

AN AUTOMATIC SYSTEM FOR CLASSIFICATION OF  
BREAST CANCER LESIONS IN ULTRASOUND IMAGES

BEHNAM KARIMI

A THESIS  
IN  
THE DEPARTMENT  
OF  
COMPUTER SCIENCE

PRESENTED IN PARTIAL FULFILLMENT OF THE REQUIREMENTS  
FOR THE DEGREE OF DOCTOR OF PHILOSOPHY  
CONCORDIA UNIVERSITY  
MONTRÉAL, QUÉBEC, CANADA

AUGUST 2014

© BEHNAM KARIMI, 2014

CONCORDIA UNIVERSITY  
School of Graduate Studies

This is to certify that the thesis prepared

By: **Mr. Behnam Karimi**

Entitled: **An automatic system for classification of breast cancer  
lesions in ultrasound images**

and submitted in partial fulfillment of the requirements for the degree of

**Doctor of Philosophy (Computer Science)**

complies with the regulations of this University and meets the accepted standards  
with respect to originality and quality.

Signed by the final examining committee:

<u>Dr. Otmane Ait Mohamed</u>	Chair
<u>Dr. Farida Cheriet</u>	External Examiner
<u>Dr. Ching Y. Suen</u>	Examiner
<u>Dr. Nawwaf Kharma</u>	Examiner
<u>Dr. Thomas G. Fevens</u>	Examiner
<u>Dr. Adam Krzyżak</u>	Supervisor

Approved \_\_\_\_\_  
Chair of Department or Graduate Program Director

# Abstract

An automatic system for classification of breast cancer lesions in ultrasound images

Behnam Karimi, Ph.D.

Concordia University, 2014

Breast cancer is the most common of all cancers and second most deadly cancer in women in the developed countries. Mammography and ultrasound imaging are the standard techniques used in cancer screening. Mammography is widely used as the primary tool for cancer screening, however it is invasive technique due to radiation used.

Ultrasound seems to be good at picking up many cancers missed by mammography. In addition, ultrasound is non-invasive as no radiation is used, portable and versatile. However, ultrasound images have usually poor quality because of multiplicative speckle noise that results in artifacts. Because of noise segmentation of suspected areas in ultrasound images is a challenging task that remains an open problem despite many years of research.

In this research, a new method for automatic detection of suspected breast cancer lesions using ultrasound is proposed. In this fully automated method, new de-noising and segmentation techniques are introduced and high accuracy classifier using combination of morphological and textural features is used.

We use a combination of fuzzy logic and compounding to denoise ultrasound images and reduce shadows. We introduced a new method to identify the seed points and then use region growing method to perform segmentation. For preliminary classification we use three classifiers (ANN, AdaBoost, FSVM) and then we use a majority voting to get the final result. We demonstrate that our automated system performs better than the other state-of-the-art systems. On our database containing ultrasound images for 80 patients we reached accuracy of 98.75% versus ABUS method with 88.75% accuracy and Hybrid Filtering method with 92.50% accuracy.

Future work would involve a larger dataset of ultrasound images and we will extend our system to handle color ultrasound images. We will also study the impact

of larger number of texture and morphological features as well as weighting scheme on performance of our classifier. We will also develop an automated method to identify the "wall thickness" of a mass in breast ultrasound images. Presently the wall thickness is extracted manually with the help of a physician.

# Acknowledgments

I would like to express my special appreciation and thanks to my advisor Professor Adam Krzyżak, you have been a tremendous mentor for me. I would like to thank you for encouraging my research and for allowing me to grow as a researcher. Your advice on both research has been priceless. I would also like to thank my committee members: Professor Ching Y. Suen, Professor Thomas Fevens, Professor Nawwaf Kharma and Professor Farida Cheriet for serving as my committee members. I also want to thank you for letting my defense be an enjoyable moment, and for your brilliant comments and suggestions, thanks to you.

Special thanks to Professor Hengda Cheng who provided me with the database of ultrasound images. I could not have done this research without it.

# Contents

<b>List of Figures</b>	<b>x</b>
<b>List of Tables</b>	<b>xii</b>
<b>Acronyms</b>	<b>xv</b>
<b>1 Introduction</b>	<b>1</b>
1.1 The problem . . . . .	5
1.2 The approach . . . . .	5
1.3 Structure of the thesis . . . . .	6
<b>2 Breast cancer and its diagnosis using ultrasound</b>	<b>8</b>
2.1 Biology of cancer . . . . .	9
2.2 Sonography . . . . .	10
2.2.1 Examining margins, shape, and echogenicity . . . . .	11
2.2.2 Sonographic features of benign and malignant nodules . . . . .	12
2.2.3 Ultrasound characteristics typical of malignant breast masses . . . . .	12
2.2.4 Benign breast masses ultrasound . . . . .	16
2.3 Ultrasound interpretations . . . . .	19
2.4 Use of computer in analysis of breast ultrasound images . . . . .	19
2.5 Computer-aided screening . . . . .	20
2.6 Stages in CAD . . . . .	20
2.6.1 Pre-processing . . . . .	20
2.6.2 Segmentation . . . . .	20
2.6.3 Feature extraction . . . . .	20
2.6.4 Classification . . . . .	21

<b>3</b>	<b>Literature survey</b>	<b>22</b>
3.1	State-of-the-art CAD systems . . . . .	22
3.2	Pre-processing . . . . .	24
3.3	Segmentation . . . . .	28
3.3.1	Histogram thresholding . . . . .	28
3.3.2	Model-based methods . . . . .	29
3.3.3	Machine learning methods . . . . .	31
3.4	Feature extraction . . . . .	33
3.4.1	Morphological features . . . . .	34
3.4.2	Texture extraction . . . . .	35
3.5	Feature selection . . . . .	38
3.6	Classification . . . . .	42
3.7	Summary . . . . .	53
<b>4</b>	<b>Proposed computer system</b>	<b>54</b>
4.1	Pre-processing . . . . .	55
4.1.1	Fuzzy logic for de-noising . . . . .	55
4.1.2	Compounding and correlation of images . . . . .	56
4.2	Segmentation . . . . .	63
4.3	Feature extraction . . . . .	69
4.3.1	Morphological features . . . . .	69
4.3.2	Texture features . . . . .	71
4.3.3	Moments features . . . . .	72
4.3.4	Convolutional neural network for feature extraction . . . . .	74
4.3.5	Combination of texture features with morphological features . . . . .	75
4.4	Feature selection . . . . .	76
4.4.1	Using MI, SFS and SBS techniques for feature selection . . . . .	76
4.4.2	Selected morphological and texture features . . . . .	76
4.5	Classification . . . . .	77
4.6	Stages in our proposed CAD system . . . . .	78
<b>5</b>	<b>Experimental results</b>	<b>81</b>
5.1	Ultrasound image database . . . . .	81
5.2	Formulas used for evaluation . . . . .	81

5.3	Pre-processing . . . . .	82
5.3.1	Compounding . . . . .	84
5.3.2	Performance of our pre-processing methods . . . . .	85
5.4	Segmentation . . . . .	86
5.5	Feature extraction and selection . . . . .	86
5.6	Classification . . . . .	88
5.7	Performance of our proposed CAD system . . . . .	89
5.8	Performance of our proposed CAD system with different set of features	91
5.8.1	Experiment using manually extracted feature (wall thickness)	91
5.8.2	Experiment using CNN to extract texture features . . . . .	92
5.8.3	Experiment using Hu moments to extract texture features . . . . .	92
5.8.4	Experiment using texture features and only Fuzzy for pre-processing	93
5.9	Using concurrent computing . . . . .	93
5.10	Complete list of experiments . . . . .	94
5.11	Conclusion of our experiments . . . . .	94
<b>6</b>	<b>Conclusions</b>	<b>96</b>
<b>A</b>	<b>Implementation notes</b>	<b>98</b>
A.1	Statistical Analysis . . . . .	98
A.2	Accord.NET library . . . . .	98
A.2.1	Scientific computing . . . . .	98
A.3	Basic linear algebra - DotNetMatrix library . . . . .	113
A.3.1	Background . . . . .	114
A.3.2	Using the library . . . . .	115
<b>B</b>	<b>Ultrasound database</b>	<b>118</b>
<b>C</b>	<b>All Experiments</b>	<b>121</b>
C.1	Experiment #1 - Experiment using no pre-processing and using morphological features only . . . . .	121
C.2	Experiment #2 - Experiment using fuzzy logic for de-noising and using morphological features only . . . . .	131
C.3	Experiment #3 - Experiment using fuzzy logic for pre-processing and using morphological and texture features . . . . .	141



C.4	Experiment #4 - Experiment using fuzzy logic and compounding for de-noising and using morphological and texture features . . . . .	151
C.5	Experiment #5 - Experiment using an extra feature (wall thickness) .	160
C.6	Experimental results using combination of different methods . . . . .	164

<b>Bibliography</b>		<b>166</b>
---------------------	--	------------

# List of Figures

1.1	Female Breast Cancer Death Rates by Race and Ethnicity, U.S., 1999 to 2010 . . . . .	2
1.2	A sonography image from breast that shows a suspicious mass . . . . .	2
1.3	Pathology report . . . . .	4
2.1	An example of a solid breast nodule . . . . .	9
2.2	(a) illustrates a sonographic instrument and (b) shows a transducer . . . . .	11
2.3	a) Benign tumour b) Malignant tumour . . . . .	14
2.4	An example of calcification in breast ultrasound . . . . .	15
2.5	Irregular borders . . . . .	16
2.6	Well-defined border . . . . .	17
2.7	Enlarged lymph node that can be interpreted as metastasis of breast cancer . . . . .	18
2.8	Ultrasound image interpretations challenges . . . . .	19
2.9	Stages in CAD . . . . .	21
3.1	Fully automated ROI labelling system . . . . .	22
3.2	Speckle reduction . . . . .	27
3.3	Detection of contours in slices(taken from [152]) . . . . .	30
3.4	A mass with irregular shape and with branches . . . . .	33
3.5	Window of some pre-determined size . . . . .	37
3.6	(a) Sequential forward search (b) Sequential backward search . . . . .	41
3.7	Sequential forward search algorithm (taken from [45]) . . . . .	41
3.8	Sequential backward search algorithm (taken from [45]) . . . . .	42
3.9	Eigenfaces generation process . . . . .	44
3.10	Cluster separation . . . . .	44
3.11	Multi Artificial Neural Network model . . . . .	46
3.12	Multi Classifier Scheme model (taken from [129]) . . . . .	47

3.13	Image classifier . . . . .	48
3.14	Image classifier . . . . .	49
3.15	Aggregation of sub-images using SVM . . . . .	52
4.1	Membership functions for input gray level values . . . . .	56
4.2	An ultrasound transducer is rotated fully around the female breast to acquire data from multiple angles (taken from Techavipoo et al. [128])	58
4.3	B-scan vs. compounding (taken from [132]) . . . . .	60
4.4	Coordinate system for paired angle compounding (taken from [132]) .	61
4.5	Different views of breast . . . . .	63
4.6	Incorrect seed point selection using method by Ulagamuthalvi and Srid- haran [135] . . . . .	63
4.7	a) Original Image b) Binarized image . . . . .	64
4.8	a) Binarized image b) After deleting boundary-connected region . . .	65
4.9	a) After deleting boundary-connected region b) Winning region . . .	66
4.10	a) Original image b) Clustered image c) Winning region . . . . .	68
4.11	CNN structure used for feature extraction . . . . .	75
4.12	Proposed classifier - combination of FSVM, AdaBoost, ANN and Ma- jority base classifiers . . . . .	78
4.13	Proposed system . . . . .	79
5.1	Fuzzy logic for de-noising . . . . .	82
5.2	Segmentation . . . . .	83
5.3	Segmentation without using Fuzzy logic for de-noising . . . . .	83

# List of Tables

2.1	Selected Features . . . . .	13
3.1	Selected features by Chen et al. [22] - A: 77 auto-covariance matrix; B: SGLDM; C: GLDM; D: BDIP; E: BVLC; F: NGTDM . . . . .	36
3.2	GLRLM features . . . . .	36
3.3	Comparison between different classification methods to detect suspicious lesions in kidney ultrasound images [2] . . . . .	51
4.1	Comparison between proposed segmentation method, region growing method and neurotrophic I-means clustering method . . . . .	67
4.2	Comparison between proposed segmentation methods (using binarized image to select seed point and using k-means algorithm to select seed points) . . . . .	68
4.3	All possible texture features by Chen et al. [22] - A: 77 auto-covariance matrix; B: SGLDM; C: GLDM; D: BDIP; E: BVLC; F: NGTDM . . . . .	72
4.4	Selected morphological and texture features . . . . .	77
5.1	Applying fuzzy logic for de-noising (TP: True Positive; TN: True Negative; FP: False Positive; FN: False Negative) . . . . .	83
5.2	No fuzzy logic for de-noising . . . . .	84
5.3	Experiment using compounding (Gold stand.: Cold standard, Comp.: Compounded) . . . . .	85
5.4	Results with compounding . . . . .	85
5.5	Comparison between several de-noising methods . . . . .	86
5.6	Comparison between proposed segmentation method, region growing method and neurotrophic I-means clustering method . . . . .	86
5.7	Selected morphological features used in our experiments . . . . .	87
5.8	Comparison between different feature selection algorithms . . . . .	87
5.9	Methods used in each stage . . . . .	88

5.10	Comparing our proposed classifiers with state-of-the-art classifiers - using k-fold cross-validation . . . . .	88
5.11	Comparing our proposed classifiers with state-of-the-art classifiers . . . . .	89
5.12	Proposed CAD system - Selected features (A: 77 auto-covariance matrix; B: SGLDM; C: GLDM; D: BDIP; E: BVLC; F: NGTDM) . . . . .	90
5.13	Proposed CAD system - Methods used in each stage . . . . .	90
5.14	Proposed CAD system - Results . . . . .	90
5.15	Proposed CAD system - Comparison with other methods . . . . .	91
5.16	Results . . . . .	91
5.17	Comparison with other methods . . . . .	91
5.18	Result of comparing our proposed classifiers with state-of-the-art classifiers - using CNN for texture feature extraction and using k-fold cross-validation . . . . .	92
5.19	Result of comparing our proposed classifiers with state-of-the-art classifiers - Using CNN for texture feature extraction . . . . .	92
5.20	Experiment - Using Hu moments - Results using k-fold cross-validation . . . . .	92
5.21	Experiment - Using Hu moments - Results . . . . .	93
5.22	Experiment using texture features and Fuzzy logic - Results . . . . .	93
5.23	Computational time for our proposed system (in seconds) . . . . .	94
A.2	DotNetMatrix library capabilities . . . . .	117
B.1	Breast ultrasound database - B: Benign, M: Malignant . . . . .	120
C.1	Experiment #1 - Selected morphological features . . . . .	122
C.2	Experiment #1 - Methods used in each stage . . . . .	122
C.3	Experiment #1 - Results . . . . .	122
C.4	Experiment #1 - Comparison with other methods . . . . .	123
C.5	Experiment #1 - Output . . . . .	131
C.6	Experiment #2 - Selected morphological features . . . . .	131
C.7	Experiment #2 - Methods used in each stage . . . . .	132
C.8	Experiment #2 - Results . . . . .	132
C.9	Experiment #2 - Comparison with other methods . . . . .	132
C.10	Experiment #2 - Output . . . . .	140
C.11	Experiment #3 - Selected features (A: 77 auto-covariance matrix; B: SGLDM; C: GLDM; D: BDIP; E: BVLC; F: NGTDM) . . . . .	141

C.12 Experiment #3 - Methods used in each stage . . . . .	142
C.13 Experiment #3 - Results . . . . .	142
C.14 Experiment #3 - Comparison with other methods . . . . .	142
C.15 Experiment #3 - Output . . . . .	150
C.16 Experiment #3 - Selected features (A: 77 auto-covariance matrix; B: SGLDM; C: GLDM; D: BDIP; E: BVLC; F: NGTDM) . . . . .	151
C.17 Experiment #4 - Methods used in each stage . . . . .	152
C.18 Experiment #4 - Results . . . . .	152
C.19 Experiment #4 - Comparison with other methods . . . . .	152
C.20 Experiment #4 - Output . . . . .	160
C.21 Experiment #5 - Selected features (A: 77 auto-covariance matrix; B: SGLDM; C: GLDM; D: BDIP; E: BVLC; F: NGTDM) . . . . .	161
C.22 Experiment #5 - Methods used in each stage . . . . .	162
C.23 Experiment #5 - Results . . . . .	162
C.24 Experiment #5 - Comparison with other methods . . . . .	162
C.25 Experiment #5 - Sample output . . . . .	163
C.26 Summary of experiments (Spec.: Specificity, Sen.: Sensitivity) . . . . .	164
C.27 Experiments with different combination of methods in each stage of the CAD system . . . . .	165
C.28 Result of comparing our proposed classifiers with state-of-the-art clas- sifiers . . . . .	166

# Acronyms

**AdaBoost** Adaptive Boost.

**ANN** Artificial Neural Network.

**BDIP** Block Difference of Inverse Probabilities.

**BDS** Bidirectional Search.

**CAD** Computer Aided Diagnosis.

**CNN** Convolutional Neural Network.

**DCT** Discrete Cosine Transform.

**DWT** Discrete Wavelet Transform.

**FLD** Fisher's Linear Discriminant.

**FN** False Negative.

**FP** False Positive.

**FSVM** Fuzzy Support Vector Machine.

**GLDM** Gray-Level Difference Matrix.

**IDWT** Inverse Discrete Wavelet Transform.

**KNN**  $k$ -nearest neighbor.

**LDA** Linear Discriminant Analysis.

**MANN** Multi Artificial Neural Network.

**MI** Mutual Information.

**MSE** Mean-Squared Error.

**NGTDM** Neighborhood Gray-Tone Difference Matrix.

**NN** Neural Network.

**NPV** Negative Predictive Value.

**PCA** Principal Component Analysis.

**PPV** Positive Predictive Value.

**PSNR** Peak Signal to Noise Ratio.

**ROI** Region of Interest.

**ROI** Volume of Interest.

**SBS** Sequential Backward Search.

**SFS** Sequential Forward Search.

**SGLDM** Spatial Gray-Level Dependence Matrices.

**SRI** Speckle Reduction Imaging.

**SVM** Support Vector Machine.

**TN** True Negative.

**TP** True Positive.

**US** Ultrasound.



# Chapter 1

## Introduction

Mammography is one of the screening tests that has been shown to decrease the breast cancer death rate for women. Where the breast tissue is dense, cancers can be hidden on mammogram. Mammography is less able to show cancers in younger women, between 40 and 49 years old, than in women 50 years or older, although mammography is beneficial in both age groups. Sonography shows many cancers not seen on mammography, especially when the tissue is dense. This success has stimulated interest in using sonography for breast cancer screening. It is not known at this time whether patients with cancers found only by sonography have the same outcome as those with cancers found on mammography or whether treating cancers found only by sonography saves lives. Most of cancers found only on sonography are small invasive cancers. Figure 1.1 illustrates breast cancer death rates for women from 1999 to 2010.

Usually, when there is a suspicious lesion found in mammography, it is recommended to perform sonography for better analysis. If the suspicious growth detected by mammography is confirmed by sonography, then the patient will be sent to perform biopsy in order to get the final diagnosis. It is very important to know that mammography and sonography are not diagnosis tests but rather screening tests. Figure 1.2 illustrates a sample sonography image of breast.

A suspicious mass or nodule is typically darkest in the sonogram. The reason is that the more dense the tissue is, the more unlikely that the sound passes through the tissue. That is why that area becomes darker. When a dark area in sonography image is found, sonographer examines that area carefully to see the type of the mass.

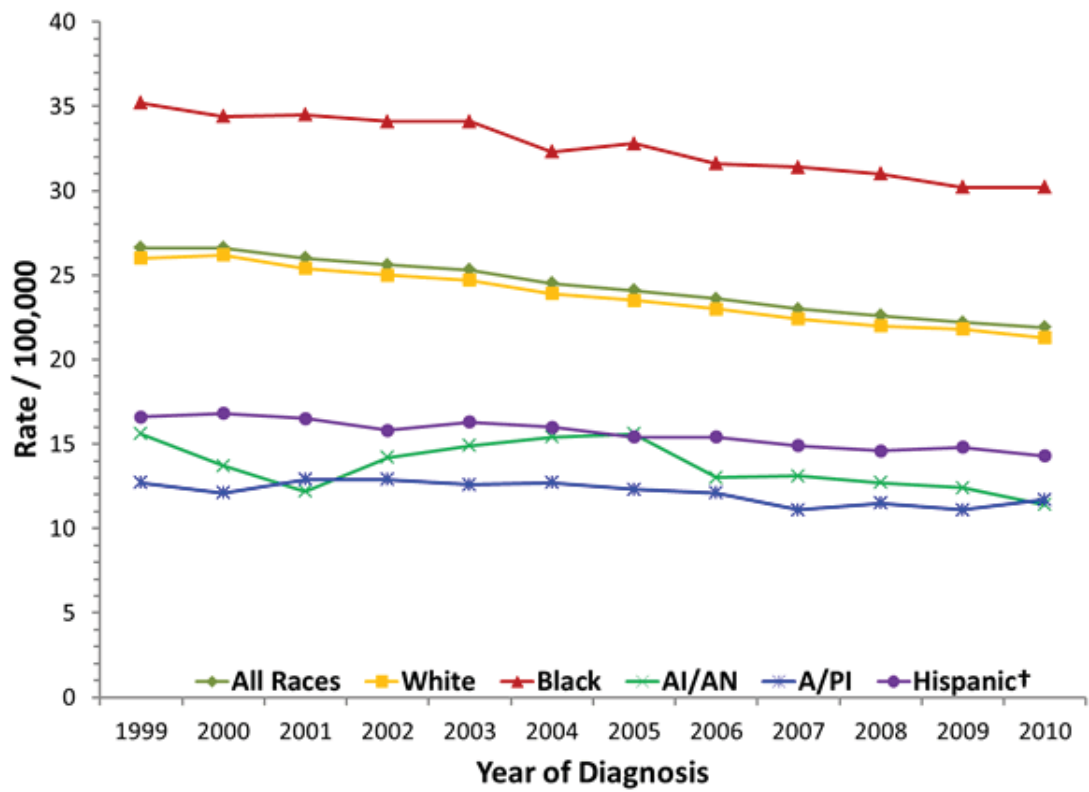


Figure 1.1: Female Breast Cancer Death Rates by Race and Ethnicity, U.S., 1999 to 2010

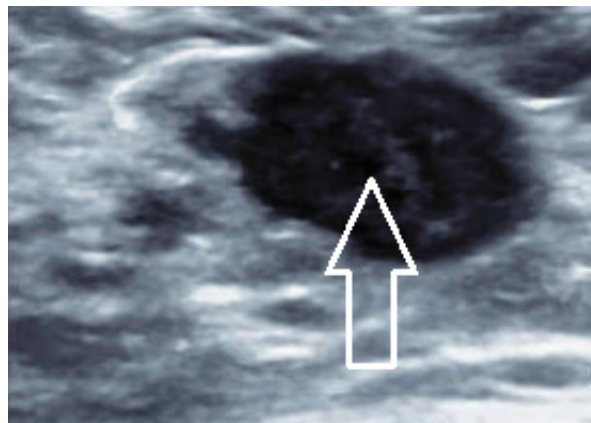


Figure 1.2: A sonography image from breast that shows a suspicious mass

Radiologists usually use heuristic and measurable criteria to identify if a mass is suspicious for carcinoma. The most important features of a mass that could raise the red flag are the size, the shape, the area and the texture. Upon completion of image analysis the radiologist decides whether a patient requires a diagnostic test, i.e., biopsy.

Tumors are sometimes cancerous but this does not mean that tumors and cancers are synonyms (as most people think). Therefore a proper examination of lumps is very important. Differences between cancer, carcinoma and tumor are:

- Cancer: Class of diseases occurring due to uncontrolled growth of groups of cells. Cancerous cells are malignant.
- Carcinoma: Is a cancer that begins in the skin or in tissues that line or cover internal organs
- Tumor: A tumor is the name for swelling or lesion formed by an abnormal growth of cells. A tumor can be benign, pre-malignant or malignant, whereas cancer is by definition malignant.

When biopsy is recommended, the abnormality identified on a mammogram or ultrasound is surgically removed. Biopsy is an excisional biopsy, meaning that the abnormality seen on mammogram is surgically removed. You will be given the anesthesia that you and your physician have discussed. The surgeon uses the wire implanted earlier to locate the abnormality and remove it in the operating room. The specimen, once removed from the breast, is then sent to radiology to be X-rayed. The radiologist and the surgeon communicate to confirm that the abnormality seen on mammogram or ultrasound has been removed. The abnormality that is removed is then sent to pathologist to determine if the sample contains cancerous cells and also some other information life grade and type of cancer is determined during pathological analysis. Figure 1.3 illustrates a sample pathology report.

#2. Received fresh, consists of a fragment of fibroadipose tissue measuring 1.6 x 1.2 x 0.6 cm. One lymph node (LN) is identified on cross-section measuring 1.3 x 0.7 x 0.6 cm: bisected and touch prints made. The LN is submitted in toto in one cassette labelled "LN". SH/mc

**SYNOPTIC REPORT:**

**Tumor type:** INVASIVE DUCTAL CARCINOMA, no special type

**Invasive tumor size:** 2.0 x 1.5 x 1.3 cm

**Nottingham histologic Grade:** 3/3

Score for tubules: 2-3/3

Score for nuclei: 2/3

Score for mitoses: 3/3 (40/10 HPF; field size: 0.56 mm diameter)

Lymphovascular space invasion: Present

Perineural invasion: Absent

Invasive tumor necrosis: Absent

Pushing border: Yes: less than 25%

Lymphocytic infiltrate in stroma: Present, diffuse

Syncytial growth: Absent

DCIS: Present

DCIS type: solid, micropapillary

Nuclear grade of DCIS: 2/3

DCIS necrosis: central (comedo), focal

% DCIS in tumor: <1 %

Number of slides involved: 10 out of 14 slides

Calcifications: In DCIS

Skin involvement: Absent

**Hormone Receptor Status:** POSITIVE estrogen and progesterone receptors protein as per previous core biopsy # SB-09-13704

**HER2/neu Protein:** NEGATIVE (as repeated on block 1C)

% of cells positive: 0%

Antibody used: 4B5

**Resection margins:**

**Invasive carcinoma:**

NEGATIVE . The distance to the closest margin is 3 mm.

The closest margins are MEDIAL and POSTERIOR. All other margins area > 5

**DCIS margins:**

NEGATIVE . The distance to the closest margin is 1.0 mm (slices 5,6,7)

The closest margin is POSTERIOR. Other margins > 5 mm

**Lymph Node Dissection:**

Number of nodes resected 1 Number involved: 0

**Other abnormalities in breast tissue :**

- Fibrocystic changes: (apocrine metaplasia, sclerosing adenosis, cyst formation, stromal fibrosis)
- Biopsy tract identified

Figure 1.3: Pathology report

## 1.1 The problem

Interpretation of breast ultrasound images is a very critical step in diagnosing breast cancer. The radiologist analyzes the ultrasound images and makes a decision to send the patient for biopsy.

There are some challenges in interpretation of ultrasound images. Sometimes even experienced radiologists have difficulties to identify if a lesion is suspicious for cancer. If a radiologist decides that a lesion is not suspicious for cancer, and in reality it is cancer, then it is called a false negative result. Unfortunately, false negative results happen and it is not unheard of. False negatives are very dangerous because the patient will not seek medical treatment and cancer can spread to the other organs in the body.

There are some reasons that make interpretation of breast ultrasound images a challenging task. One of the reasons is that ultrasound images (specially breast ultrasound images) are very noisy. This makes the interpretation very difficult as sometimes normal breast tissues are considered as part of the lesion and vice versa.

The other reason that radiologists sometimes have difficulties analyzing breast ultrasound images is shadowing. Shadowing is not part of the normal breast tissue or lesion but it is an artifact that can be seen in ultrasound images. The shadows are sometimes mistakenly considered part of the lesions and make the analysis very difficult.

When radiologist finds the boundary of the lesion, limited number of features are considered to define if the lesion is suspicious for cancer. Those limited number of features might not be enough to cover all the possible cases. Radiologists sometimes use their own experience for making their decision. Therefore interpretation of ultrasound images can be very subjective.

## 1.2 The approach

In this thesis a new method to automatically detect suspicious lesions in breast ultrasound images is proposed. The goal of this study is to remove as much noise as possible from ultrasound images so we can identify lesions easier. Also, our method tries to eliminate or reduce the shadows appearing in ultrasound images.

The other challenge we are trying to overcome is to consider a better set of features

with higher discriminatory power. We consider morphological features and texture features.

To summarize, in this thesis a new CAD system with high performance and accuracy is introduced. Here are the main contributions of this thesis:

- Implementation of a new method for de-noising to eliminate as much noise as possible while preserving important information in ultrasound images
- Implementation of a new segmentation method with more accuracy than the state-of-the-art segmentation methods
- Finding proper set of features with better discriminatory power
- Combination of different types of features (i.e. morphological and texture features) and study the effect of those features on the performance and accuracy of the system
- Considering ultrasound images from different angles to get more information about the lesions seen in those images
- Introduction of a new two class classification method with high accuracy for classifying lesions in breast ultrasound images
- Comparison between state-of-the-art methods and our method to validate the performance and accuracy of our proposed system

Based on the mentioned items, we have done several experiments to prove our system could perform better than other state-of-the-art systems.

### **1.3 Structure of the thesis**

This thesis consists of six chapters preceded by a list of figures and tables. Chapter 2 illustrates the characteristics of ultrasound images and discusses some difficulties that radiologists have for interpretation of ultrasound images.

In chapter 3 different methods of pre-processing and segmentation are studied and the advantages and disadvantages of those methods are discussed. We also discuss

existing methods for feature selection. Finally we discuss the state-of-the-art classification methods to classify lesions in breast ultrasound images and we also discuss advantages and disadvantages of each method.

Our contribution in this thesis is discussed in chapter 4. We used fuzzy logic and compounding for de-noising of breast ultrasound images. We also introduced a new approach for segmentation of lesions in ultrasound images based on automatic selection of seed points and region growing algorithm. We used combination of texture features and morphological features and selected proper set of features. Our new classification method is shown in this chapter along with implementation details and proper methods of validation and verification. Finally, the complete system to classify lesions in breast ultrasound images is proposed.

In chapter 5 we show the result of our experiments based on the new method we introduced. A comparison between our method and other methods is done and we show representative outputs of our algorithm.

We finally conclude the thesis in chapter 6 and discuss future work.

## Chapter 2

# Breast cancer and its diagnosis using ultrasound

Ultrasound is a useful diagnostic tool for breast cancer, especially for younger patients. Most of the time breast ultrasound is used as a way to distinguish solid from cystic masses and often to determine the extent of cancer in known or suspected cases. A cystic mass is a closed capsule or sac-like structure, typically filled with liquid, semisolid or gaseous material - very much like a blister.

For young women (younger than 30) ultrasound imaging may be the first step in which a clinical exam reveals either a palpable mass or nipple discharge. (Since breast cancer tends to happen with older post-menopausal women, doctors try not to expose younger women to unnecessary radiation of a mammogram). But sonography can help establish the differentiation between benign and malignant solid tumors as well. A lack of circumscribed margins, heterogeneous echo patterns, and an increased anteroposterior dimension can indicate a higher probability of malignancy in solid breast nodules as shown in Fig. 2.1 [124, 146].



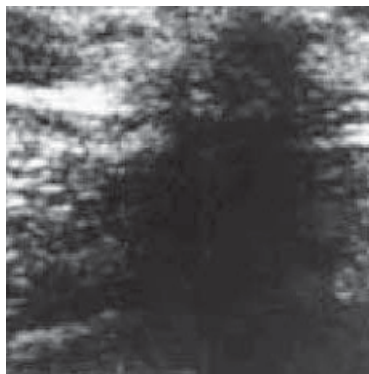


Figure 2.1: An example of a solid breast nodule

## 2.1 Biology of cancer

Cells are fundamental unit of life. Organs in the body (i.e. breast, colon, brain, etc.) are made of specialized cells that carry out the organs functions. This may include transporting oxygen to other parts of the body, digestion, excretion of waste, reproduction, etc. [31].

When a cell is worn out, it has to be replaced to allow organs to perform. The cells might also increase in number in response to changes in the environment. Reproduction of cells happens by cell division. When the cell is normal, the division is happening in a regulated way. When cell grows, inheritance and containment is being controlled by DNA. DNA is considered as cells brain. It is like a blueprint of the functions of the cell. In humans, cells DNA is arranged in 46 sections. Those sections are called chromosomes. Chromosomes are in pairs (23 chromosomes from each biological parent).

The 46 chromosomes contain more than 100,000 genes. Gene is a segment of DNA that makes the structure of a protein. Protein is the main source for development and growth of the cells and it carries out vital chemical functions in the body. Genes are also arranged in pairs (like DNA). The pair of gene consists of gene from the mother and gene from the father. Gene responsibility is to tell a cell to make different proteins. Some genes send a message to the cell to produce structural proteins that serve as building blocks. Other genes tell the cell to make hormones, which exit the cell and communicate with other cells.

Cells division happens when they receive signals from growth factors that circulate in the bloodstream or from another cell. When cells receive signals to divide, they

go through a cycle called cell cycle. Each step has a checkpoint to make sure the process is performed the way it should. When the process goes wrong, a cell might become cancerous. In another word, a cancer cell is a cell that grows uncontrollably. These cells do not respond to signals to stop the division. When the cells grow in an uncontrollable manner and they are not able to recognize their own natural boundary, the cells may spread to other parts of the body, where they do not even belong to.

A cancer cell is a defective cell that goes through mutation. Mutation means several genes changes happen. There are two types of mutations. The first type is called dominant mutation, which is caused by an abnormality in one gene in a pair. An example is a gene that produces defective protein and makes the growth-factor receptor on a cells surface to be always on, when there is no growth-factor even present. The second type of mutation is called recessive mutation. In this type of mutation, both pairs are damaged. For example, a normal gene called p53 produces a protein that turns off the cell cycle and helps to control cell growth.

When a cell becomes cancerous, many mutations are necessary. In some cases, both types of mutation (dominant and recessive) may occur in order for a cell to become cancerous. A gene mutation can cause an abnormal cell to invade normal tissues, where the cancer started or it can travel in the bloodstream, which is called metastasize, and reach remote parts of the body. To summarize, cancerous cells are defective cells which divide uncontrollably. They can invade the surrounding tissues and spread by vascular and/or lymphatic systems. These defects are the result of gene mutation [67].

## 2.2 Sonography

Ultrasound is cyclic sound pressure with a frequency greater than the upper limit of human hearing. It is used in different fields, typically to penetrate a medium and measure the reflection signature or supply focused energy. The reflection signature can show the details about the inner structure of the medium. The most well-known application of ultrasound is its use in sonography.

Sonography is a procedure widely used in medicine. It can be used for screening, diagnosis and therapeutic procedures, using ultrasound to guide interventional procedures such as biopsy. The procedure of sonography is usually performed by



(a)



(b)

Figure 2.2: (a) illustrates a sonographic instrument and (b) shows a transducer

Radiologists, who are physicians specialized in the application and interpretation of a wide variety of medical imaging modalities. To perform sonography, a hand-held probe is typically used (called transducer) that is placed directly on and moved over the patient. As the transducer moved over the patient, an ultrasound image can be seen on the sonographic instrument monitor. This instrument can take snapshots of different areas for further reference. The snapshots can then be printed and be filed. Fig. 2.2 illustrates a sonographic instrument. Using sonographic instrument, sonographer can analyze the images seen on the monitor.

### 2.2.1 Examining margins, shape, and echogenicity

The most important features in a breast ultrasound are the clarity and contour of the mass margins, the orientation and shape of the mass, the echo texture and echogenicity (reflecting ultrasound waves), and the effects on distal echoes. Others aspects of the mass such as compressibility and vascularity may also be noted. Some of the features one might usually find in a sonograph of a malignant breast mass would include a marked hypoechogenicity, acoustic shadowing, a branch pattern or microlobulation,

or a duct extension. Other malignant features might be a 'taller than wide' shape, angular margins, the presence of calcification, and speculation, which probably has the highest positive predictive value for malignant breast cancer. Benign breast lesions on the other hand tend to appear on ultrasound with intense and uniform hyperechogenicity, as an oval shape with a thin, consistent capsule, and they may have two to three gentle lobulations.

### **2.2.2 Sonographic features of benign and malignant nodules**

A breast sonograph can help in diagnosis in differentiating between benign and malignant tumors, often without the need for a biopsy. The absence of a well-circumscribed margin, heterogeneous echo patterns, as well as an increased anteroposterior dimension to the image does tend to indicate a higher probability of malignant cancer in solid breast nodules. A 'probably benign' and with recommended short term follow up only, can only be given if there is an absence of any of these clearly suspicious features.

### **2.2.3 Ultrasound characteristics typical of malignant breast masses**

The typical sonographic presentation of a malignant breast mass would be an irregular, heterogeneous, hypoechoic mass, with speculations and angular margins. And, these kinds of masses tend to have that 'taller-than-wide' appearance, and also demonstrate acoustic shadowing. Figure 2.3 compares a malignant tumour with a benign tumour. In the malignant tumour, an ill-defined border, an irregular shape, microlobulations, and speculations (which appears as a hyperechoic 'band' around the mass) can clearly be seen. The lesion also appears to be 'taller-than-wide', with an angular margin. This would all be highly predictive of invasive ductal carcinoma, and the lesions would be biopsied.

Speculations often represent breast tumor 'tentacles' or desmoplastic reactions. On ultrasound, speculations will often consist of straight lines that 'radiate' in a perpendicular fashion from the surface of the breast mass.

Table 2.1: Selected Features

Sonographic Features	Benign	Potentially Malignant
Absence of malignant findings	*	
Hyperechoic/ intense, fibrous tissue like	*	
Two or three microlobulations	*	
Ellipsoid shape/ wider than tall, parallel to the skin	*	
Pseudocapsule/ thin, echogenic, well-circumscribed	*	
Speculations/ alternating hyper and hypoechoic straight lines		*
Height divided by width greater than 1 or non-parallel to the skin		*
Angular margins		*
Shadowing/ through transmission attenuated		*
Branch pattern extensions / multiple radial projections, peri or intra-ductal, nipple oriented		*
Markedly hypoechoic (sound waves not absorbed)		*
Microcalcifications		*
Duct extension / single radial projection, peri or intra-ductal, nipple oriented		*
Microlobulations		*
Intracystic nodule (cyst inside a mass), parietal thickening (thickening of the border of the mass)		*

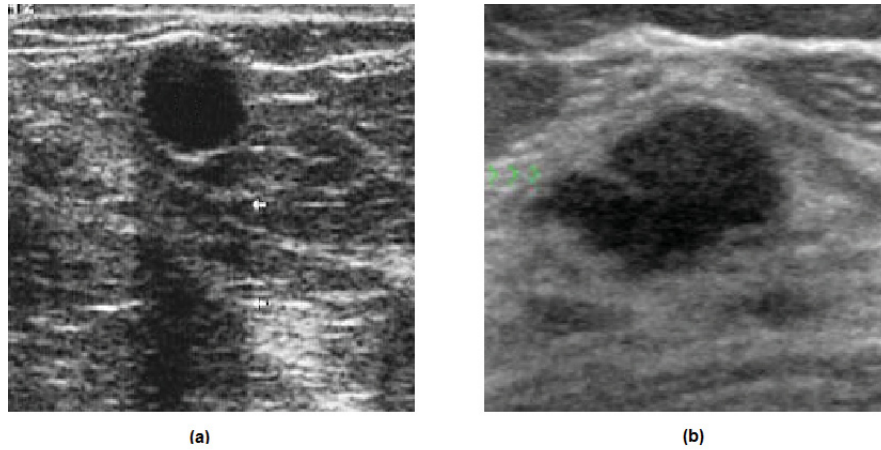


Figure 2.3: a) Benign tumour b) Malignant tumour

An 'angular margin' is observed as an angular configuration to the junction between relatively hypoechoic or isoechoic central portion of a solid mass and surrounding tissue. Sometimes these features are referred to as 'jagged' or 'irregular' margins. Angular margins are quite distinct from 'lobulations' which tend to be smooth and rounded. Angular margins observed on breast ultrasound are highly predictive of malignancy.

If a solid breast nodule appears on ultrasound to be 'taller-than-wide', this is quite suspicious of malignancy. When a patient is scanned by ultrasound, they are usually in a supine position, and as a result the normal 'tissue planes' on the breast will have a horizontal orientation. If a mass or part of the mass seems longer in the anteroposterior dimension (tallness) compared to either the sagittal or transverse dimensions (depth and width) then one can conceive that this might likely be caused by a malignancy 'aggressive enough' to overcome normal breast tissue barriers and planes, and grow vertically.

Hypoechoic breast lesions are suspicious for malignancy, and on ultrasound imaging they will tend to look intensely black compared to the surrounding isoechoic fat. But malignancies can also be isoechoic and hyperechoic on breast ultrasound, so it is not a 'hard and fast' finding by any means.

'Microlobulations' observed on breast ultrasound indicate the presence of lots of very small (1mm to 2 mm) lobulations on the surface of a solid breast nodule, and will be quite similar to mammogram findings. As the number of these microlobulations increase, the probability that the breast mass is malignant also increases.

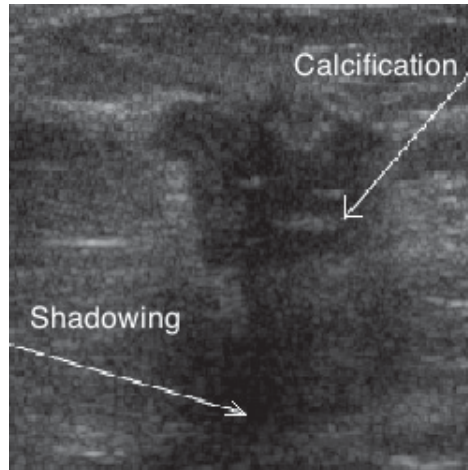


Figure 2.4: An example of calcification in breast ultrasound

A 'duct extension' appears on ultrasound as a 'radially oriented' projection that seems to arise from the lesions an axis oriented towards the nipple. These projections are often observed either within or around breast duct. Sometimes a duct extensions/projection can be observed which has developed as a 'bridge' between multifocal malignancies. This is different from a 'branch pattern' in which multiple extensions are seen to arise from the mass but extend away-from the nipple. A branching pattern tends to indicate a tumor growth advancing away from the nipple. Any apparent growth that is long enough to visibly fill a duct and branch, no matter what direction is goes, will be suspicious for malignancy and be biopsied.

### **Calcifications**

Mammography is more sensitive than ultrasound when it comes to the detection of micro calcifications. Calcifications on a solid mass which appear 'punctate' are highly suspicious of malignancy, and will usually appear on ultrasound as bright, punctate foci. Since malignant breast lesions are typically either intensely or mildly homogenous hypoechoic solid masses, on ultrasound this provides a 'background' which makes it easier to view calcifications sonographically. So, while calcifications are usually not seen on ultrasound, when they do appear vividly, it is highly suspicious for malignancy. An example of calcification is shown in Figure 2.4.

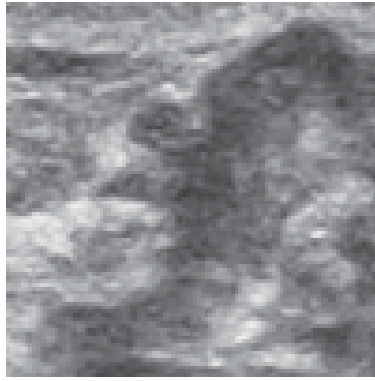


Figure 2.5: Irregular borders

### **Irregular borders**

Speculated margins have a positive predictive value for malignant breast cancer in about the 85% range. Masses showing an irregular shape or non-parallel orientation are also quite suggestive of malignancy, with a positive predictive value in the 62% to 69% range. Other studies place a higher predictive value on the presence of an irregular border (about 88% predictive of malignancy) and evidence of increased vascularity in the mass predicts malignancy about 82% of the time. The sonograph image below shows an irregular vascularized retroareolar mass, with calcifications. This is very likely to be infiltrating ductal carcinoma and a biopsy sample would likely be taken right away. Figure 2.5 illustrates a mass with irregular borders.

## **2.2.4 Benign breast masses ultrasound**

### **Hyperechogenicity, thin well defined border**

On ultrasound, a benign breast mass will typically be well defined and with smooth margins. The lesion might also be microlobulated or with just 2 to 4 mild lobulations. Benign breast lesions also tend to be ovoid or round in shape, and are often 'wider-than-tall' (which indicates a parallel orientation to the chest wall). The echo texture of a benign mass will usually be homogeneous with an isoechoic, hyperechoic, to mildly hypoechoic echogenicity. Some benign breast masses will also exhibit mild acoustic enhancement on ultrasound, and might be slightly compressible. Vascularity in an ultrasound of a benign mass is variable and will depend on the specific histology of the suspicious mass.



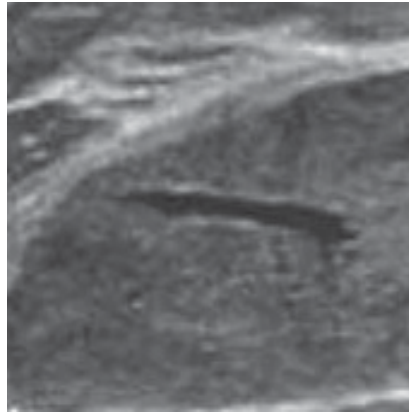


Figure 2.6: Well-defined border

In terms of sonographic features suggestive of benign breast lesions, a well circumscribed margin has a positive predictive value for being benign about 90% of the time, and an 'oval shape' about 84% of the time. Breast lesions with a 'parallel' orientation are predictive of benignity almost 80% of the time.

The quality of the margins of a breast lesions scanned with ultrasound is sometimes referred to as its 'capsule'. If the margin of the suspected mass seems well-circumscribed in both its inner and outer edges, and seems thin and even, this tends to be a sign of a benign mass. The lesion is 'encapsulated' by the compressed adjacent breast tissue, and the mass itself is 'pushing against' this tissue, rather than infiltrating and invading that tissue. Figure 2.6 illustrates an example of a mass with well-defined border.

Sometimes you do see a mild undulation in contour on ultrasound with a benign fibroadenoma. But there should not be many of these mild 'lobulations', and usually any more than three is considered a potentially malignant sign. Of greater concern are more numerous, smaller, and sharper microlobulations than one tends to find in malignant breast cancer tumors.

Breast lesions which appear as having a marked and uniform hyperechogenicity are highly predictive of a benign lesion. This feature typically represents normal fibrous changes within the breast. But when there are some regions are either hypoechogenicity or isoechogenicity that are larger than normal (larger than either normal ducts or terminal ductal-lobular units), that would indicate a 'medium' level of concern and would probably result in a biopsy, particularly if these areas were not contained within fat lobules.

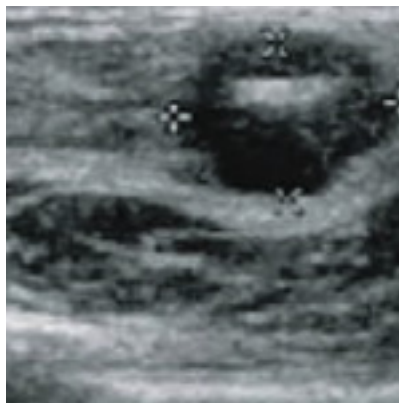


Figure 2.7: Enlarged lymph node that can be interpreted as metastasis of breast cancer

The 'compressibility' of a breast lesions scanned with ultrasound refers to changes in the shape of a lesion as a result of the pressure applied by the probe. A solid, likely malignant, breast lesion will not 'compress' at all from the pressure of the probe, but a tumor of benign fibrous or glandular tissue, such as a fibroadenoma, will show some compressibility. A benign breast fibroadenoma is usually oriented horizontally, more wide than tall. Often the compression of the scanner will cause a 'flattened' oval shape of a fibroadenoma, which would not occur with solid, malignant breast lesions. the

Sometimes a breast ultrasound will pick up an enlarged node in axilla. Many breast cancer oncologists would take an enlarged axillary node on ultrasound as proof positive for lymph node metastasis, even without a lymph node dissection. (Sometimes patients will not agree to a lymph node dissection to check for breast cancer metastasis). Figure 2.7 illustrates an example of an abnormal lymph node.

If the findings of ultrasound imaging of suspicious breast nodules were expressed as an odds ratio (the odds of a person with these features as having breast cancer, as compared to an breast ultrasound where these features are not present) it may be suggested that breast lesions without a well-circumscribed margins are almost 17 times more likely to indicate malignant breast cancer. Breast sonographs showing a heterogeneous echo texture are about 8x more likely to be breast cancer. The 'incompressibility' of a breast lesion on ultrasound would tend to be almost 9 times more likely to be malignant.

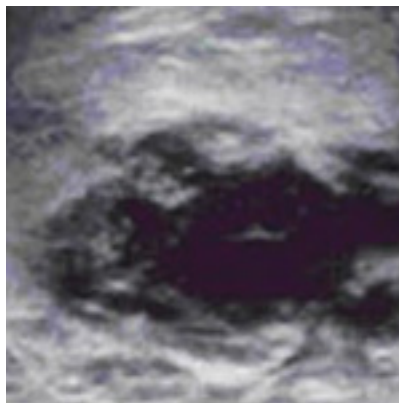


Figure 2.8: Ultrasound image interpretations challenges

## 2.3 Ultrasound interpretations

Not all suspicious breast lesions will be straightforward in their ultrasound appearance and diagnosis. In some cases the findings are still inconclusive, with a recommendation for short interval follow-up, or biopsy. But, one of the reasons to use ultrasound in the first place is because there is a high suspicion of a benign mass to begin with, and the use of ultrasound is mostly to confirm the cystic nature of the lesion. For example, ultrasound cannot always reliably confirm the diagnosis of a breast abscess. Figure 2.8 illustrates an example of a mass that is challenging for professional to diagnose.

## 2.4 Use of computer in analysis of breast ultrasound images

Computer-aided diagnosis (CAD) has been used more and more in past two decades. It is used to assist radiologists to interpret medical images by using a computer system to provide second opinions. Studies on CAD systems shows that it could dramatically reduce the workload and reduce cancer missed by other methods and give more information to the radiologist [39].

Since breast ultrasound is much more operator-dependent than mammography, reading ultrasound image requires very well-trained and experienced radiologists. Even among well-trained experts, they might have a high inter-observer variation

rate. Therefore, computer-aided diagnosis (CAD) has been investigated to help radiologists in making accurate decisions.

## **2.5 Computer-aided screening**

CAD systems are used to provide radiologists with second opinion. They can extract some features, such as computational features and statistical features. Those features cannot be obtained by visual cues. Another advantage is that CAD can help with eliminating workload and minimize the operator-dependent nature inherent in ultrasound imaging and make the diagnosis process more reproducible [50].

## **2.6 Stages in CAD**

In a Computer-aided diagnosis system for ultrasound images, there are four stages as shown in Figure 2.9.

### **2.6.1 Pre-processing**

This stage is used to enhance the ultrasound image and to reduce noises without eliminating important features in the image.

### **2.6.2 Segmentation**

This state is used to find non-overlapping segments that can be distinguished from the background. Those segments are believed to be the lesions in interest.

### **2.6.3 Feature extraction**

In this stage, features for each segment identified in previous stage are extracted for classification purposes. These features will be used to distinguish benign from malignant in classification stage.

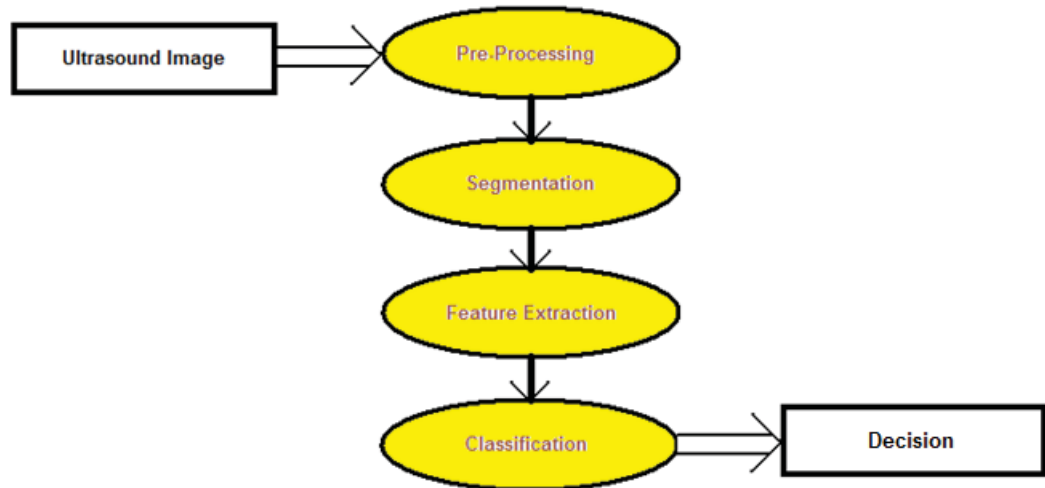


Figure 2.9: Stages in CAD

#### 2.6.4 Classification

In this final stage, lesions are categorized into groups such as benign or malignant. Several classification methods can be used in this stage such as linear discriminant analysis (LDA), support vector machine (SVM) and artificial neural network (ANN).

# Chapter 3

## Literature survey

### 3.1 State-of-the-art CAD systems

Many research has been done in recent years and not many methods have been proposed to automate detection of breast cancer.

A method is proposed by Yap [145] that uniquely combines histogram equalization as a preprocessing stage and then uses hybrid filtering, multifractal analysis, thresholding segmentation, and a rule-based approach in fully automated ROI labeling as shown in as shown in Figure 3.1.

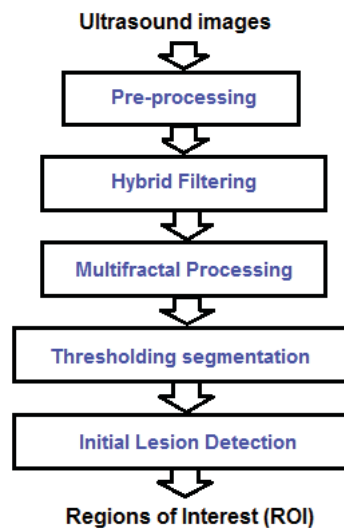


Figure 3.1: Fully automated ROI labelling system

The proposed method is able to very accurately label most lesions, with its best performance being the identification of malignant lesions (90%) and its worst being the identification of fibroadenomas (77.59%). It appears that even by using Hybrid Filtering and Multifractal Processing, the accuracy of the result to identify fibroadenomas is not very high. It appears that noise and shadowing in the images still prevents high accuracy identifying fibroadenomas.

Another method was introduced by Ikedo et al. [51] that uses a bilateral subtraction technique to reduce false positives in mass candidate regions detected by detection scheme for whole breast ultrasound images. It was found that the bilateral subtraction technique could reduce false positives effectively. In this technique, Normal left and right breasts on same subject are architectural symmetry. This method is based on the symmetrical features in both breasts. This is used by radiologists as a useful tool to interpret ultrasound images. Even if there is such a region like a mass, the region is classified normal tissue if same position in the other breast image has similar feature region. This method uses this feature to reduce false positives. The method involves (1) image feature extraction; (2) registration of bilateral breasts; and (3) reduction of false positives. This method removes 67.3% of false positives but requires more improvements. It appears the accuracy of the system can be improved by employing a better pre-processing technique for noise and shadow removal.

Another method was proposed by Moon et al. [91] that uses speckle features of automated breast ultrasound images (ABUS). The ABUS images of 147 pathologically proven breast masses (76 benign and 71 malignant cases) were used. For each mass, a volume of interest (VOI) was cropped to define the tumor area, and the average number of speckle pixels within a VOI was calculated. In addition, first-order and second-order statistical analyses of the speckle pixels were used to quantify the information of gray-level distributions and the spatial relations among the pixels. Receiver operating characteristic curve analysis was used to evaluate the performance. It achieves the accuracy of 84.4%. The performance indices of the speckle features were comparable to the performance indices of the morphological features, which include shape and ellipse-fitting features. Accuracy of the system is not ideal and therefore could be improved. Addition of morphological and texture features could improve the accuracy of the system.

In the next sections state-of-the-art methods for each stage in a CAD system are

studied. We identified advantages and disadvantages of each method and tried to overcome the disadvantages by proposing new methods.

## 3.2 Pre-processing

Ultrasound images are usually deteriorated by noise because of various sources of interferences and other phenomena. The noise usually appears as bright and dark spots and called Speckle, which obscures fine details and makes it difficult to detect low-contrast lesions. Speckle noise occurrence is often undesirable, as it does make it difficult to interpret the lesions and diagnosis. Thus in a computerized system for detection of ultrasound images, pre-processing to eliminate the noise is an important stage [51, 91, 42].

In the past years a lot of image enhancement algorithms have been introduced. They usually belong to two categories: spatial domain- and transform-domain-based. The spatial domain algorithms include image operations on a whole image or a local region based on the image statistics. This category includes methods such as histogram equalization, image averaging, sharpening of images using edge detection and morphology operators, and nonlinear median filtering [11]. In transform-domain-based algorithms, operations are performed in the transform domain. This category includes methods such as in the Fourier and wavelet domain. The frequency transform methods facilitate the extraction of certain image features that cannot be derived from the spatial domain [107].

Image enhancement algorithms use mathematics to improve the quality of a given image. The result is another image that contains certain features in a manner that is better in some sense as compared to their appearance in the original image.

A method for speckle reduction of ultrasonic images was implemented in Matlab [94] based on median filtering, Wiener filtering, and Wavelet transform methods. Median filter is a nonlinear filter that is widely used to replace the original grey level of a pixel by the median of the grey values of pixels in a specific neighborhood. Another name for median filter is order specific filter because it is based on statistics related to ordering of the elements rather than taking the mean. This method is extremely popular and works well for reducing noise without blurring edges of the image [125]. The noise-reducing effect of the median filter depends on two factors: the



spatial extent of the neighborhood and the number of pixels involved in the median calculation.

Because noises can be easily identified in frequency domain, filtering using frequency domain is much easier than filtering in spatial domain. For example, when an image is transformed into the Fourier domain, it is known that low frequency components correspond to smooth regions or blurred structures of the image, and high-frequency components correspond to image details, edges, and noises. By knowing that, we can design filters according to image frequency components to remove undesirable noises [51]. Low-pass filtering will usually smooth images by attenuating high-frequency components, and high-pass filtering will emphasize the image edges or sharp details by attenuating low-frequency components. The Wiener filter is an optimal filter derived under a minimum of mean-squared error criteria [89] but has some limitations.

Another method to represent images is wavelets. A wavelet is a wave-like oscillation with amplitude that starts out at zero, increases, and then decreases back to zero. It can typically be visualized as a "brief oscillation" like one might see recorded by a seismograph or heart monitor. They can be used for analysis of multi-scale image structures. Wavelet functions are distinguished from other transformations such as Fourier transform because they not only dissect signals into their component frequencies but also vary the scale at which the component frequencies are analyzed. As a result, wavelets are exceptionally suited for applications such as data compression, noise reduction, and singularity detection in signals.

Wavelets have been used widely to enhance medical images including ultrasound images. Wavelet de-noising involves three steps: (1) Compute the DWT (discrete wavelet transform) of the image; (2) Threshold details wavelet coefficients; (3) Compute the IDWT (inverse discrete wavelet transform) to obtain the de-noised estimate. The main idea of using this method is to separate signal from noise.

How to choose the wavelet filter is based on the signal itself. Signals have different characteristics and are coming from different sources. For example, for ultrasound images, it is not clear what wavelet filter is the best. The problem is to represent typical signals with a small number of convenient computable functions [85].

Another method (called SRI) of speckle reduction was introduced by Ahn et al. [6]. The algorithm is based on Figure 3.2. In the Analyze phase, the image is examined

pixel-by-pixel and classified as Mostly Speckle or Mostly Feature. This classification is performed by examining the relative difference between neighboring pixel values and determining whether the grey-scale variations have a sharp difference, follow a trend, or are random in nature. It claims to have better edge detection and uniform grey-scale output. It is also said that it enhances the overall quality of the image without losing the features. SRI, or Speckle Reduction Imaging, is the first real-time algorithm that provides a significant reduction in speckle without the disadvantages that have plagued implementations to date. The adaptive nature of the SRI algorithm allows it to smooth regions where no feature, or edges, appear and maintain or enhance edges and borders. It has been shown that SRI increases contrast resolution by increasing the signal to noise ratio. Lastly, the algorithm does not eliminate any information, so diagnostic criteria are preserved. These image quality improvements will help to improve consistency in diagnosis, reduce patient and operator dependence and may ultimately improve diagnostic accuracy and confidence and increase patient throughput. SRI methods may also enable computer aided diagnostic techniques.

Several methods have been introduced to use angular compounding to reduce shadows in ultrasound images. In all the methods, ultrasound scans at each insonification angle have simply been regarded as relatively independent estimates, which can be averaged to increase the information content. One method introduced by Treece et al. [132] goes above just averaging, where various forms of median and maximum filter is also investigated. It is possible to combine two approaches and use insonification from variety of known angles to deduce the attenuation, rather than simply averaging results from each angle. It is also possible to calculate lateral variations in attenuation in a sample from the single envelope of a pair of scans from equal and opposite steered angles. This information then can be used to provide a compounded backscatter image free from shadows and enhancements.

Despite all of the noise reduction techniques that have been introduced, one study suggested that Speckle reduction imaging of breast ultrasound does not improve the diagnostic performance of morphology-based CAD System [140]. In this study one hundred ten patients with pathologically proven breast lesions were enrolled consecutively from April 2008 to October 2008. SRI (Speckle Reduction Imaging) and non-SRI ultrasound images were both obtained at the same examination for each patient. The regions of interest were manually sketched by an experienced physician

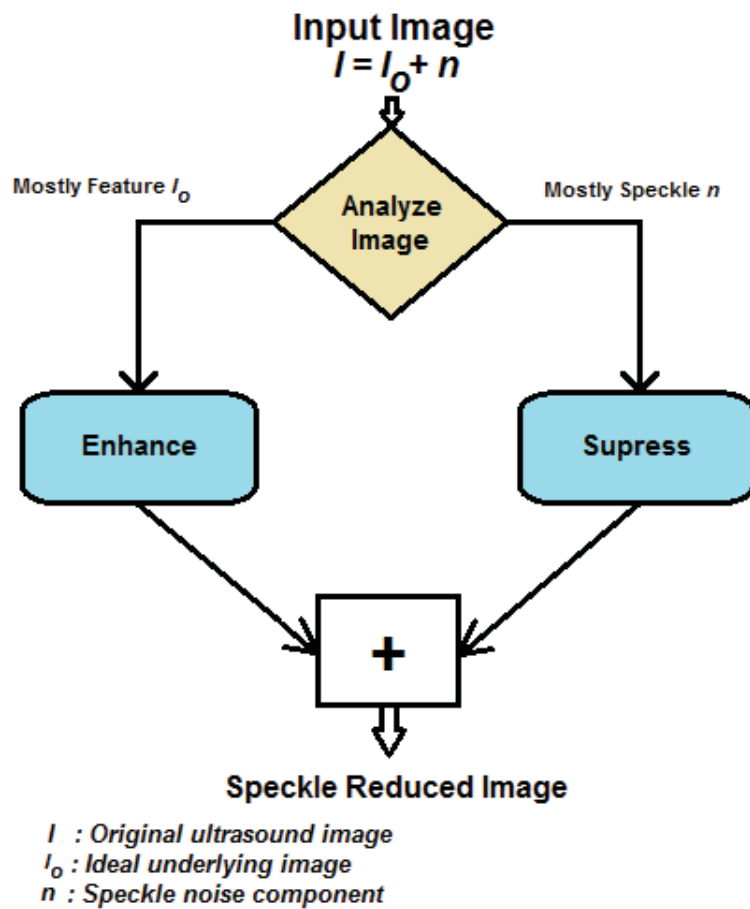


Figure 3.2: Speckle reduction

without histological information. Nineteen practical morphologic features from the extracted contour were calculated and a support vector machine classifier identified the breast tumour as benign or malignant. Conventional binomial receiver operating characteristics curve analysis was used to represent the diagnostic performance of both SRI and non-SRI. Between SRI and non-SRI methods, there were no significant differences in the area under the receiver operating characteristics curve (z-value: 0.82 versus 0.81), the sensitivity (78.9% versus 84.2%), and the specificity (73.6% versus 70.8%).

## 3.3 Segmentation

There are several segmentation methods that were applied to breast ultrasound images. Here, we are going to review different segmentation methods used in breast ultrasound images and discuss the advantage and disadvantage of each of them [140, 110].

### 3.3.1 Histogram thresholding

Simple histogram thresholding [152] can find the preliminary lesion boundary. In a histogram thresholding method, an intensity threshold is chosen at the valley of the image histogram to separate the image into background and foreground. The oversimplified approach in these methods results in imprecise generation of boundaries. They are also very sensitive to noise. But they can definitely be used as intermediate step to provide a rough contour or can be combined with post-processing procedures such as morphological operations [62], disk expansion [56] and Bayesian neural network [21, 148, 32].

As an example in Wu et al. [140] and Yu and Acton [152], a 44 median filter was used to reduce noise in the regions of interest (ROI). Then, a 33 unsharp filter was constructed using the negative of a two-dimensional Laplacian filter to enhance the contrast between object and background. At last, the ROIs were converted to a binary image by thresholding and selected nodules boundary pixels were obtained using morphologic operations. The algorithm determines breast nodule malignancy using digital image processing and ANN based on multiple sonographic features. The typical accuracy for classifying benign and malignant tumors in US is 91.4% with 92.3% sensitivity (the proportion of actual positives which are correctly identified) and 90.7% specificity (the proportion of negatives which are correctly identified). In addition, the results indicate that 53.3% of biopsies on benign nodules can be avoided with 99.3% sensitivity. This performance of the system is comparable to the clinical study by Stavros in the similar patient populations.

Another method of histogram thresholding is introduced by Kenjiro and Nishimura [65]. The proposed method uses an iterative cluster unification to develop a dendrogram iteratively until two groups of gray levels are obtained. Initially, it assumed that each gray level is assigned to a different cluster. If there are  $K$  gray levels used

in the image, then we can assume there are  $K$  classes,  $C_1, C_2, C_K$ , which gray level  $T_k$  is contained in  $C_k$ , and satisfy  $T_1 < T_2 < \dots < T_K$ . For convenience to describe the parameters, we add  $T_0 = 0$ . Similarity is measured between two adjacent clusters in the histogram to know the closeness between both cluster distributions. The distance measurement between cluster  $A$  and  $B$ ,  $Dist_{AB}$  is using discriminant analysis adapted from the criterion function defined by Otsu. The smaller value of the distance, the better pair to merge. Therefore, the closest pair is determined as the pair that can be merged. Since thresholding algorithm can be generalized to deal with the multi-level threshold problem, we can assume the initial problem as the multi-level threshold problem.

Histogram thresholding uses very simple concept and has a very high performance. The disadvantage for this method is that this method works only for bimodal histograms and is not accurate for ultrasound images. It is also very sensitive to noise [57]. These methods might not be suitable for segmentation of breast ultrasound images because breast ultrasound images are very noisy.

### 3.3.2 Model-based methods

These methods perform well with noise present in the ultrasound images and seem to be very stable. Commonly used models are level set [Zaina2006], active contours [92, 19] and Markov random fields [83].

The idea in Markov random fields is to fix the problems with conventional segmentation methods based on intensity. Those methods do not work well under speckle noise and intense tissue. Even methods that reduce speckle noise are not working well in boundary preserving [113].

A method is introduced by Yu and Acton [152] that assumes a representative template of a contour is available, and then a physician will select a slice, call it  $p$  and will manually deform the template with the mouse. The result of this will be an adjusted template. The adjusted contour will have center  $(C_x^a(p), C_y^a(p))$  and contour vectors  $\rho^a(p)$  and  $\theta^a(p)$ . The model will refine the adjusted template in the current slice, which is unsupervised. Then the model automatically detects the contours for the rest of the slices within the volume data. The summary of the procedure is shown in Figure 3.3.

Lihua et al. [77] proposes a level set maximum likelihood method to achieve a

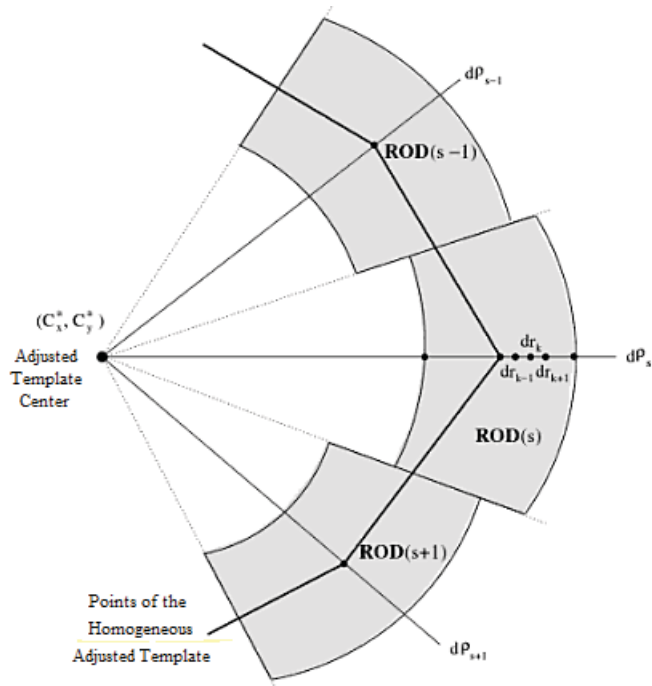


Figure 3.3: Detection of contours in slices(taken from [152])

maximum likelihood segmentation of the target. The Rayleigh probability distribution was used to model grey level behavior of ultrasound images. A partial differential equation-based flow was derived as the steepest descent of an energy function taking into account the density probability distribution of the gray levels, as well as smoothness constraints. A level set formulation for the associated flow was derived to search the minimal value of the model. Finally, the image was segmented according to the minimum energy.

Liao et al. [76] proposes a novel level set-based active contour model. It is argued that because of the low signal/noise ratio, low contrast and blurry boundaries, segmentation of ultrasound images is a challenging task. Thus a novel level set-based active contour model is proposed for breast ultrasound image segmentation. The first step is to formulate an energy function based on the differences between the actual and estimated probability densities of the intensities of the regions in ultrasound images. The probability densities are calculated directly. For calculating the estimated probability densities, the probability density estimation method and background knowledge are utilized. The energy function is formulated with level set approach, and a partial differential equation is derived for finding the minimum of

the energy function. For performing numerical computation, the derived partial differential equation is approximated by the central difference and non-re-initialization approach. The result shows that the proposed method performs well, is robust and is reliably.

Most of model based methods are not sensitive to noise in ultrasound images and they are robust. Disadvantages of these methods are that they are very time consuming to run and also some of them do not work well under speckle noises. Also they all require pre-labelled region of interest (ROI) or initial contour. Because of the noisy nature of breast ultrasound images, these methods might not be a good choice for segmentation.

### 3.3.3 Machine learning methods

Machines learning methods are widely used in image classification. Machine learning is a branch of artificial intelligence that uses learning technique from some generally unknown probability distribution. Then the system predicts the result based on a set of input feature and based on the experience. Example of classifiers are neural networks and support vector machines.

Dokur and Olmez [30] proposes a segmentation method based on neural network. Images are divided into blocks of squares. Features are extracted from each block using discrete cosine transform (DCT). After that, a three-layer hybrid neural network is trained to classify the blocks into background and foreground.

Reference Lui et al. [82] uses a support vector machine (SVM) with a radial basis function kernel to classify different patterns. In this method a window of size of 15x15 is selected and is ran over the image. If the central point of the running window falls inside a circular lesion, then the training pattern is labeled as positive, otherwise it is labeled as negative. For the training purposes, several positive patterns and negative patterns were extracted from the training set. The result shows that this method performs better when the training set is larger.

A system is proposed by Ulagamuthalvi and Sridharan [135] that applies the co-occurrence matrix features and gray level run-length features for identifying the seed point for given ultrasound liver images. After the detection of automated seed point, segmentation of the image is done by applying the region growing algorithm using gray space map and Otsu algorithm for segmenting the ultrasound image. These

co-occurrence matrix features and the run length also used for the classification of the ultrasound images. The algorithm of region growing is very simple. The seed gray level is computed:  $U$ , then it looks for structures which have the same gray level than the seed overlapping the seed position. At the second iteration, it looks for structures having a small gray level difference from the seed. In other words a set of gray levels from  $U-D$  to  $U+D$  is defined. Then those structures which overlap the seed position are kept. In each iteration, the difference  $D$  is increased by 1. In this way structures which are closed from a spatial AND intensity point of view to the seed are highlighted with higher values. In new image if we are far spatially and from an intensity point of view from the seed, the lower intensity is labelled. The resulted image is Gray Space map of image. For segmentation, the maximum area variation is found in which means that from this intensity to 0 we are sure that this is not the ROI. Then the histogram from MAX to 0 is cut. After that, the threshold from MAX to the highest intensity is found which separates the uncertainty area from the ROI. This is simply done using the well-known Otsu thresholding method. This is a parameter free thresholding technique which maximizes the inter-class variance. It is interesting to observe that the Otsu method is more accurate in cutting into two classes. Otsu also takes care to get compact clusters using the inter-class variance.

Shan et al. [119] introduces a segmentation method that utilizes a novel phase feature to improve the image quality, and a novel neutrosophic clustering approach to detect the accurate lesion boundary. First, a region of interest is generated to cut off complex background. After speckle reduction, an enhancement algorithm based on phase in max-energy orientation (PMO) is developed to further improve the image quality. The PMO is a newly proposed 2D phase feature obtained by filtering the image in the frequency domain and calculating the phase accumulation in the orientation with maximum energy. Finally, the authors propose a novel clustering approach called neutrosophic l-means (NLM) to detect the lesion boundary. NLM is a generalized clustering method that can be used to solve other clustering problems as well. In this paper, NLM is used to segment images with vague boundaries, and to deal with uncertainty better. To evaluate the performance of the proposed method, the authors compare it with the traditional fuzzy c-means clustering, active contour, level set, and watershed-based segmentation methods, using a common database. Radiologist's manual delineations are used as the golden standards. The proposed method



generates the most similar boundaries to the radiologist’s manual delineations (TP rate is 92.4%, FP rate is 7.2%), which outperforms the other mentioned segmentation methods.

By using machine learning methods we can incorporate different lesion characteristics using feature extraction. But the disadvantage is that these methods require long training time and we might face over-training problem. Also the test images should come from the training images. Another disadvantage is that they are machine dependent, meaning that we can get different results based on different type of sonographic machines.

### 3.4 Feature extraction

After segmentation, we need to find the features in the regions to be able to categorize the lesions into malignant or benign categories. In the diagnosis of breast cancer, a mass is regarded as an important criterion. Features of the mass playing a significant role in breast cancer diagnosis include shape, boundary, branch, internal structures, and the micro calcifications. For example, when a doctor observes a mass in an ultrasound image, which usually is the darkest area of the image, the first thing he does is to see if the mass is in irregular shape and has branched. If the mass is branched or if the mass has irregular shape, with sharp edges, or if the height of the mass is not in synch with the width, then the mass is considered suspicious for carcinoma. Figure 3.4 shows a mass that is both branched and is in irregular shape.

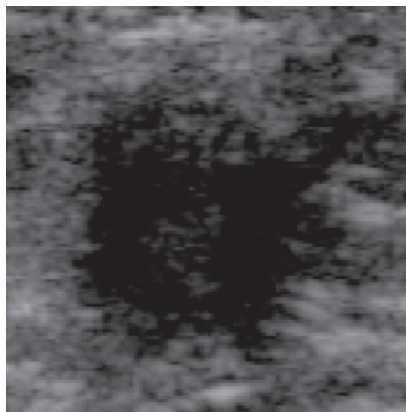


Figure 3.4: A mass with irregular shape and with branches

### 3.4.1 Morphological features

The following geometrical features are extracted from ultrasound images:

- Perimeter
- Area
- NSPD (number of substantial protuberances and depressions)
- LI (lobulation index)
- ENC (elliptic-normalized circumference)
- ENS (elliptic-normalized skeleton)
- LS Ratio (long axis to short axis ratio)
- Aspect Ratio
- Roundness
- Solidity
- Convexity
- Extent
- TCA Ratio (tumor area to convex area ratio)
- TEP Ratio (tumor perimeter to ellipse perimeter ratio)
- TEP Difference (difference between tumor perimeter and ellipse perimeter)
- TCP Ratio (tumor perimeter to circle perimeter ratio)
- TCP Difference (difference between tumor perimeter and circle perimeter)
- AP Ratio (area to perimeter ratio)
- Thickness of the wall

### 3.4.2 Texture extraction

Extracting morphological features for classification purposes requires lots of computational time. Although these features result in accurate classification, it is worth it to consider other types of features for this purpose [135]. For extracting texture feature information, there are two primary methodologies. The first class of methods applies a linear transform, filter, or filter bank globally to the image. The local energy of the filter responses represents the local texture feature values. Generally these methods have high computational complexity. The second class of methods divides the whole image into many small non-overlapping pixel blocks, and then applies some transform, such as a wavelet transform, to each block to get the local information. These methods extract texture features for a block of pixels. Both methodologies have the problem of generating texture information for each individual pixel.

Part of the manual diagnosis by a physician is to see the texture of the lesions and decide whether they look suspicious or not. As texture is a very important feature in manual diagnosis, it could be used as part of CAD systems to provide more accurate information. Extracting those features are not very time consuming and combining them with morphological features could give better and more accurate classification results [28, 99, 141, 104].

Singh et al. [121] discusses that extracting texture features are not time consuming and have a very strong discriminatory power for classification. They discuss that because physicians always look at the texture of the mass in ultrasound images, that is a very good indication that these types of features are very powerful for diagnosis.

Chen et al. [22] studies several different texture features used to process ultrasound images. These features include BDIP (Block difference of inverse probabilities), 2D normalized auto-covariance coefficients, SGLDM (Spatial gray-level dependence matrices, GLDM (Gray-level difference matrix) and NGTDM (Neighborhood gray-tone difference matrix. After extraction of features, PCA is applied to reduce the dimension. After applying PCA, the study considers all the possible combination texture features and ranks all the possible combinations to extract the best features. Table 3.1 shows the result of the study that selects seven texture features for classification. The accuracy of this method is reported in a range of about 65-84%.

Gomez et al. [40] uses an statistical approach that considers co-occurrence texture

Table 3.1: Selected features by Chen et al. [22] - A: 77 auto-covariance matrix; B: SGLDM; C: GLDM; D: BDIP; E: BVLC; F: NGTDM

Rank	Feature set	$A_z$	std
1	AD	0.9253	0.0196
2	ADE	0.9240	0.0199
3	AEF	0.9209	0.0217
4	ABCF	0.9184	0.0218
5	A	0.9173	0.0206
6	ADF	0.9129	0.0219
7	ACDE	0.9114	0.0250

features. It extracts 22 texture features and ranks them using the mutual information (MI) technique, which is in agreement to minimal-redundancy-maximal-relevance (mRMR) criterion. The final extracted features are: contrast, correlation I, correlation II, cluster prominence, cluster shade, difference variance, information measure of correlation I, information measure of correlation II, and inverse difference moment normalized. The accuracy of the classification based on the selected features is at 83.05%.

Krishnan and Sudhakar [69] proposes a CAD system and eliminates segmentation step in the process. It uses GLRLM texture features for the whole image and uses a classifier to classify lesions into benign and malignant classes. It is concluded that the overall accuracy of the system is 92.91%. The list of features that are extracted in this study is shown in Table 3.2.

Table 3.2: GLRLM features

Rank	Feature
1	Short Run Emphasis
2	Long Run Emphasis
3	Gray Level Non-uniformity
4	Run-length Non-uniformity
5	Run Percentage
6	Low Gray Level Run Emphasis
7	High Gray Level Run Emphasis
8	Short Run Low Gray Level Emphasis
9	Short Run High Gray Level Emphasis
10	Long Run Low Gray Level Emphasis
11	Long Run High Gray Level Emphasis

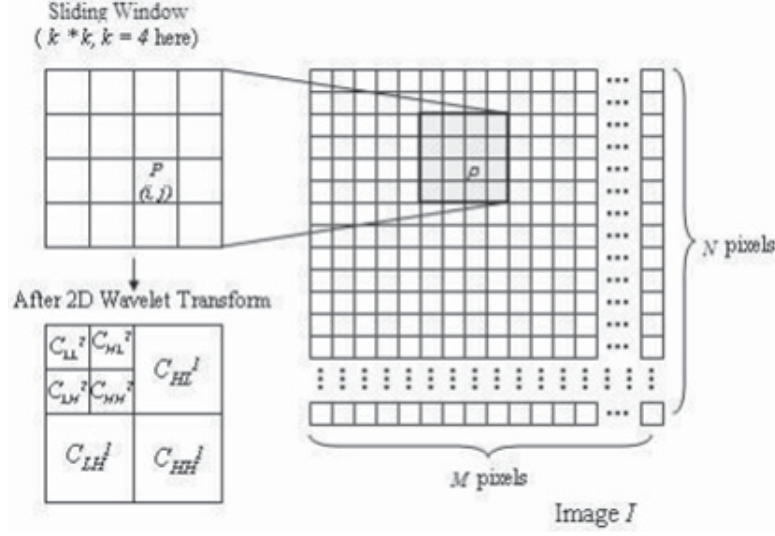


Figure 3.5: Window of some pre-determined size

Zhang et al. [156] proposes a method to extract texture features for each pixel. It applies a window of some pre-determined size,  $k * k$ , to each pixel, as illustrated in Figure 3.5. The centre of the window slides over every pixel and performs the wavelet transform (Daubechies-4 wavelet is used) at each location to determine each pixels texture feature.

Let  $I$  be the whole image,  $M, N$  indicate the width and height of the image (as measured in pixels) respectively, and  $p(i, j)$  be the pixel for which we want to extract the texture information, where  $0 \leq i < M$ ,  $0 \leq j < N$ . Let  $k * k$  be the size of the transform window. Since the texture values are defined in three orientations, the horizontal, vertical and oblique directions, we use  $V_t^h(p)$ ,  $V_t^v(p)$ ,  $V_t^o(p)$  to denote the texture in these directions, respectively. Assume  $C_x^r(x, y)$  denotes the wavelet coefficient in sub-band  $s$  at position  $(x, y)$ , after the  $r^{th}$  level wavelet transform, where  $s \in LL, HL, LH, HH$ ,  $0 \leq x < k$ ,  $0 \leq y < k$  and  $r \leq \log_2 k$ . Then the texture-orientation equations are defined in 1, 2 and 3. This will give us texture feature in three different orientations. This method is a very fast method but does not discuss the accuracy for medical imaging.

$$V_t^h(p(i, j)) = \frac{\left[ \sum_{r=1}^{\log_2 k} r * \left[ \frac{\sqrt{\sum_{x=\frac{k}{2^r}}^{\frac{k}{2^{r-1}}-1} \sum_{y=0}^{\frac{k}{2^r}-1} (C_{HL}^r(x, y))^2}}{k * 2^{-r}} \right] \right]}{\sum_{r=1}^{\log_2 k} r} \quad (1)$$

$$V_t^v(p(i, j)) = \frac{\left[ \sum_{r=1}^{\log_2 k} r * \left[ \frac{\sqrt{\sum_{x=0}^{\frac{k}{2^r}-1} \sum_{y=\frac{k}{2^r}}^{\frac{k}{2^r}-1} (C_{LH}^r(x, y))^2}}{k * 2^{-r}} \right] \right]}{\sum_{r=1}^{\log_2 k} r} \quad (2)$$

$$V_t^o(p(i, j)) = \frac{\left[ \sum_{r=1}^{\log_2 k} r * \left[ \frac{\sqrt{\sum_{x=0}^{\frac{k}{2^r}-1} \sum_{y=\frac{k}{2^r}}^{\frac{k}{2^r}-1} (C_{HH}^r(x, y))^2}}{k * 2^{-r}} \right] \right]}{\sum_{r=1}^{\log_2 k} r} \quad (3)$$

Another method of extracting texture feature is proposed by Srinivasan and Shobha [123]. This is one of the most well-known texture feature, diagonal moment, that is used in different applications. This method is an statistical method that uses joint probability distributions of pairs of pixels. It shows how often each gray level occurs at a pixel located at a fixed geometric position relative to each other pixel, as a function of gray level.

As part of this research, we will find the optimum number and set of features that provide the highest accuracy and performance. We are not able to consider all the combination of the features as it is practically impossible to compute but we are going to try to find a sub-set of features that are highly discriminative.

### 3.5 Feature selection

Two broad categories of optimal feature subset selection have been proposed: filter and wrapper. In filter approaches, features are scored and ranked based on certain statistical criteria and the features with highest ranking values are selected. Frequently used filter methods include t-test, chi-square test, Wilcoxon Mann-Whitney test, mutual information, Pearson correlation coefficients and principal component analysis (PCA) [38].

Filter methods are fast but lack robustness against interactions among features and feature redundancy. In addition, it is not clear how to determine the cut-off point for ranking s to select only truly important features and exclude noise.

In the wrapper approach, feature selection is wrapped in a learning algorithm. The learning algorithm is applied to subsets of features and tested on a hold-out set, and prediction accuracy is used to determine the feature set quality. Generally,

wrapper methods are more effective than filter methods. Since exhaustive search is not computationally feasible, wrapper methods must employ a search algorithm to search for an optimal subset of features.

Sohail et al. [122] combines the concept of between-class distance and within-class divergence. Therefore, the ultimate objective becomes to select a subset of image features that (i) Maximizes the distances among the classes, and (ii) minimizes the divergence within each class. Let  $T_S$  be a labeled training set with  $N_S$  samples. The classes  $\omega_k$  represented by subsets  $T_K \subset T_S$ , each class having  $N_K$  samples  $\sum N_K = N_S$ . Measurement vectors in  $T_S$  (without reference to their class) are denoted by  $z_n$ . Measurement vectors in  $T_K$  (vectors coming from class  $\omega_k$  denoted by  $z_{k,n}$ ). The sample mean of a class and that of the entire training set can be defined respectively as:  $\hat{\mu}_k(T_k) = \frac{1}{N_k} \sum_{n=1}^{N_k} z_{k,n}$  and  $\hat{\mu}_k(T_S) = \frac{1}{N_S} \sum_{n=1}^{N_S} z_n$ . The following formula defines the partial within-class scattered matrix for one specific class:

$$S_k(T_k) = \frac{1}{N_k} \sum_{n=1}^{N_k} (z_{k,n} - \hat{\mu}_k)(z_{k,n} - \hat{\mu}_k)^T \quad (4)$$

The following formula represents the within-class scattered matrix.

$$S_\omega(T_S) = \frac{1}{N_S} \sum_{k=1}^K N_k S_k(T_k) = \frac{1}{N_S} \sum_{k=1}^K \sum_{n=1}^{N_k} (z_{k,n} - \hat{\mu}_k)(z_{k,n} - \hat{\mu}_k)^T \quad (5)$$

The following formula provides the between-class scattered matrix:

$$S_b(T_S) = \frac{1}{N_S} \sum_{k=1}^K N_k (\hat{\mu}_k - \mu)(\hat{\mu}_k - \mu)^T \quad (6)$$

Peng et al. [98] discusses a mutual information (MI) technique that is extensively used for ranking the feature space in agreement to minimal-redundancy-maximal-relevance (mrMR) criterion. The minimal redundancy condition selects the features such that they are mutually exclusive, whereas the maximal relevance condition measures the level of dependency between an individual feature and the target class. Therefore, the whole  $M$ -dimensional feature set is ranked, where the first feature has the largest dependency on the target class. For discrete variables, the MI of two random variables  $x$  and  $y$  could be computed by subtracting the conditional entropy of  $x$  given  $y$  from the marginal entropy of  $x$ .

Haralick and Watson [45] introduces the methods of Sequential Backward Search (SBS) and Sequential Forward Search (SFS). In sequential forward search, first the

best single feature is found. Then among the remaining features, the feature that best discriminates between the classes when used along with already selected features is chosen and added to the list of selected features. The procedure is repeated until the addition of new features increases the error rate or no feature remains to be added. In sequential backward search, the search space is drawn like an ellipse to emphasize the fact that there are fewer states towards the full or empty sets. The main disadvantage of SFS is that it is unable to remove features that become obsolete after the addition of other features.

In sequential backward search, we eliminate the features that have smallest contribution to separation of classes. In this procedure, first all the subsets obtained by removing one of the features are compared and the subset with lowest error rate is selected. Then among the subsets containing one feature lower than the selected subset the best subset in terms of error rate is picked up. The procedure is continuing until the removal of features result in higher rate error rate.

Sequential backward search works best when the optimal feature subset is large, since sequential backward search spends most of its time visiting large subsets. The main limitation of sequential backward search is its inability to re-evaluate the usefulness of a feature after it has been discarded. Figure 3.6 visualizes the two mentioned methods.

Probably the most effective feature selection techniques is sequential backward search and sequential forward search. Basically, in the case of forward search, the algorithm starts with a null feature set and, for each step, the best feature that satisfies some criterion function is included with the current feature set, i. e., one step of the sequential forward selection is performed. The algorithm also verifies the possibility of improvement of the criterion if some feature is excluded. In this case, the worst feature (concerning the criterion) is eliminated from the set, that is, it is performed one step of sequential backward search. Therefore, the sequential forward search proceeds dynamically increasing and decreasing the number of features until the desired is reached [45].

The backward search works analogously, but starting with the full feature set (of size  $m$ ) and performing the search until the desired dimension  $d$  is reached. The time complexity of these methods is  $O(d)$  for sequential forward search and  $O(m - d)$  for sequential backward search.



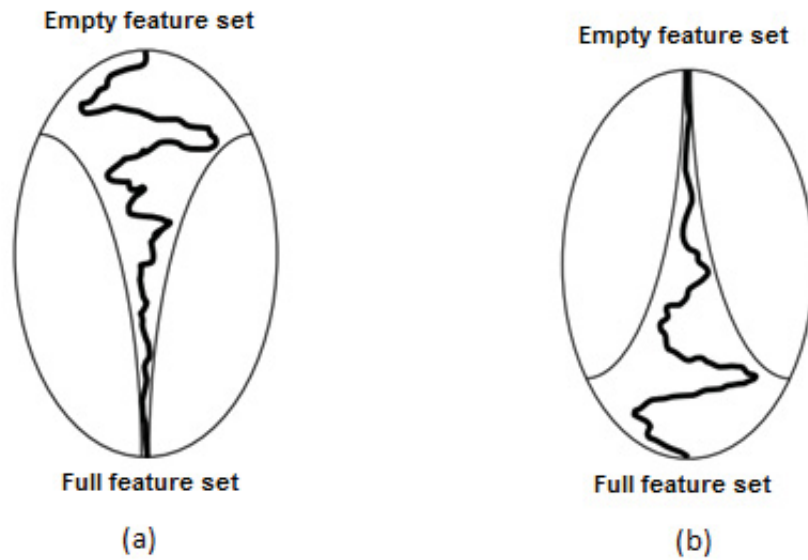


Figure 3.6: (a) Sequential forward search (b) Sequential backward search

Figure 3.7 illustrate the algorithm used for sequential forward search and Figure 3.8 illustrates the algorithm for sequential backward search.

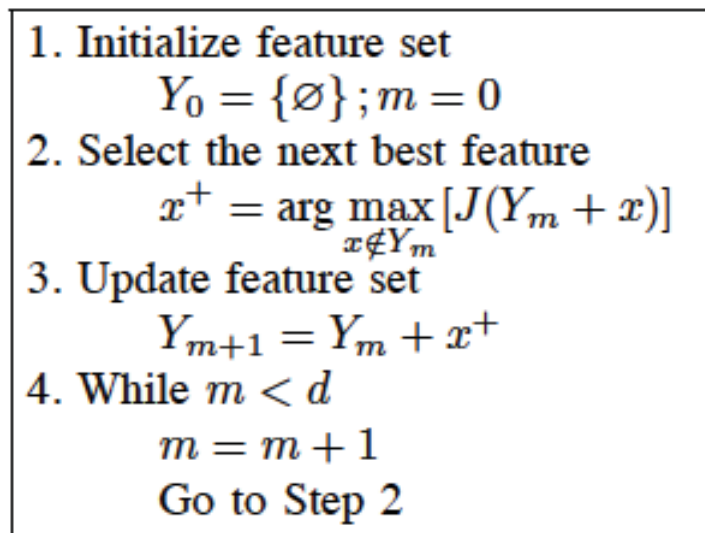


Figure 3.7: Sequential forward search algorithm (taken from [45])

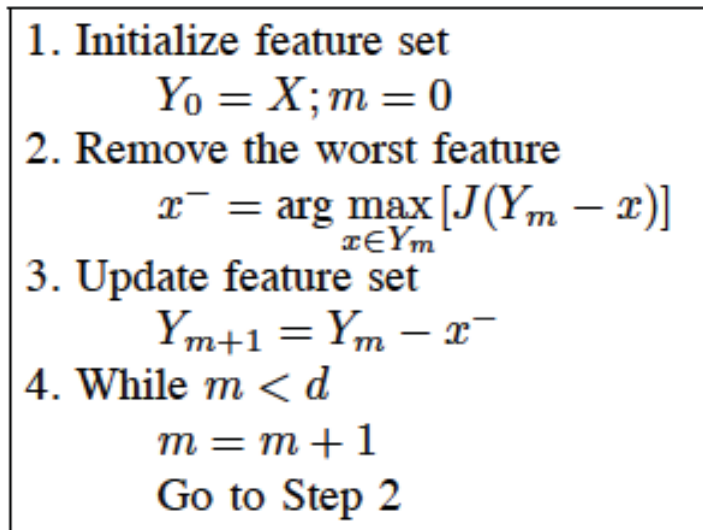


Figure 3.8: Sequential backward search algorithm (taken from [45])

The problem with these sequential approaches is that they gravitate toward local minima due to the inability to re-evaluate the usefulness of features that were previously added or discarded. Therefore they might miss some of the important features. In order to avoid that, in our proposed method, we used a combination of sequential forward search, sequential backward search and mutual information (MI) techniques. This will be discussed in details when we discuss our proposed method.

Lauera et al. [72] introduces a method of Convolutional neural network that is independent of a classifier and extracts the features from handwritten digits. This is a feed-forward neural network that extracts topological features of the image. Although the research is about handwritten digits and this method was not applied to medical images, it could still be beneficial to try this method on a database of breast ultrasound images.

## 3.6 Classification

The main goal of this study is to help radiologists in interpreting ultrasound images. After the features are extracted from the ultrasound image, we need to perform a classification in order to see if the lesion is suspicious based on the extracted features. Image classification is one of classical problems in image processing. The goal of image classification is to predict the categories of the input image using its features. There

are various approaches for solving this problem such as principal component analysis (PCA), Fisher’s linear discriminant (FLD), k nearest neighbor (KNN), adaptive boost (Adaboosted), artificial neural network (NN), support vector machine (SVM), tree classifier, etc. [34, 129].

In statistics, principal components analysis (PCA) is a technique that can be used to simplify a dataset; more formally it is a linear transformation that chooses a new coordinate system for the data set so that the greatest variance by any projection of the data set comes to lie on the first axis (then called the first principal component), the second greatest variance on the second axis, and so on. PCA can be used for reducing dimensionality in a dataset while retaining those characteristics of the dataset that contribute most to its variance by eliminating the later principal components (by a more or less heuristic decision). These characteristics may be the "most important", but this is not necessarily the case, depending on the application [9, 52]. Image space is redundant so the goal of PCA is to reduce the space dimension to get fewer variables for recognition. PCA is also called the Karhunen-Love transform (named after Kari Karhunen and Michel Love) or the Hotelling transform (in honor of Harold Hotelling). PCA has the specialty of being the optimal linear transformation for keeping the subspace that has largest variance. However this comes at the price of greater computational requirement, e.g. if compared to the discrete cosine transform. Unlike other linear transforms, PCA does not have a fixed set of basis vectors. Its basis vectors depend on the data set.

Assuming zero sample mean (the sample mean has been subtracted away from the data set), the principal component  $w_1$  of a dataset  $x$  can be defined as:

$$w_1 = \arg \max_{\|w\|=1} E(W^T x)^2 \quad (7)$$

with the first  $k - 1$  components, the  $k - th$  component can be found by subtracting the first  $k - 1$  principal components from  $x$ :

$$\hat{x}_{k-1} = x - \sum_{i=1}^{k-1} w_i w_i^T x \quad (8)$$

There are two phases in PCA: 1) The training phase and; 2) the recognition phase. In the training phase, training images are selected and PCA variables are calculated. In the recognition phase, the calculated variables are used to recognize an

unidentified image. In this algorithm, the training set is transformed into eigenfaces. Then required variables are calculated for each image in the training set (weights). After weights are calculated, weights for an unknown image are calculated as well. In the last step, the difference between the weights in the training set and the weights for the unknown image are compared and the closest difference based on the threshold  $\theta$  is considered as the recognized image, i.e. the test image is categorized as benign or malignant. Figure 3.9 shows the conversion of training image into eigenfaces.

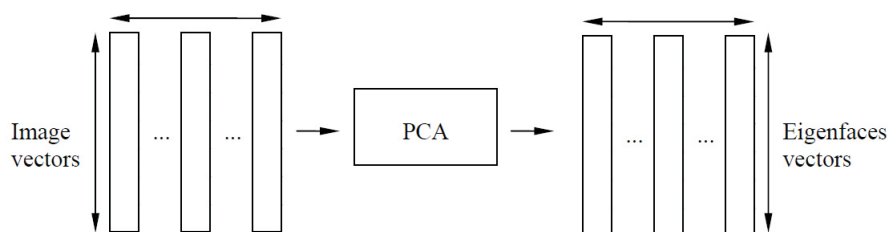


Figure 3.9: Eigenfaces generation process

The Fisherface method was suggested by Belhumeur et al. [9]. Both the Eigenface algorithm and the Fisherface methods project images into a feature space. However, Fisherface uses Fishers Linear Discrimination (FLD), a class-specific method. FLD, on the other hand, tries to find a projection, which separates data clusters. Figure 3.10 illustrates good cluster separation and poor cluster separation.

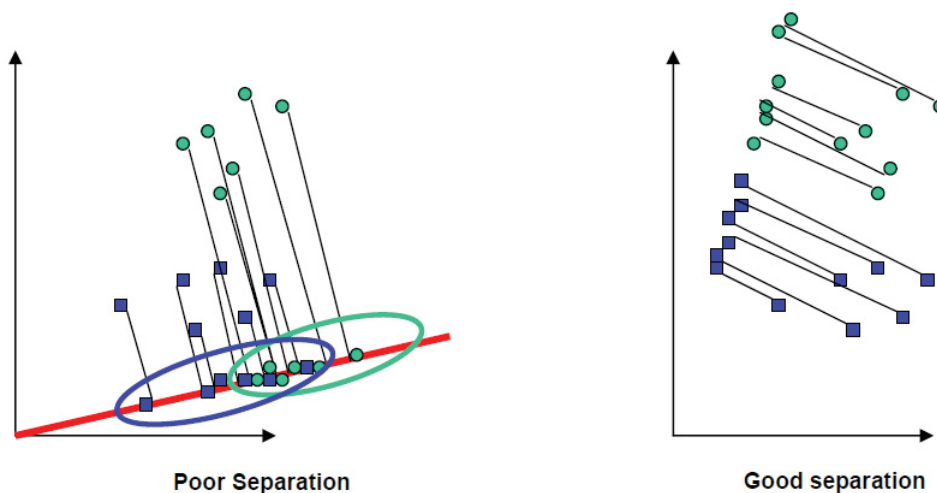


Figure 3.10: Cluster separation

In PCA, projection is best for reconstruction of images from a low dimensional basis. However, the projection does not make use of the betweenclass variance. The projection may not be optimal for discrimination for different classes. In FLD, the projection maximizes the ratio of the between-class scatter to that of the within-class scatter. It tries to reshape the scatter to make it more reliable for classification. The between-class scatter is defined as following:

$$S_B = \sum_{k=1}^c m_i (\Psi_k - \Psi)(\Psi_k - \Psi)^T \quad (9)$$

where  $c$  is the number of classes and  $m_i$  is the number of samples in class  $T_i$ . The within-class scatter matrix is defined as:

$$S_W = \sum_{i=1}^c \sum_{X_k \in C_i} (X_k - \Psi_i)(X_k - \Psi_i)^T \quad (10)$$

The k-NN classifier, a conventional non-parametric, calculates the distance between the feature vector of the input image (unknown class image) and the feature vector of training image dataset. Then, it assigns the input image to the class among its k-NN, where k is an integer.

Adaboost is a good classifier based on the set of weak classifiers. Weak classifiers label a sub-region of an image,  $x$ , as belonging to either the object or clutter class by comparing  $f$  to a threshold  $\theta$ . A weak classifier based on Haar-Like features can be defined as:

$$h_j = \begin{cases} 1 & \text{if } p_j f(x) \leq p_j \theta_j \\ 0 & \text{otherwise.} \end{cases} \quad (11)$$

where  $x$  is a sub-window, and  $\theta$  is a threshold and  $p_j$  indicates the direction of the inequality sign.

AdaBoost (Adaptive Boost) is an iterative learning algorithm to create a "strong" classifier using a training dataset and a "weak" learning algorithm. They are called weak because they are expected to perform only slightly better than a random guesser. At every iterative step, the "weak" classifier with the minimum classification error is selected.

Artificial Neural Network (ANN), a brain-style computational model, has been used for many applications. Researchers have developed various ANNs structure

relevant to their problems. After the network is trained, it can be used for image classification. One of the best known methods in pattern classification and image classification is SVM. It is designed to separate a set of training images into two different classes,  $(x_1, y_1), (x_2, y_2), \dots, (x_n, y_n)$  where  $x_i$  in  $R^d$ ,  $d$ -dimensional feature space, and  $y_i$  in  $-1, +1$ , the class label, with  $i = 1..n$ . SVM builds the optimal separating hyper planes based on a kernel function ( $K$ ). All images, of which feature vector lies on one side of the hyper plane, are belong to class  $-1$  and the others are belong to class  $+1$ . Besides there are some integrated multi techniques model for classifying such as Multi Artificial Neural Network (MANN) for facial expression classification and Multi Classifier Scheme for Adult image classification. ANN model is shown in Figure 3.11.

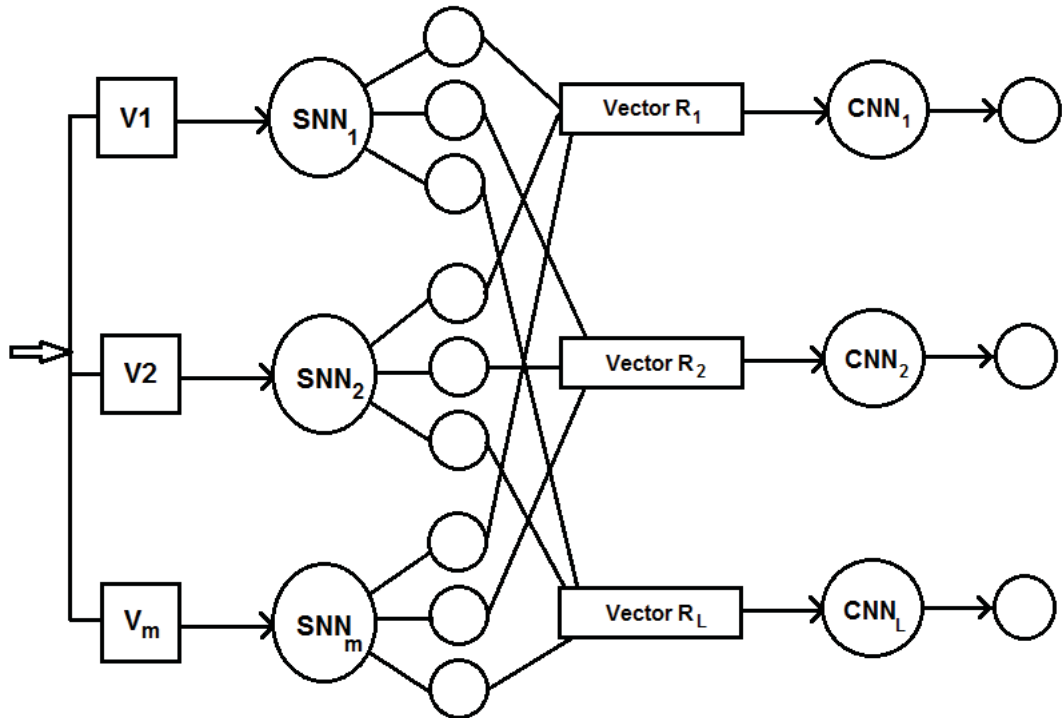


Figure 3.11: Multi Artificial Neural Network model

In Figure 3.11, Multi Artificial Neural Network (MANN), applying for pattern or image classification with parameters  $(m, L)$ , has  $m$  Sub-Neural Network (SNN) and a global frame (GF) consisting  $L$  Component Neural Network (CNN). In particular,  $m$  is the number of feature vectors of image and  $L$  is the number of classes. This model uses many Neural Networks so that the training phrase is complex and long. Besides, it is not suitable in case the number of classes  $L$  is high. MANN is the

2-layers classifier model using Neural Network.

Multi classifier scheme has been proposed for adult image classification with low level feature. This model contains two-layer classifier. Layer 1 uses Support Vector Machine (SVM) classifier and AdaBoost classifier. Layer 2 is the majority base classifier integrating the classified results of layer 1. Multi Classifier Scheme model is shown in Figure 3.12 (CLD: Color Layout Descriptor, SCD: Scalable Color Descriptor, EHD: Edge Histogram Descriptor).

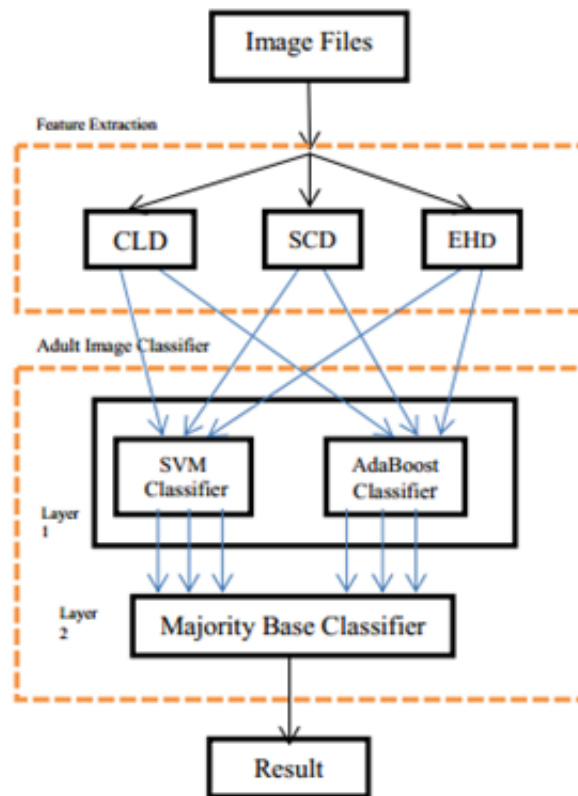


Figure 3.12: Multi Classifier Scheme model (taken from [129])

In Figure 3.12, the Multi Classifier Scheme model is two layers classifier. The output of SVM classifier and AdaBoost classifier has been combined by Majority Base Classifier. This experiment has showed that we need to choose the appropriate classifiers for the feature extraction to increase the precision of image classification. On the other hand, the precision of classification system depends on the feature extraction and the classifier.

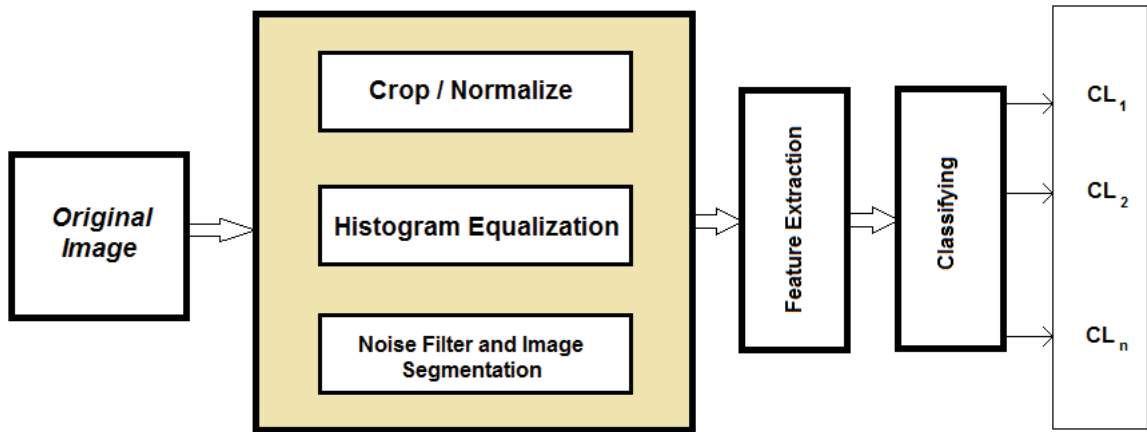


Figure 3.13: Image classifier

In Figure 3.13,  $CL_1, CL_2, \dots, CL_n$  refers to the classes or categories that images are classified into. Step 1, pre-processing, is required before applying any image analysis methods. The images are normalized, performing histogram equalization, applying the noise filter and segmenting. In the step 2, feature extraction, using the suitable transform to decompose an image for example, wavelet, PCA, ICA... The features of images are the input of our classification system. Finally, images are classified into the responsive classes by the suitable techniques (K-NN, NN, SVM ...).

There are various approaches for image classification. Most of classifiers, such as maximum a posterior probability, minimum distance, neural network, decision tree, k-NN and support vector machine, are supervised classifiers making a definitive decision about the test sample class and require a training sample. On the contrary, clustering based algorithm, e.g. K-mean or ISODATA, are unsupervised classifier, and fuzzy-set classifier are soft classification providing more information and potentially a more accurate result. Besides, the knowledge based classification, using knowledge and rules from expert, or generating rules from observed data, is becoming attractive. In recent years, combining of multiple classifiers received considerable attention. Some researchers combine NN classifier, SVM classifier or AdaBoost classifier for image classification [7].

After the images were preprocessed and extracted features, they would present in the large representation space. Thus, they would be projected into the Sub-space in order to analysis easily and reduce dimensions of images feature as illustrated in Figure 3.14



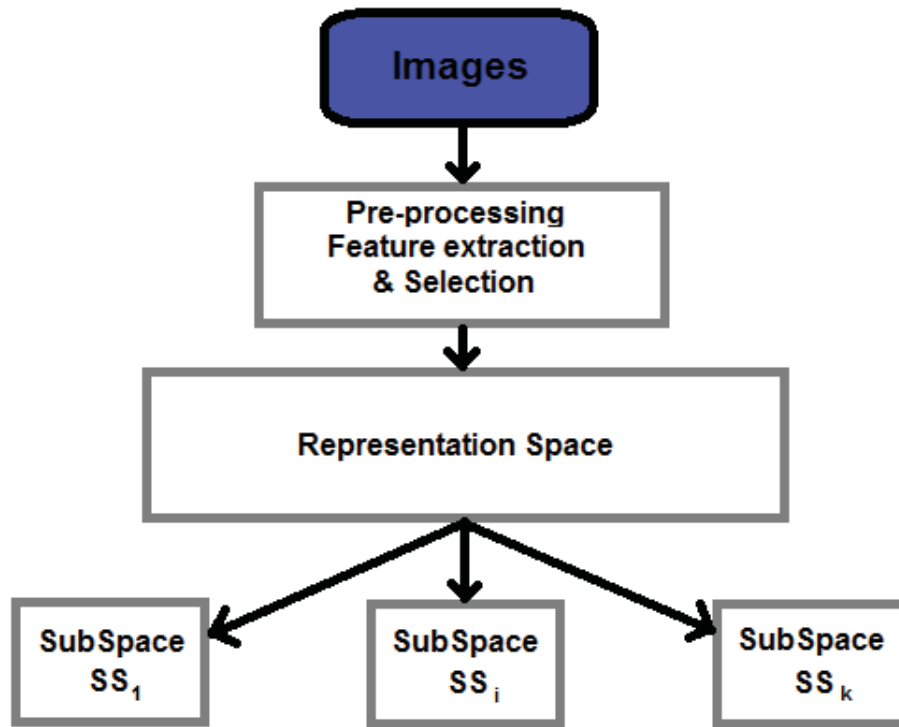


Figure 3.14: Image classifier

### Using ANN to classify each sub-image

In the Figure 3.14, for each sub-space, an image would be extracted the feature vector. This feature vector is the input of ANN for image classification based on a sub-space. Every ANN has 3 layers: input, hidden and output. The number nodes of input layer are equal to the dimension of feature vector, called in. The number nodes of output are equal to  $n$ , the number of classes. We have  $k$  sub-spaces so that there are  $k$  classification results of sub-space, called  $CL_{SS_1}, CL_{SS_2}, \dots, CL_{SS_k}$ . Thus the problem is how to integrate all of those results. The simple integrating way is to calculate the mean value:

$$CL = \frac{1}{k} \sum_{i=1}^k CL_{SS_i} \quad (12)$$

or weighted mean value:

$$CL = \frac{1}{k} \sum_{i=1}^k w_i CL_{SS_i} \quad (13)$$

where  $w_i$  the weight of classification is result of sub-space  $SS_i$  and satisfies:

$$CL = \sum_{i=1}^k w_i = 1 \quad (14)$$

MANN has used Neural Network for identify the weights or importance of the local results. In this research, we suggest that the parameter of the hyperplanes of SVM is instead of the weight  $sw_i$ . Although SVM need to be trained first, the parameter of SVM is adjusted to suitable for the training data in the specific problem.

### SVM and Fuzzy SVM

Image classification is one of classical problems of concern in image processing. The goal of image classification is to predict the categories of the input image using its features. There are various approaches for solving this problem such as k nearest neighbor (KNN), Adaptive boost (AdaBoost), Artificial Neural Network (NN), Support Vector Machine (SVM).

The learning method in SVMs is motivated by statistical learning theory. SVMs are powerful in solving two-class classification problem but some limitations exist in the SVM theory [2]. Traditionally, we know each sample  $x_i, y_i$  in the training dataset belongs to either one class or the other, i.e., the value of  $y_i$  is only assigned to 1 or -1. All samples in training dataset are treated uniformly in the same class during the learning process of SVMs.

In practical classification problems, the effects of the samples in training dataset may be different. Usually, some of samples in training dataset are corrupted by noise, which is introduced during sampling. These samples are called outliers, and usually less important than others. In fact, that we care about the meaningful samples can be classified correctly.

In short, a sample in the training dataset may not completely belong to one class. For example, 90% of the samples belongs to one of the two classes and 10% is meaningless, or we say that the sample belongs to one of two classes with 90% confidence. In other words, each training sample  $x_i, y_i$  is associated with a fuzzy membership  $(0s_i1)$ . This fuzzy membership  $s_i$  indicates the certainty that the sample belongs to one of two classes is  $s_i$ , and the value  $(1-s_i)$  can be regarded as meaningless in the classification problem.

An FSVM (fuzzy SVM) is proposed in Lin and Wang [78]. In FSVM, each sample  $x_i, y_i$  in the training data is weighted by using fuzzy membership function. It becomes as  $x_i, y_i, s_i$ , where  $s_i$  is the fuzzy membership, i.e., the confidence of this sample belong to one of two classes. Then the optimization problem in SVM is reformulated as:

Minimize

$$L(\alpha) = \frac{1}{2} \sum_{i=1}^n \sum_{j=1}^n y_i y_j \alpha_i \alpha_j K(x_i, x_j) - \sum \alpha_i \quad (15)$$

subject to

$$\sum_{i=1}^n y_i \alpha_i = 0, 0 \leq \alpha_i \leq s_i C, i = 1, 2, \dots, n \quad (16)$$

The significant difference of FSVM from SVM is that the sample with smaller fuzzy member  $s_i$  is less important than all other samples in SVM during training. It indicates that the importance of the training sample can be measured by the fuzzy membership  $s_i$ .

A comparison between different classification methods was done by Gab [2] as shown in Table 3.3.

Table 3.3: Comparison between different classification methods to detect suspicious lesions in kidney ultrasound images [2]

	Radiologist	ANN	SVM	FSVM
Accuracy (%)	74.71	88.51	87.36	94.25
Sensitivity (%)	88.89	86.11	86.11	91.67
Specificity (%)	64.71	90.20	88.24	96.08

In Figure 3.15, SVM is used to combine all of ANNs classify results. Here SVM is the solution for identifying the weight of the ANNs result.

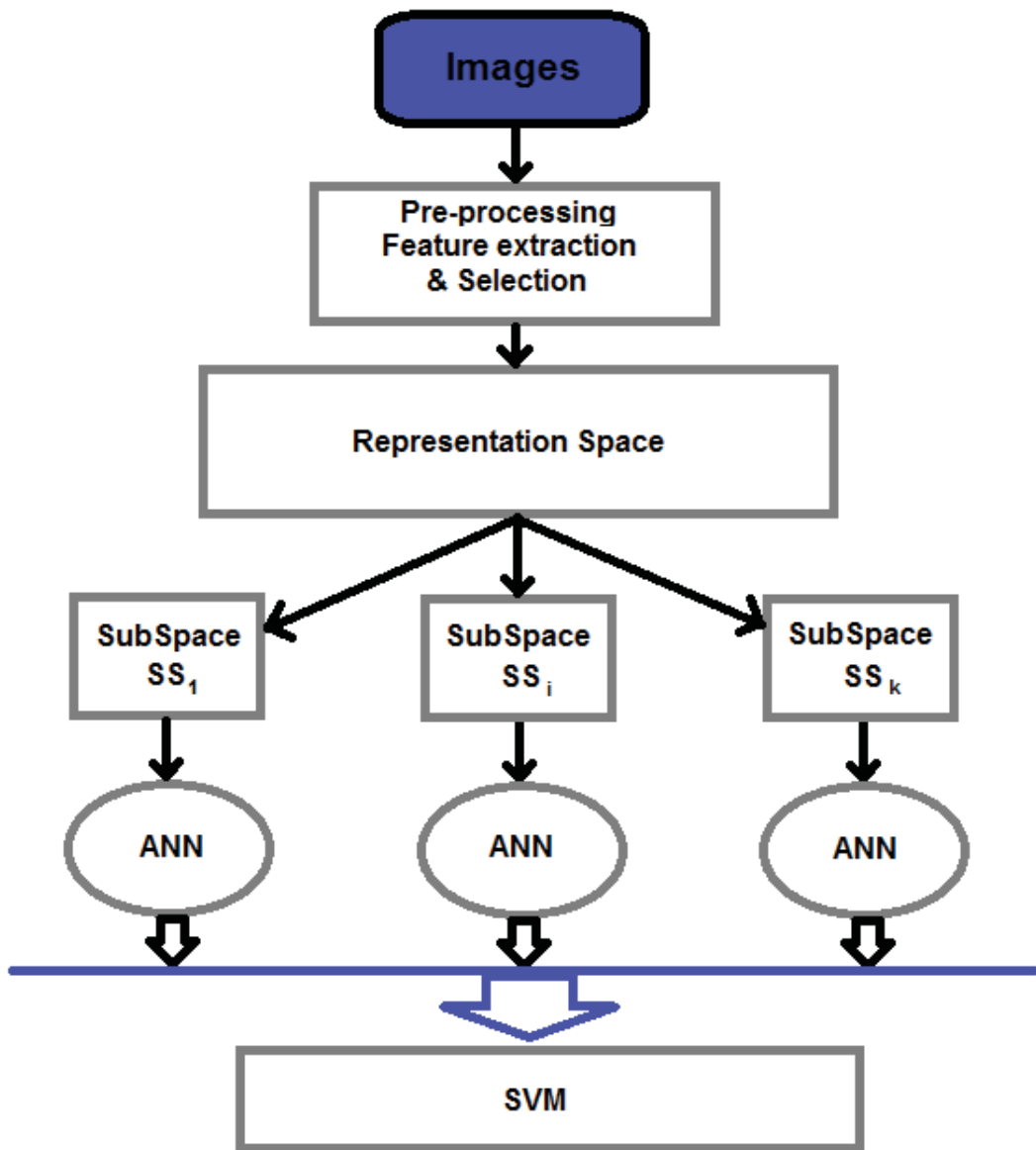


Figure 3.15: Aggregation of sub-images using SVM

## 3.7 Summary

Several pre-processing techniques have been introduced but they have some limitations. Some techniques do not make good separation between foreground and background and some techniques do not remove shadows in ultrasound images. Some of the techniques remove the important information in ultrasound images. These deficiencies require a better pre-processing method to improve the quality of the image while preserving important information in ultrasound images.

In segmentation techniques, some techniques are very sensitive to noise and not suitable for ultrasound images. Some others are very time consuming to run. Some of the methods do not perform well when the training dataset is small. These problems suggest the use of a technique that is not sensitive to noise and is suitable for ultrasound images.

For feature selection, it appears that SFS and SBS are probably the most effective methods for feature selection. These methods require the features to be ranked. In feature ranking methods, MI appears to be one of the best and widely used techniques.

Among classification methods, some do not perform well on medical imaging applications. It appears that ANN and SVM perform better in applications for medical imaging. Also AdaBoost appears to be good as a two class classifier.

# Chapter 4

## Proposed computer system

The detection of structures is crucial for the diagnosis of a vast number of illnesses including breast cancer in breast ultrasound images. Being blurred in nature, with little contrast or immerse in noise, most standard techniques of Digital Image Processing, do not yield optimum results in these images.

The main problem with most of the computer aided diagnosis (CAD) systems is that they are sensitive to noises and noise is unavoidable in ultrasound images. Another problem with some of the CAD methods is that they produce different results for images from different types of sonographic machines.

The mentioned problems suggest using a method to be able to make a clear separation between background and foreground of the ultrasound images. By doing so, the segmentation is expected to be more accurate. The uncertainty to identify the lesions and lesions boundaries suggest the use of fuzzy logic. The use of fuzzy logic that uses both the global and local information and has the ability to enhance the fine details of the ultrasound images is a suitable choice for low-contrast ultrasound images as their details cannot be obtained easily in those images. Also one of the artifacts in ultrasound images is shadowing. A compounding technique could reduce the shadows and made the classification more accurate.

## 4.1 Pre-processing

### 4.1.1 Fuzzy logic for de-noising

The enhancement can be done to better distinguish the background from the actual image. It is logical that the better we can distinguish the background from foreground, the better the final detection of cancer would be.

An interval-valued fuzzy set constitutes that the membership degree of every element to the set is given by a closed subinterval of interval  $[0, 1]$ . The concept of type 2 fuzzy sets was introduced by Zadeh [153, 154] as a generalization of an ordinary fuzzy set. The membership degree of an element to a type 2 fuzzy set is a fuzzy set in  $[0, 1]$ .

An interval type 2 fuzzy set  $\overline{\overline{A}}$  in  $U$  is defined as

$$\overline{\overline{A}} = \{(u, A(u), \mu_u(x)) | u \in U, A(u) \in L([0, 1])\} \quad (17)$$

where  $A(u) = [\underline{A}(u), \overline{A}(u)]$  is a membership function; i.e., a closed subinterval is  $[0, 1]$ , and function  $\mu(x)$  represents the fuzzy set associated with the element  $u \in U$  obtained when  $x$  is within  $[0, 1]$ ;  $\mu_u(x)$  is given in the following way:

$$F(x) = \begin{cases} a & \text{if } \underline{A}(u) \leq x \leq \overline{A}(u) \\ 0 & \text{otherwise.} \end{cases} \quad (18)$$

Sahba et al. [109] proposes fuzzy rules for image enhancement, in which fuzzy rules such as the following have been used:

- IF the pixel does not belong to the object, THEN leave it unchanged.
- IF the pixel belongs to the breast object AND is dark, THEN make it darker.
- IF the pixel belongs to the breast object AND is gray, THEN make it dark.
- IF the pixel belongs to the breast object AND is bright, THEN make it brighter.

The degree of belonging of each pixel to the object is a function of its distance to the central point of the object or the inside of an initial/coarse segment. For initial segment, we used the region growing algorithm proposed by Ulagamuthalvi and Sridharan [135]. The initial segment is required to identify if a pixel belongs to

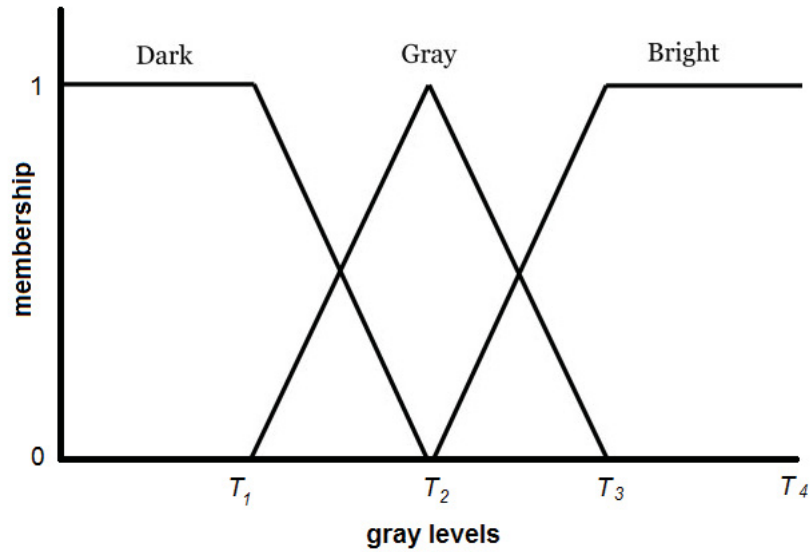


Figure 4.1: Membership functions for input gray level values

the lesion. The main idea of enhancement is to eliminate the noise in the images and enhance the gray levels of selected area (regional contrast enhancement). In this method, each pixel is fuzzyfied depending on its intensity with a membership function that is constructed taking into account the mean level of gray of the surroundings and the position of the selected point. The fuzzy membership function that is used in this research is shown in Figure 4.1.

In Figure 4.1,  $T_4$  is the brightest gray level in the image. For simplicity we used  $T_1 = 25$ ,  $T_2 = 50$  and  $T_3 = 80$ .

In this research, this method has been applied to breast ultrasound images for eliminating unwanted noise. The idea is to map the image space to a fuzzy space using fuzzy rules and then apply segmentation techniques to detect lesions.

### 4.1.2 Compounding and correlation of images

Real time compounding of ultrasound images has been investigated for long time. Special equipments have been designed to perform compounding of ultrasound images from different angles. But despite that, conventional ultrasound still being used [35]. In conventional ultrasound, radiologist investigate the breast from different angles. These images from different angles could be used to get more information about the lesions in breast ultrasound images (i.e. using compounding). This information can



be used to improve the classification results of our proposed system.

Although the application of ultrasound images is usually promising, there are some restrictions due to the physical nature of imaging:

- Image noise is high because of systematic noise in ultrasound images.
- Due to anisotropic resolution in ultrasound images and due to differences in the propagation velocity of sound waves in different types of tissues, the geometric representation of objects is strongly dependent on the angle of insonification.
- Some artifacts like shadowing may hamper a clear delineation of the lesion.

Because of the points mentioned above, ultrasound imaging is an interactive process and requires lots of experience to capture and interpret ultrasound images. Findings in the ultrasound images sometimes are not reproducible and often vary between different interpreters.

The limitation mentioned above might be overcome by considering correlation between images from different angles (i.e. multiple viewing angles all around the breast). The concept is known as Full Angle Spatial Compounding (FASC). When the ultrasound is being performed, the investigator usually moves the transducer around the female breasts to capture images from different angles. The correlation between those images could give more information and makes the investigation easier. The method of capturing images from different angles is illustrated in Figure 4.2.

This method has capability of improving diagnosis for the following reasons:

- As noise is uncorrelated in images from different angles, it will be reduced by using this technique.
- Compound images exhibit an isotropic resolution which is a combination of the axial and lateral resolution of the individual images.
- Shadowing are suppressed because of varying angle of insonification.
- Structures, which cause specular reflection are imaged and delineated in the compound image.

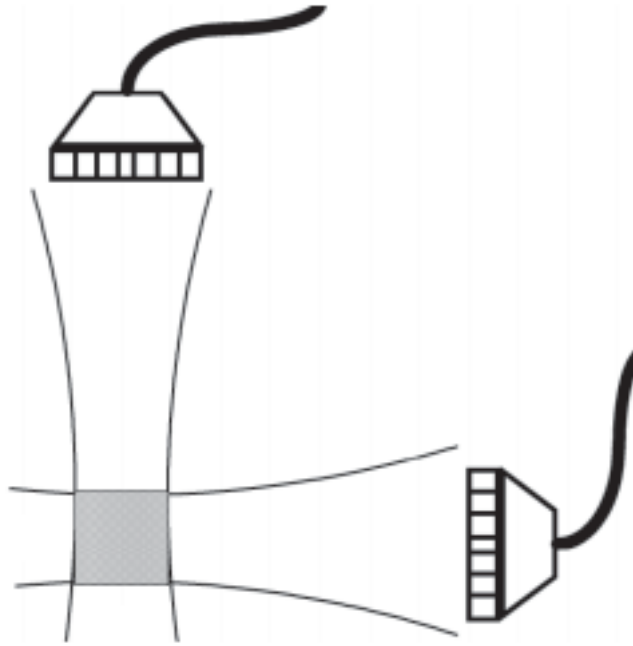


Figure 4.2: An ultrasound transducer is rotated fully around the female breast to acquire data from multiple angles (taken from Techavipoo et al. [128])

### Compounding

Ultrasound images contain many artifacts due to the complex nature of sound transmission and reflection in anatomical structures. Because of the variations in attenuation throughout the image, shadowing and enhancement are happening. This can be compensated in the vertical direction by a set of time-gain sliders which control the gain in horizontal bands across the image. Gain variations in the horizontal direction remain, but they appear as over-compensated bright patches under regions of low attenuation (enhancement) or under-compensated dark patches under regions of high attenuation (shadowing).

In some cases, shadows and enhancements have clinical significance. For instance, this has been demonstrated in detecting liver disease [78] or certain tumors [112]. However, some other cases they can simply be confusing. Especially in 3D data that the visualization planes are not in general along the direction of insonification. In such planes, shadows or enhancements can appear without the corresponding anatomy which generated them.

In any case, it would seem logical to display attenuation effects separately from signal backscatter (or reflection) which is the main component of ultrasound images.

Certainly this would ease the interpretation of ultrasound images, and make downstream processing (for instance segmentation) more reliable. We can display the estimated attenuation as a completely separate image rather than having to infer it from artifacts in an image of ultrasound backscatter.

Several methods have been introduced to use angular compounding. In all the methods, ultrasound scans at each insonification angle have simply been regarded as relatively independent estimates, which can be averaged to increase the information content.

It is possible to combine two approaches and use insonification from variety of known angles to deduce the attenuation, instead of just simply averaging results from each angle. It is also possible to calculate lateral variations in attenuation in a sample from the single envelope of a pair of scans from equal and opposite steered angles. This information then can be used to provide a compounded backscatter image free from shadows and enhancements.

We have applied the mentioned algorithm on ultrasound images consists of three images per patient. Out of the three images per patient, one is obtained from the front, and the other two obtained in 90 degrees angle, opposite to each other [133].

### **Attenuation estimation**

One way to reduce shadowing and enhancing is to estimate the attenuation independently from the backscatter. If we estimate the attenuation at all points in an image, it is going to be very straightforward to adjust the image for this known attenuation and removing the artefact (i.e. shadowing).

One algorithm proposed by Bevan and Sherar [12] deduces attenuation directly from the backscattered signal by assuming that the attenuation is directly proportional to the backscatter. Also it is assumed that the ultrasound pulse has a broadly Gaussian spectrum, and use the shift in centre frequency to estimate attenuation. Both of the mentioned methods require the scattering spectrum of the sample to be the same as in a calibration object.

### **Angular compounding**

In angular compounding the transducer is steered to various angles and the resulting image is averaged. The main benefit of this method is to increase the signal to speckle

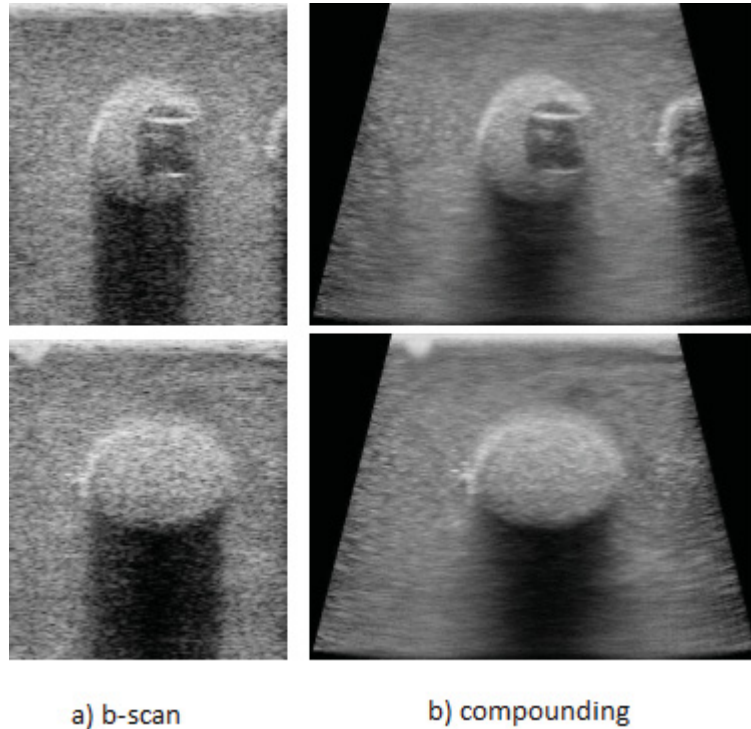


Figure 4.3: B-scan vs. compounding (taken from [132])

ratio and reduce the dependency of reflection from planar interfaces on relative angle to the transducer. But because we know that shadowing and enhancements will always lie in the direction of insonification, angular compounding also has subsidiary effect that these artifacts are blurred by the compounding procedure. Figure 4.3 shows some examples, in which the strength of the shadow is not substantially reduced by compounding, but appearance is different than conventional B-scan.

### **Attenuation and backscatter model**

In the presentation we will follow [132]. In order to simplify the process, two assumptions are made:

- At least over a small range of insonification angles, both the backscatter and attenuation from a particular location are isotropic.
- Effect of attenuation on the center frequency of the ultrasound pulse is small compare to the center frequency.

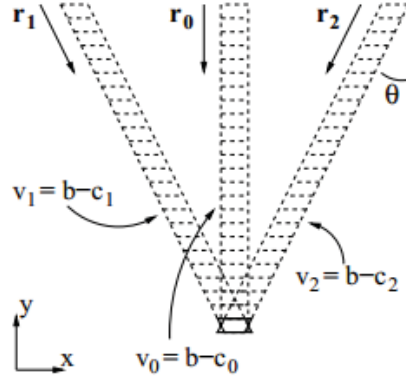


Figure 4.4: Coordinate system for paired angle compounding (taken from [132])

By making the above assumptions, we can model the tissue with two scalar fields,  $b(x, y)$  giving the backscatter coefficient in  $dB$  at  $(x, y)$  and  $a(x, y)$  giving the attenuation coefficient in  $dB/cm$  at the average center frequency of ultrasound pulse in the tissue.

We also assume that the ultrasound pulse is everywhere focused and that the speed of sound is constant in the medium. Now the cumulative attenuation  $c(x, y)$  from the pulse origin  $o$  to the scanned location  $(x, y)$  is twice the line integral of  $a(x, y)$  along this path:

$$c(x, y) = 2 \int_0^{r(x)} a(r, \theta) dr \quad (19)$$

where  $r$  is distance along the insonification direction  $\mathbf{r}$  and  $a(r, \theta)$  is a scatter field expressed in polar coordinates  $r, \theta$ . The signal  $v(x, y)$  (in  $dB$ ) received at the transducer corresponding to the location  $(x, y)$  is

$$v(x, y) = b(x, y) - c(x, y). \quad (20)$$

### Derivation of paired angle compounding

We now can consider a point  $(x, y)$  that is imaged from three different insonification directions at steering angles  $-\theta^\circ, 0^\circ, \theta^\circ$  as shown in Figure 4.4. It has to be said that the underlying backscatter and attenuation coefficients in all three directions are the same. Because the attenuation at a point is the derivative of the cumulative

attenuation along the direction of insonification, then comparing the two equal and opposite angle scans, attenuation  $a$  at a point is defined as:

$$a(x, y) = \nabla c_1(x, y) \cdot \mathbf{r}_1 = \nabla c_2(x, y) \cdot \mathbf{r}_2 \quad (21)$$

where the subscript 1 corresponds to an insonification angle of  $-\theta^\circ$ , subscript 2 to an insonification angle of  $\theta^\circ$  and  $\cdot$  denotes the dot product.  $\mathbf{r}_1$  is a unit vector along the  $-\theta^\circ$  and  $\nabla$  is the gradient operator.

The previous equation implies:

$$\nabla b(x, y) \cdot \mathbf{i} = \frac{1}{2} \nabla (v_2(x, y) + v_1(x, y)) \cdot \mathbf{i} + \frac{1}{2 \tan \theta} \nabla (v_2(x, y) - v_1(x, y)) \cdot \mathbf{j}, \quad (22)$$

where  $\mathbf{i}$  and  $\mathbf{j}$  are unit vectors in the x and y directions, respectively.

Angular compounding is usually performed over more than two angles. We can combine estimates for  $b$  from multiple pairs of angles by taking the weighted average of the difference images before we calculate the gradient. Therefore the final equation for the compounded backscatter image is

$$c_{comp}(x, y) = \int_0^x [\nabla \sum_{\theta}^{| \theta |} [\frac{1}{2 \tan \theta} (v_2(t, y) - v_1(t, y))] \cdot \mathbf{j}] dt + K(y), \quad (23)$$

where  $\sum$  is summation over all the angles involved and  $K(y)$  is undetermined function. Even though  $K$  cannot be determined it is not required to correct shadows in the ultrasound data (we refer reader to [132] for details).

We have applied the mentioned algorithm to the database of ultrasound images which consists of three images per patient. Out of the three images per patient, one is obtained from the front, and the other two are obtained for 90 degrees angle, opposite to each other as shown in Figure 4.5.

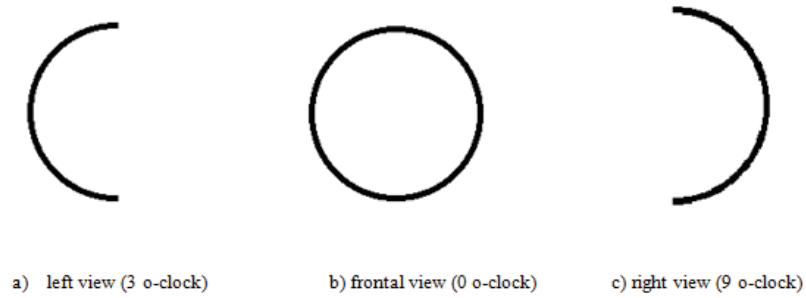


Figure 4.5: Different views of breast

## 4.2 Segmentation

A region growing method for segmentation of ultrasound images by Ulagamuthalvi and Sridharan [135] is proposed. This method applies the co-occurrence matrix features and gray level run-length features for identifying the seed point for given ultrasound liver images. We have implemented the method and ran it against our breast ultrasound images. We used fuzzy method to de-noise our images before applying the method. Using this method, the seed points are not selected correctly in some of the cases. An example is shown in Figure 4.6.

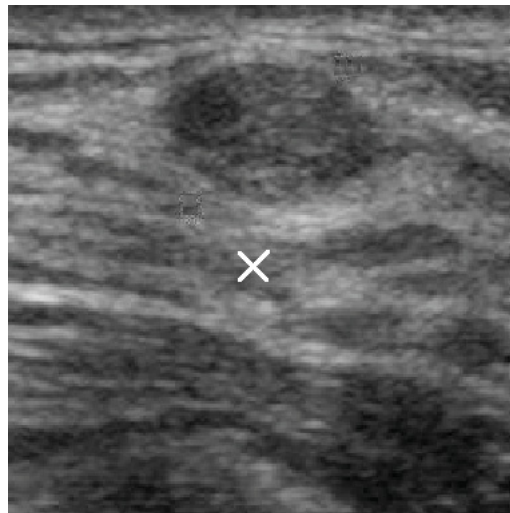


Figure 4.6: Incorrect seed point selection using method by Ulagamuthalvi and Sridharan [135]

The reason for this inaccurate result is the fact that there are other noise areas

in the image that are considered as lesion. Therefore the seed point is not selected correctly.

To overcome that problem, we used a method to identify the regions in the image, remove the noise region and rank the remaining regions based on importance and select the main region of interest [117]. In order to achieve this, we first calculate all the local minimums of the image histogram. Then we need to find a good threshold to separate the lesion from the background. This threshold should be one of the local minimums. We used well-known Otsu thresholding method to achieve this [86]. This is a parameter free thresholding technique which maximizes the inter-class variance. It is interesting to observe that the Otsu method is more accurate in cutting into two classes (foreground and background).

After finding the proper threshold, we then binarize and reverse ultrasound images using that threshold (lesions become white and background become black). An example of binarized images is shown in Figure 4.7.

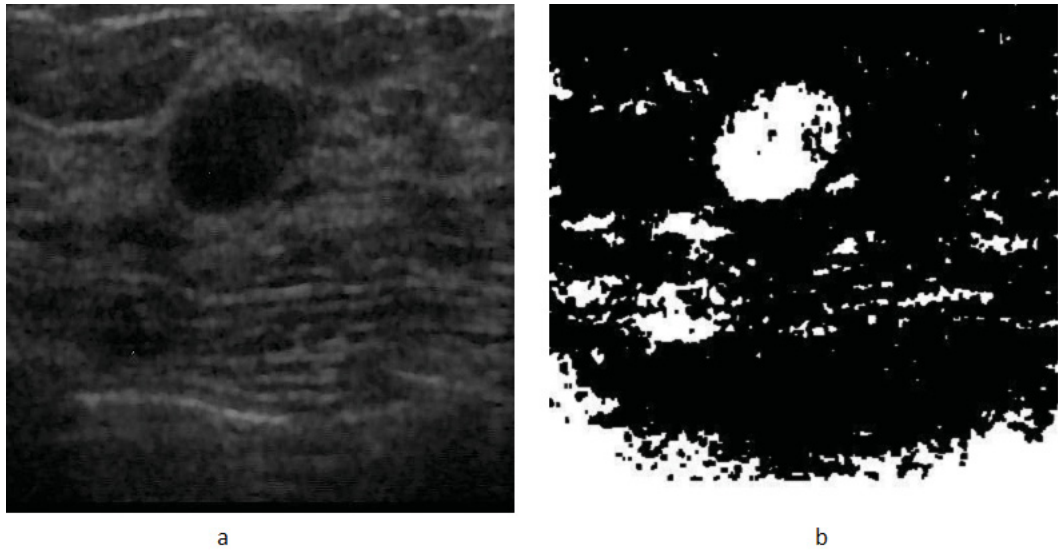


Figure 4.7: a) Original Image b) Binarized image  
(taken from [117])

After binarizing image, we use a center window to evaluate every boundary region. The center window is about 1/2 size of the whole image and centered at the image center. We only leave the regions that have an intersection with the image center window. In cases that no region has intersection with the image center window, we



reduce the size of the window by half and repeat the same procedure. Figure 4.8 illustrates this method.

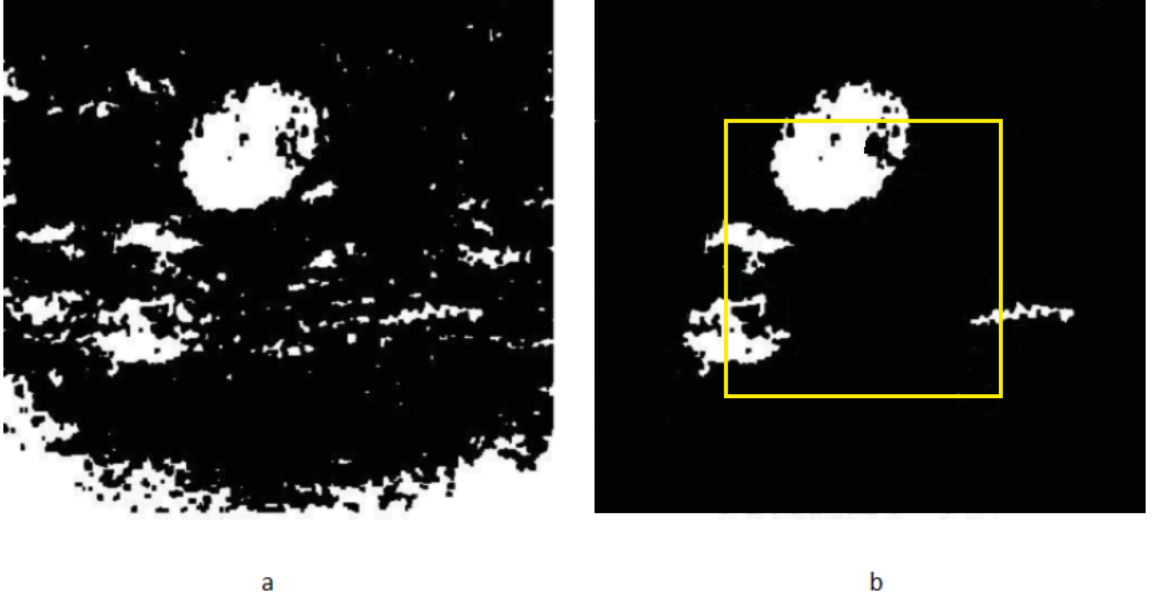


Figure 4.8: a) Binarized image b) After deleting boundary-connected region

We use the following score formula to rank each left region. The one with the highest score is considered as the lesion region.

$$S_n = \frac{\sqrt{Area}}{dis(C_n, C_0) \cdot var(C_n)}, n = 1, \dots, k \quad (24)$$

where  $k$  is the number of regions,  $Area$  is the number of pixels in the region,  $C_n$  is the center of the region,  $C_0$  is the center of the image, and  $var(C_n)$  is the variance of a small circular region centered at  $C_n$ . Figure 4.9 illustrates the selected region.

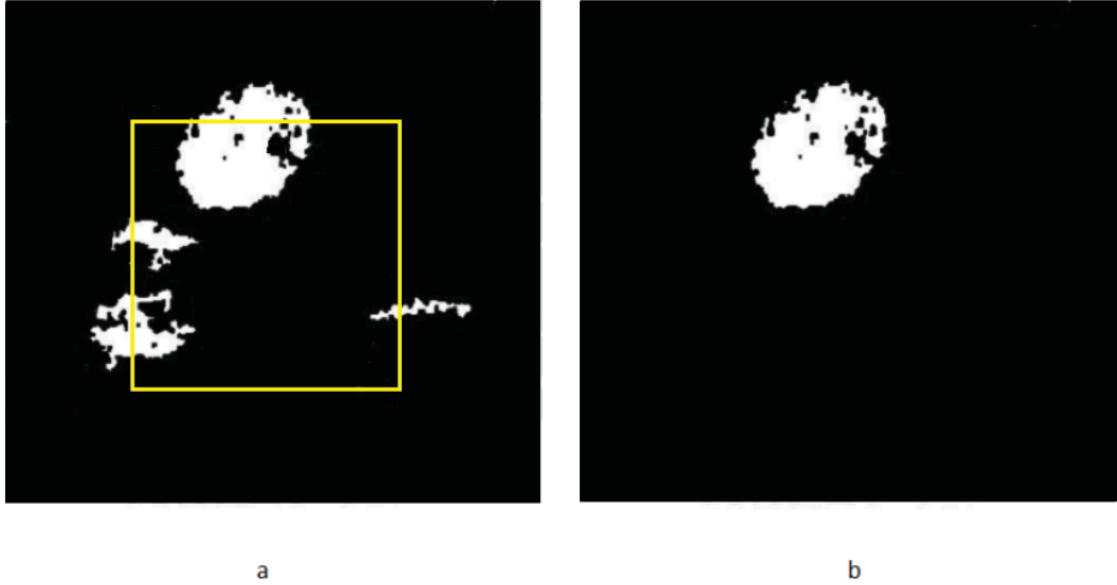


Figure 4.9: a) After deleting boundary-connected region b) Winning region

Now that we identified the winning region, we can select the seed point. To select a seed point, we use a simple approach. Lets consider the minimum rectangle containing winning region  $[x_{min}, x_{max}; y_{min}, y_{max}]$ . In most cases the center of the minimum rectangle could be considered as a seed point. However is some cases that the region shape is irregular, center point might be outside of the lesion. For those cases we can consider  $x_{seed} = \frac{(x_{min}+x_{max})}{2}$  and  $y_{seed} = \{\forall y|(x_{seed}, y) \in lesion\ region\}$

Now that we have identified our seed point, we use the region growing method introduced by Ulagamuthalvi and Sridharan [135] to complete our segmentation process.

The gold standard to define the accuracy of a segmentation method is a physician. The segmentation has to be performed and be verified by a physician in order to conclude if segmentation is done correctly. As it is practically impossible to ask a physician to verify the result of several methods, we relied on existing research in combination with our own experiments.

Shan et al. [119] introduces a novel method based on neutrosophic l-means clustering and compares the method with other state-of-the-art segmentation methods. This method is compared with the state-of-the-art segmentation methods introduced by Madabhushi and Metaxas [83] , Zhang [158] and Liu et al. [79]. Shan et al. [119] claims to outperform other state-of-the-art segmentation methods.

We introduced a new region growing method that seems to be very accurate for segmentation of ultrasound images. Our approach was to run the neutrosophic I-means clustering method introduced by Shan et al. [119] and the region growing method we introduced against our breast ultrasound images database and choose the best performing segmentation method for our experiments. Table 4.1 summarizes the result of our comparison.

Table 4.1: Comparison between proposed segmentation method, region growing method and neurotrophic I-means clustering method

Method	# of patients	Segmented Correctly	Accuracy %
Region growing	80	74	92.50
I-means clustering	80	75	93.75
Proposed method	80	78	97.50

For selection of seed points, we also considered using K-means algorithm to classify ultrasound images into two classes (lesion and none-lesion) [58]. K-Means algorithm is an unsupervised clustering algorithm that classifies the input data points into multiple classes based on their inherent distance from each other. The algorithm assumes that the data features form a vector space and tries to find natural clustering in them. The points are clustered around centroids  $\mu_i \forall i = 1 \dots k$  which are obtained by minimizing the objective:

$$V = \sum_{i=1}^k \sum_{x_j \in S_i} (x_j - \mu_i)^2 \quad (25)$$

where there are  $k$  clusters  $S_i, i = 1, 2, \dots, k$  and  $\mu_i$  is the centroid or mean point of all the points  $x_j \in S_i$ . The algorithm can be summarized as follows:

- Computer the intensity distribution(also called the histogram) of the intensities.
- Initialize the centroids with  $k$  random intensities.
- Repeat the following steps until the cluster labels of the image does not change anymore.
- Cluster the points based on distance of their intensities from the centroid intensities.

$$c^{(i)} := \arg \min_j \|x^{(i)} - \mu_j\|^2 \quad (26)$$

- Compute the new centroid for each of the clusters.

After clustering, we use a center window to evaluate every boundary region. The center window is about 1/2 size of the whole image and centered at the image center. We only leave the regions that have an intersection with the image center window. In cases that no region has intersection with the image center window, we reduce the size of the window by half and repeat the same procedure. Figure 4.10 shows this method.

After removing noise regions, we use the simple approach that was used before to select the seed point. Lets consider the minimum rectangle containing winning region  $[x_{min}, x_{max}; y_{min}, y_{max}]$ . In most cases the center of the minimum rectangle could be considered as a seed point. However is some cases that the region shape is irregular, center point might be outside of the lesion. For those cases we can consider  $x_{seed} = \frac{(x_{min}+x_{max})}{2}$  and  $y_{seed} = \{\forall y|(x_{seed}, y) \in lesion\ region\}$ . Now that we have identified our seed point, we use the region growing method to complete our segmentation process. Table 4.2 shows the comparison between two proposed methods: 1) region growing using binarized image to select seed point 2) region growing using k-means algorithm.

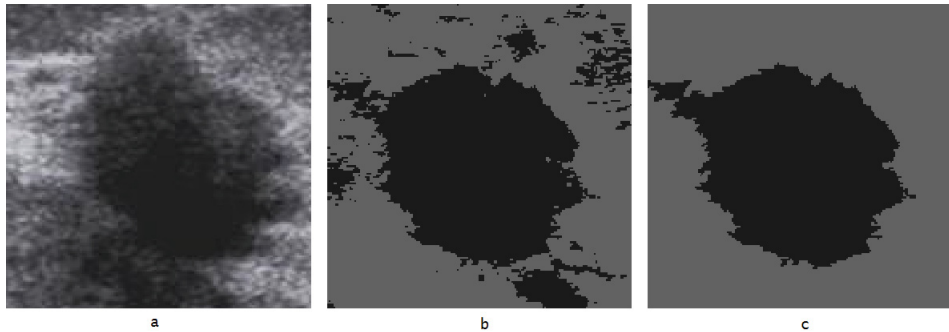


Figure 4.10: a) Original image b) Clustered image c) Winning region

Table 4.2: Comparison between proposed segmentation methods (using binarized image to select seed point and using k-means algorithm to select seed points)

Method	# of patients	Segmented Correctly	Accuracy %
Region growing (k-means)	80	76	95.00
Region growing (binarizing)	80	78	97.50

The comparison shows the proposed method that uses binarized image to select seed point is performing better than using k-means to select seed point.

## 4.3 Feature extraction

### 4.3.1 Morphological features

Below is the list of all morphological features we use for our experiments in this thesis:

- Perimeter. The Perimeter feature represents the length of the tumor perimeter. As malignant tumors usually have irregular shapes, a large tumor perimeter is associated with the likelihood that a tumor is malignant.
- Area. The Area feature is the area of a breast tumor. Malignant tumors frequently have a large area compared with benign tumors.
- NSPD (number of substantial protuberances and depressions). The NSPD feature can be utilized to calculate the level of boundary irregularity.
- LI (lobulation index). According to the definition for a concave point from the NSPD, the lobe region enclosed by a lesion contour and a line connected by any two adjacent concave points can be obtained. Usually, a malignant tumor has a larger LI than does a benign one.
- ENC (elliptic-normalized circumference). The angle of inclination for each tumor, with respect to the  $x-y$  coordinate plane, can be obtained by using the second order moment.
- ENS (elliptic-normalized skeleton). The skeleton of a tumor region expresses a set  $S$ , and ENS is defined as the sum of the skeleton points in  $S$ . When a tumor has a twisted boundary, the skeleton is also complex. A malignant lesion always has a twisted boundary and generates a large ENS.
- LS Ratio (long axis to short axis ratio). The LS Ratio is the length ratio of the major (long) axis and minor (short) axis of the equivalent ellipse defined in the ENC feature.

- Aspect Ratio. The Aspect Ratio is the ratio of a tumor's depth and width. If a tumor depth exceeds its width, the Aspect Ratio is greater than 1 and the tumor has a high probability of being malignant.

$$FormFactor = \frac{4\pi \times Area}{Perimeter^2} \quad (27)$$

when Form Factor is close to 1, the tumor shape is nearly round.

- Roundness

$$Roundness = \frac{4 \times Area}{\pi \times Max\ Diameter^2} \quad (28)$$

where Max Diameter denotes the length of the major axis from the equivalent ellipse of a tumor.

- Solidity

$$Solidity = \frac{Area}{Convex\ Area} \quad (29)$$

where Convex Area is the area of the convex hull of a tumor. When Solidity is close to 0, the tumor is malignant.

- Convexity

$$Convexity = \frac{Convex\ Perimeter}{Perimeter} \quad (30)$$

where Convex Perimeter is the perimeter of the convex hull of a tumor.

- Extent

$$Extent = \frac{Area}{Bounding\ Rectangle} \quad (31)$$

where Bounding Rectangle is the smallest rectangle containing the tumor.

- TCA Ratio. The TCA Ratio (tumor area to convex area ratio) is defined as:

$$TCARatio = \frac{Area}{Convex\ Area} \quad (32)$$

- TEP Ratio (tumor perimeter to ellipse perimeter ratio). The TEP Ratio is the ratio of a tumor perimeter and the corresponding ellipse perimeter. The major and minor axes of the corresponding ellipse are calculated based on the proportion of width to depth of a tumor to acquire the same area for the ellipse and tumor.

- TEP Difference (difference between tumor perimeter and ellipse perimeter). The TEP Difference is defined as the difference between tumor perimeter and the corresponding ellipse perimeter.
- TCP Ratio (tumor perimeter to circle perimeter ratio). The TCP Ratio is the ratio of a tumor perimeter and the corresponding circle perimeter, the corresponding circle having the same area as the tumor.
- TCP Difference (difference between tumor perimeter and circle perimeter). The TCP Difference is defined as the difference between the tumor perimeter and the corresponding circle perimeter, the corresponding circle having the same area as the tumor.
- AP Ratio (area to perimeter ratio). The AP Ratio is the ratio of the area and the perimeter of a tumor.
- Thickness of the wall. If the wall of the mass is thick, there is a better chance that it is cancerous. If it is thin, it is more possible that it is a cyst rather than a malignant tumor.

### 4.3.2 Texture features

The texture features that we used in our research are the ones extracted by Chen et al. [22] and shown in Table 4.3

Table 4.3: All possible texture features by Chen et al. [22] - A: 77 auto-covariance matrix; B: SGLDM; C: GLDM; D: BDIP; E: BVLC; F: NGTDM

Rank	Feature set	Rank	Feature set
1	AD	20	ABDF
2	ADE	21	AF
3	AEF	22	ABF
4	ABCF	23	ACEF
5	A	24	ABC
6	ADF	25	AB
7	ACDE	26	AC
8	ABCD	27	ABCEF
9	ACDEF	28	ADEF
10	ACDF	29	ABCE
11	ABCDF	30	ABD
12	ABCDE	31	ABDE
13	ACF	32	ABE
14	ABCDEF	33	C
15	ACD	34	F
16	ABDEF	35	D
17	AE	36	E
18	ACE	37	B
19	ABEF		

### 4.3.3 Moments features

Geometrical moment of order  $(p + q)$  for a two-dimensional discrete function like image is computed by using the following equation. If the image can have nonzero values only in the finite part of  $xy$  plane, then moments of all orders exist for it [48].

$$m_{pq} = \sum_{x=0}^{M-1} \sum_{y=0}^{N-1} x^p y^q f(x, y) \quad (33)$$

where  $f(x, y)$  is image function and  $M, N$  are image dimensions. Then by using



the following equation, geometrical central moments of order equal to  $(p + q)$  can be computed.

$$\mu_{pq} = \sum_{x=0}^{M-1} \sum_{y=0}^{N-1} (x - \bar{x})^p (y - \bar{y})^q f(x, y) \quad (34)$$

where  $\bar{x}$  and  $\bar{y}$  are gravity center of image and are calculated by using the following equation. Actually by image translation to coordinate origin while computing central moments, they become translation invariant.

$$\begin{aligned} \bar{x} &= \frac{m_{10}}{m_{00}} \\ \bar{y} &= \frac{m_{01}}{m_{00}} \end{aligned} \quad (35)$$

Note that in a binary image,  $m_{00} = \mu_{00}$  is count of foreground pixels and has direct relation to image scale, therefore central moments can become scale normalized using the following equation.

$$\begin{aligned} \eta_{pq} &= \frac{\mu_{pq}}{m_{00}^a} \\ a &= \frac{p + q}{2} + 1 \end{aligned} \quad (36)$$

Moment invariants are a set of nonlinear functions, which are invariant to translation, scale, and orientation and are defined on normalized geometrical central moments. Hu [48] first introduced seven moment invariants based on normalized geometrical central moments up to the third order. Then, Li [74] extended the moments and listed 52 Hu invariant moments of order 2-9. Since the higher order moment invariants have resulted higher sensitivity, a set of twelve moment invariants limited by order less than or equal to four seems to be proper in most applications [15]. Having normalized geometrical central moments of order four and the lesser ones, seven moment invariants ( $\phi_1 - \phi_7$ ) introduced by Hu and then five extended ones ( $\phi_8 - \phi_{12}$ ) developed by Li, can be computed using the following equations.

$$\begin{aligned}
\phi_1 &= \eta_{20} + \eta_{02} \\
\phi_2 &= (\eta_{20} - \eta_{02})^2 + 4\eta_{11}^2 \\
\phi_3 &= (\eta_{30} - 3\eta_{12}) + (3\eta_{21} - \eta_{03})^2 \\
\phi_4 &= (\eta_{30} + 3\eta_{12})^2 + (\eta_{21} + \eta_{03})^2 \\
\phi_5 &= (\eta_{30} - 3\eta_{12})(\eta_{30} + \eta_{12})[(\eta_{30} + \eta_{12})^2 - 3(\eta_{21} + \eta_{03})^2] \\
&\quad + (3\eta_{12} - \eta_{03})(\eta_{21} + \eta_{03})[(3\eta_{30} + \eta_{12})^2 - (\eta_{21} + \eta_{03})^2] \\
\phi_6 &= (\eta_{20} - \eta_{02})[(\eta_{30} + \eta_{12})^2 - (\eta_{21} + \eta_{03})^2] + 4\eta_{11}(\eta_{30} + \eta_{12})(\eta_{21} + \eta_{03}) \\
\phi_7 &= (3\eta_{21} - \eta_{03})(\eta_{30} + \eta_{12})[(\eta_{30} + \eta_{12})^2 - 3(\eta_{21} + \eta_{03})^2] \\
&\quad + (3\eta_{21} - \eta_{03})(\eta_{21} + \eta_{03})[(3\eta_{30} + \eta_{12})^2 - (\eta_{21} + \eta_{03})^2] \\
\phi_8 &= \eta_{40} + \eta_{22} + \eta_{02} \\
\phi_9 &= (\eta_{40} - \eta_{04})^2 + 4(\eta_{31} - \eta_{13})^2 \\
\phi_{10} &= (\eta_{40} - 6\eta_{22} + \eta_{04})^2 + 16(\eta_{31} - \eta_{13})^2 \\
\phi_{11} &= (\eta_{40} - 6\eta_{22} + \eta_{04})^2[(\eta_{40} - \eta_{04})^2 + 4(\eta_{31} - \eta_{13})^2] \\
&\quad + 16(\eta_{40} - \eta_{04}) + (\eta_{31} + \eta_{13})(\eta_{31} - \eta_{13}) \\
\phi_{12} &= (\eta_{40} - 6\eta_{22} + \eta_{04})^2[(\eta_{40} - \eta_{04})^2 + 4(\eta_{31} - \eta_{13})^2] \\
&\quad + 16(\eta_{40} - \eta_{04}) + (\eta_{31} + \eta_{13})(\eta_{31} - \eta_{13})
\end{aligned} \tag{37}$$

#### 4.3.4 Convolutional neural network for feature extraction

We identified a sub-set of morphological features and texture features for classification of breast lesions. Selection of these features depend on a classifier and the classification stage depends on these selected features. CNN is an independent method that does not rely on a classifier. The method is trained like a normal neural network using back propagation. This method uses several layers: convolutional and subsampling and they alternate (i.e. one convolutional layer followed by subsampling layer). Convolutional layer extracts elementary features of the image. It is organised in planes, also called feature maps, of simple units called neurons. It uses a  $5 \times 5$  area that forms a unit in the input image or in the previous layer. A trainable weight is assigned to each connection, as it is done in normal neural networks. The fact that an elementary feature detector is useful in a part of the image and it is likely to be useful

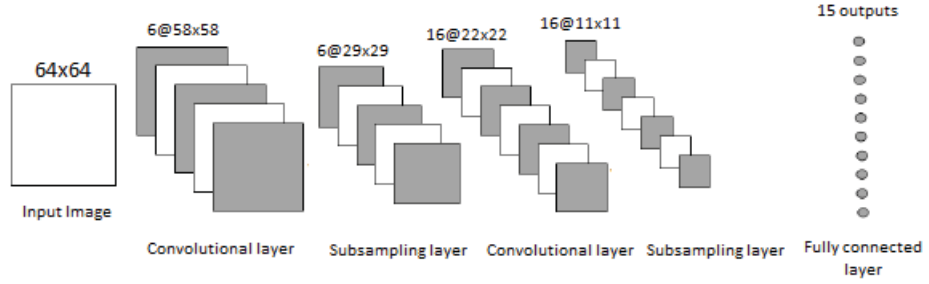


Figure 4.11: CNN structure used for feature extraction

in the entire image justifies the approach. A convolutional layer consists of several feature maps. We converted the images in our database to be the size of  $64 \times 64$ . We used a sliding window of  $7 \times 7$  to perform transformation. Fig. 4.11 illustrates the architecture of the proposed system.

In subsampling layer, we have the same number of feature maps from the previous convolutional layer but half the number of rows and columns. Each unit  $j$  is connected to a  $2 \times 2$  receptive field and we compute the average of its four inputs  $y_i$ , multiply it by a trainable weight  $w_j$  and add a trainable bias  $b_j$  to obtain the activity level  $v_j$ :

$$v_j = w_j \frac{\sum_{i=1}^4 y_i}{4} + b_j$$

The end result will be 15 features that we can use in our classifier.

### 4.3.5 Combination of texture features with morphological features

In our automated CAD system, we are able to extract morphological features and texture features. Combination of different feature sets could improve the accuracy of a CAD system. Yang et al. [143] suggests that combining different sets of features (in our case morphological and texture features) would improve computer-aided diagnosis of breast cancer. In our research, we considered two texture features that had high discriminatory power and we combined them with a sub-set of mentioned morphological features.

## 4.4 Feature selection

### 4.4.1 Using MI, SFS and SBS techniques for feature selection

We discussed morphological and texture features. We discussed how they can be extracted and how they can be used for segmentation. Now we need to find a combination of selected features that can be used to give the best performance and accuracy.

Now we can use a feature selection method to select the best feature set. We thought about using different combination of features and compare them but because there are lots of features, it is computationally not possible.

In this research As discussed before, we used a mutual information technique that ranks the features based on the discriminatory power. Then we used a selection algorithm to select a sub-set of those features. Due to limitations of Sequential Forward Search (SFS) and Sequential Backward Search (SBS) methods, a combination of those methods are used to make sure no important feature is eliminated by any of those methods. To guarantee that SFS and SBS converge to the same solution, we must ensure that features already selected by SFS are not removed by SBS and features already removed by SBS are not selected by SFS. In order to achieve that, everytime SFS attempts to add a new features, we should check if it has been removed by SBS. If it has been removed by SBS then we should attempt to add the second best feature. This method is called Bidirectional Search (BDS).

### 4.4.2 Selected morphological and texture features

Our feature selection algorithm (MI, SFS and SBS) is used to select a subset of morphological features and Chen et al. [22] selects a subset of texture features shown in Table 4.4.

Table 4.4: Selected morphological and texture features

#	Morphological Feature	#	Texture Features
1	Roundness	1	AD
2	Solidity	2	ADE
3	Convexity	3	AEF
4	TCA Ratio	4	ABCF
5	Perimeter	5	A
6	Area	6	ADF
7	NSPD	7	ACDE
8	Aspect Ratio		

## 4.5 Classification

For classification, we implemented several classification methods and concluded that ANN, AdaBoost and FSVM perform better on breast ultrasound images. The comparison between these methods and other well-know classification methods is shown in chapter 5. In our proposed method, we use a combination of Adaboost, FSVM and ANN as the first layer and then we use a majority vote classifier to combine the result of the three classifiers. A conceptual model of our classifier is shown in Figure 4.12.

For majority based classifier, we used the approach of majority votes [70]. Assume that the *label* outputs of the classifiers are given as  $c$ -dimensional binary vectors  $[d_{i,1}, \dots, d_{i,c}]^T \in \{0, 1\}^c, i = 1, \dots, L$ , where  $d_{i,j} = 1$  if  $D_i$  labels  $\mathbf{x}$  in  $\omega_j$ , and 0 otherwise. The majority vote will result in an ensemble decision for class  $\omega_k$  if majority of the classifiers classify the unknown sample into specific class.

Ties are resolved arbitrarily. This rule is often called majority vote. It will indeed coincide with the simple majority (50 percent of the votes+1) in the case of two classes ( $c = 2$ ).

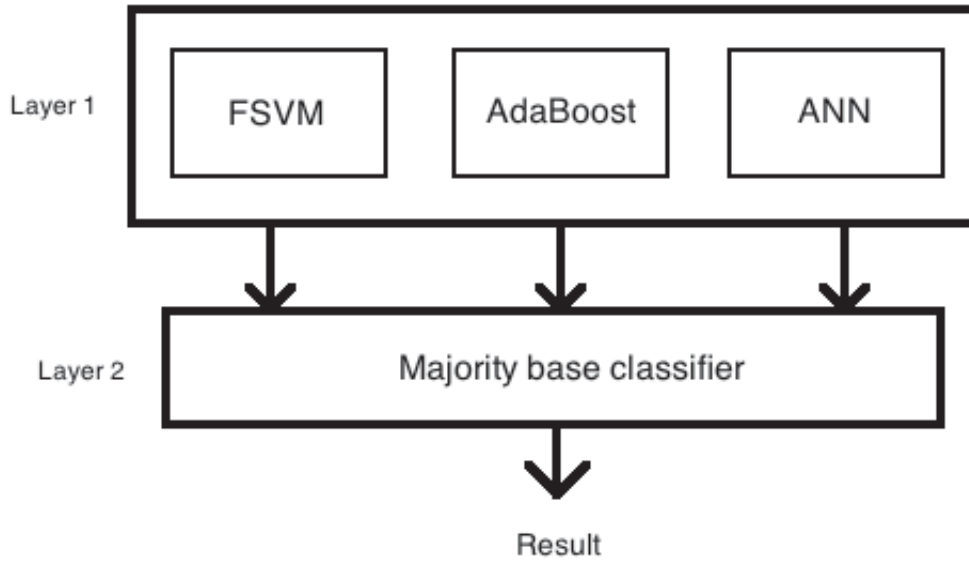


Figure 4.12: Proposed classifier - combination of FSVM, AdaBoost, ANN and Majority base classifiers

## 4.6 Stages in our proposed CAD system

In our proposed system, we use fuzzy logic and compounding for de-noising. The fuzzy nature of breast ultrasound images suggested the use of fuzzy logic and because of several other artifacts like shadowing, compounding proved to enhance the quality of ultrasound images.

We extracted several morphological and texture features. We used a MI (mutual information) approach to rank the morphological features and also used a combination of SFS and SBS methods to select the best set of features.

For segmentation, we used a new approach to select seed points and used a region growing method to perform segmentation. This method seems to perform better than other state-of-the-art segmentation methods.

For classification, we used a combination of ANN, AdaBoost and FSVM as the first layer and a majority base classifier as the second layer to classify benign and malignant lesions in breast ultrasound images.

Figure 4.13 describes the conceptual diagram of our proposed system.

**Pre-processing:** To remove noises from ultrasound images and make it ready for segmentation.

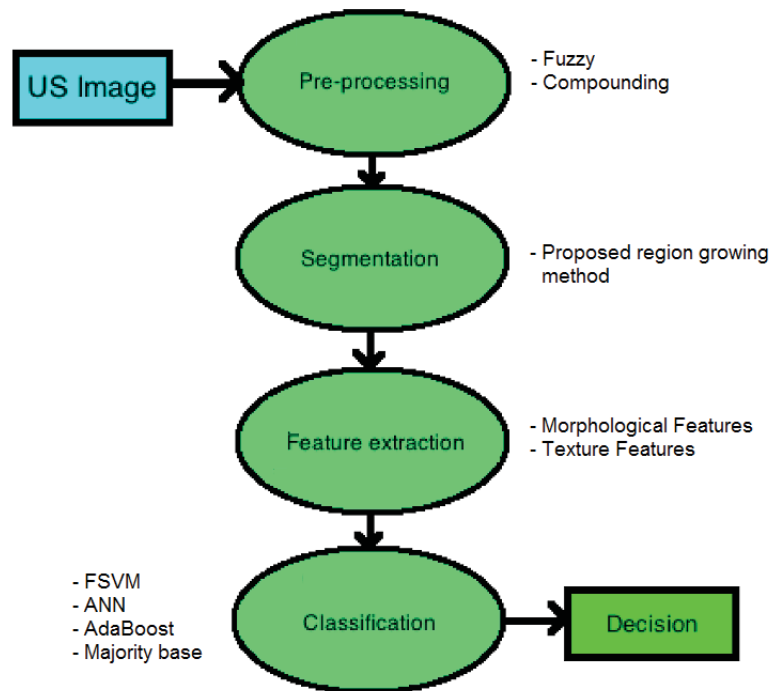


Figure 4.13: Proposed system

**Segmentation:** To determine the boundary of the suspected lesion(s).

**Feature extraction:** To identify the features for classification purpose.

**Classification:** To classify the lesion in different classes to identify if the lesion is benign or malignant.

Pre-processing is the most important stage in the system. We need to remove noise and shadow as much as possible in order to better distinguish lesions from breast tissues. We are going to study different pre-processing methods. Because of the fuzzy nature of ultrasound images, we are going to propose the use of fuzzy logic for pre-processing and perform several experiments.

We also realized that sometimes radiologists look at a lesions from different angles. The reason is that sometimes due to shadowing and noise the lesion cannot be clearly recognized. Based on that finding, we thought correlation of ultrasound images from different angles could give us more information and eliminate some of the unwanted noises and shadows. For this, compounding and perform experiments on breast ultrasound images from different angles to see if it can reduce noise and shadow while preserving important information in ultrasound images.

For segmentation of lesions in ultrasound images, we introduced a new approach

that selects seed points automatically and uses a region growing algorithm to find the boundaries of lesion.

For feature selection, we used combination of some well-known feature selection algorithms such as Sequential Forward Search, Sequential Backward Search and Mutual Information (MI) methods. We also extracted some texture features as they are not correlated to morphological features and they could provide more accuracy for classification. The methods of selecting a sub-set of morphological features and also the method for extraction texture features are described later in this thesis.

Finally, classification stage in our CAD system consists of a new classification method, which is the combination of AdaBoost, ANN, FSVM and majority-based classifier.

Implementation notes of our proposed system are given in Appendix A.



# Chapter 5

## Experimental results

### 5.1 Ultrasound image database

The database selected for experiments in this research is from HIT Pattern Recognition Research center. It consists of breast ultrasound images from 80 patients. These images are pathologically proven and consist of 59 malignant and 21 benign cases. The database of ultrasound images used in this research is shown in Appendix B.

### 5.2 Formulas used for evaluation

The following formulas are used in our experiments:

$$\text{Overall accuracy} = \frac{TP + TN}{TP + TN + FP + FN}$$

$$\text{Specificity} = \frac{TN}{TN + FP}$$

$$\text{Sensitivity} = \frac{TP}{TP + FN}$$

$$\text{Positive predictive value}(PPV) = \frac{TP}{TP + FP}$$

$$\text{Negative predictive value}(NPV) = \frac{TN}{TN + FN}$$

where  $TP = \text{True Positive}$ ,  $TN = \text{True Negative}$ ,  $FP = \text{False Positive}$ ,  $FN = \text{False Negative}$ .

### 5.3 Pre-processing

Our proposed region growing method (for segmentation) and support vector machine [83] (for classification) methods have been implemented. For de-noising, we implemented the fuzzy approach explained in chapter 4. Figure 5.1 illustrates an image after fuzzy concept is applied. As one can see, after applying fuzzy approach, the background and foreground are much better separated.

In another experiment, we used fuzzy approach for de-noising and proposed region growing method for segmentation. Figure 5.2 illustrates segmented ultrasound image.

After validation by the physician, it looks like the segmentation is done in proper way, although it does not give the best margin. This is very significant for the physician to see if the mass is branched or whether it has irregular shape.

If we do not apply fuzzy approach (do not perform de-noising) and only use proposed segmentation method, the segmented image can be seen in Figure 5.3.

As can be seen, this approach totally misses the branch of the mass. If that branch is not included, then the diagnosis could be completely different. In addition to the above experiment, we chose 20 patients and applied the method on the ultrasound images. We segmented the masses and asked a physician to tell us if the segmentation was done properly. We have not disclosed the diagnosis for the patients so it does not have impact on physician's decision.

Out of 20 patients, the masses for 19 patients were segmented correctly. The branches were identified as well as irregular shapes. We have asked the physician to

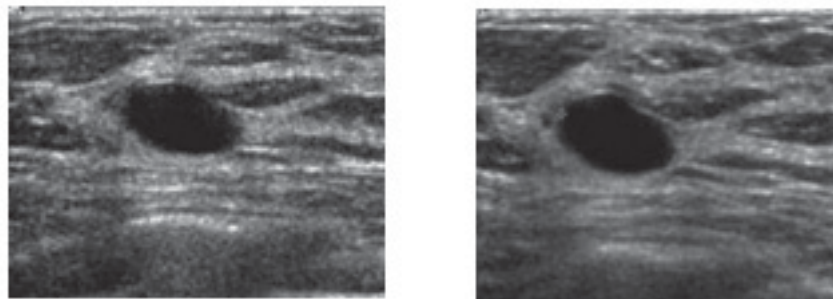


Figure 5.1: Fuzzy logic for de-noising

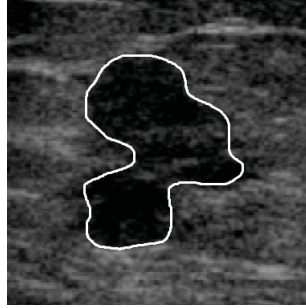


Figure 5.2: Segmentation

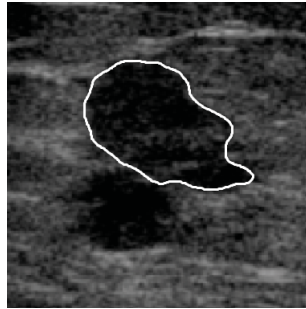


Figure 5.3: Segmentation without using Fuzzy logic for de-noising

identify the suspicious masses. Out of the 19 patients, 10 were identified by physician to be suspected for carcinoma. Out of 10 suspicious patients, 8 of those who had cancerous masses and 2 were false positive. There was no false negative. Table 5.1 summarizes the result of the experiment.

Table 5.1: Applying fuzzy logic for de-noising (TP: True Positive; TN: True Negative; FP: False Positive; FN: False Negative)

TP	TN	FP	FN	Accuracy%	Specificity%	Sensitivity%	PPV%	NPV%
15	3	2	0	90.00	60.00	100.00	88.00	100.00

For the next experiment, we did not use fuzzy approach for de-noising and repeated the same experiment. The result of the experiment is shown in Table 5.2

As you can see, in this experiment, we have one false negative, which did not exist when we applied fuzzy logic for de-noising.

Table 5.2: No fuzzy logic for de-noising

# of patients	TP	TN	FP	FN
20	14	3	2	1

### 5.3.1 Compounding

In order to find out how compounding of the images will improve the result, we applied the compounding algorithm we discussed earlier after de-noising. The algorithm is applied on 3 images per patient (9 o'clock, 0 o'clock and 3 o'clock). A sample of the result is shown in Table 5.3

Original	De-noised	Comp.	Segmented	System output	Gold stand.
				Malignant	Malignant
				Benign	Benign
				Malignant	Malignant
				Malignant	Malignant
				Malignant	Benign
				Malignant	Malignant
				Malignant	Malignant

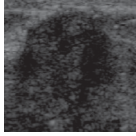
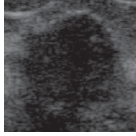
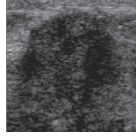
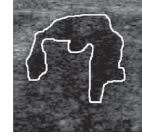
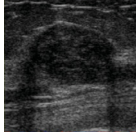
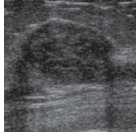
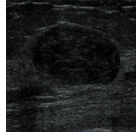
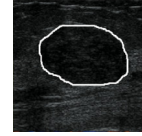
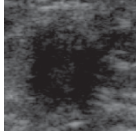
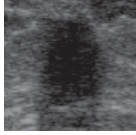
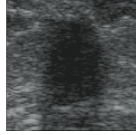

Original	De-noised	Comp.	Segmented	System output	Gold stand.
				Malignant	Malignant
				Benign	Benign
				Benign	Benign

Table 5.3: Experiment using compounding (Gold stand.: Cold standard, Comp.: Compounded)

After applying compounding, all one case of false positive is eliminated cases were identified correctly. One of the false positives that we saw before was due to shadowing that was eliminated after applying compounding to ultrasound images as illustrated in Table 5.4

Table 5.4: Results with compounding

TP	TN	FP	FN	Accuracy%	Specificity%	Sensitivity%	PPV%	NPV%
59	20	0	1	98.75	100.00	98.33	100.00	95.24

### 5.3.2 Performance of our pre-processing methods

The performance metrics used are Peak Signal to Noise Ratio (PSNR) and De-noising Time [136]. PSNR is a quality measurement between the original and a de-noised image. The higher the PSNR, the better is the quality of the compressed or reconstructed image. To compute PSNR, the block first calculates the Mean-Squared Error (MSE) and then the PSNR:

$$PSNR = 10 \log_{10} \left[ \frac{R^2}{MSE} \right] \quad (38)$$

where  $MSE = \frac{\sum [I_1(m,n) - I_2(m,n)]^2}{M*N}$  where  $M$  and  $N$ ,  $m$  and  $n$  are number of rows

and columns in the input and output image respectively. Table 5.5 shows the comparison between our proposed de-noising method (Fuzzy and Compounding) and other standard de-noising methods used in medical imaging.

Table 5.5: Comparison between several de-noising methods

Filter	PSNR
Lee	27.25
Frost	27.42
Bayes	47.21
Fuzzy	54.96
Compounding	36.45
Proposed method	63.24

## 5.4 Segmentation

Our proposed segmentation method is compared with other state-of-the-art segmentation methods. Our approach selects the seed point automatically and then uses a region growing algorithm to perform segmentation. Table 5.6 summarizes the result of our comparison.

Table 5.6: Comparison between proposed segmentation method, region growing method and neurotrophic I-means clustering method

Method	# of patients	Segmented Correctly	Accuracy %
Region growing [135]	80	74	92.50
I-means clustering [119]	80	75	93.75
Proposed method	80	78	97.50

## 5.5 Feature extraction and selection

Total of twenty morphological features and thirty seven texture features are considered. A combination of MI (mutual information), Combination of Sequential Forward Search and Sequential Backward Search has been implemented (Bidirectional Search) to select a sub-set of morphological features. Total of seven texture features (selected

by Chen et al. [22]) and eight morphological features were selected. Table 5.7 summarizes the selected morphological features and selected texture features.

Table 5.7: Selected morphological features used in our experiments

#	Morphological Feature	#	Texture Features
1	Roundness	1	AD
2	Solidity	2	ADE
3	Convexity	3	AEF
4	TCA Ratio	4	ABCF
5	Perimeter	5	A
6	Area	6	ADF
7	NSPD	7	ACDE
8	Aspect Ratio		
9	Wall Thickness		

For quantitative evaluation of our feature selection method, we used criteria that measures the separation of each class and we compared it with other feature selection methods. The criteria  $S = \text{trace}(S_b^{-1}S_w)$  is used, where  $S_b$  is between class scattered matrix and  $S_w$  is within class scattered matrix. A lower value of separability criteria  $S$  ensures that the classes are well separated by their scatter means. The result of our comparison between BDS (Bidirectional Search) method and other well-known methods are summarized in Table 5.8.

Table 5.8: Comparison between different feature selection algorithms

Method	$S$
Branch and Bound[29]	0.45
Sequential Floating Forward Search[22]	0.55
Stepwise Clustering[66]	0.52
Sequential Forward Search[22]	0.45
Sequential Backward Search[22]	0.45
Bidirectional Search (used in our CAD system)	0.42

Based on the result of the comparison, it looks like BDS makes better separation between the classes.

## 5.6 Classification

Our proposed classification method consists of a combination of three different state-of-the-art classification methods (refer to section 4.5). These three methods are: AdaBoost, ANN and FSVM.

In order to prove that our proposed classification method outperforms the other methods. We used the methods for pre-processing, segmentation and feature extraction shown in Table 5.9.

Table 5.9: Methods used in each stage

Stage	Method
Pre-processing	Fuzzy method and Compounding
Segmentation	Proposed region growing method
Feature Extraction	Morphological and texture features
Feature Selection	MI (mutual information), Sequential Forward Search and Sequential Backward Search
Classification	ANN, AdaBoost and FSVM

We used PCA, FLD, AdaBoost, ANN and FSVM classifiers separately to compare the accuracy of those classifiers with our proposed classifier. Table 5.10 and Table 5.11 compares the performance of our proposed classification method with other state-of-the-art classification methods. In table Table 5.10 we use k-fold cross-validation technique with 16 partitions. Table 5.11 does not use k-fold cross-validation.

Table 5.10: Comparing our proposed classifiers with state-of-the-art classifiers - using k-fold cross-validation

Method	Accuracy
FLD	86.25%
KNN	85.00%
PCA	87.50%
ANN	90.00%
AdaBoost	92.50%
FSVM	97.50%
Proposed classifier	98.70%



Table 5.11: Comparing our proposed classifiers with state-of-the-art classifiers

Method	Accuracy
PCA	87.50%
FLD	87.50%
KNN	87.50%
ANN	91.25%
AdaBoost	95.00%
FSVM	97.50%
Proposed classifier	98.70%

## 5.7 Performance of our proposed CAD system

In this experiment, we used fuzzy logic for pre-processing of ultrasound images. We also used compounding of three images of each patient (9 o'clock, 0 o'clock and 3 o'clock) and performed compounding on the images. Proposed region growing method is used for Segmentation. We used the morphological features that we extracted using MI (mutual information), Sequential Forward Search and Sequential Backward Search methods. We also included texture features by Chen et al. [22]. For classification, we used our proposed classification method, which uses a combination of FSVM, AdaBoost, ANN and Majority based methods. The selected morphological features and texture features are showing in Table 5.12. Methods used in each stage of our system are shown in Table 5.13.

Table 5.12: Proposed CAD system - Selected features (A: 77 auto-covariance matrix; B: SGLDM; C: GLDM; D: BDIP; E: BVLC; F: NGTDM)

#	Morphological Feature	#	Texture Features
1	Roundness	1	AD
2	Solidity	2	ADE
3	Convexity	3	AEF
4	TCA Ratio	4	ABCF
5	Perimeter	5	A
6	Area	6	ADF
7	NSPD	7	ACDE
8	Aspect Ratio		

Table 5.13: Proposed CAD system - Methods used in each stage

Stage	Method
Pre-processing	Fuzzy method + Compounding
Segmentation	Proposed region growing method
Feature Extraction	Morphological and texture features
Feature Selection	MI (mutual information), Sequential Forward Search and Sequential Backward Search
Classification	Our proposed classification method (combination of ANN, AdaBoost, FSVM and Majority base classifier)

We have performed experiments on the database of 80 patients. The results are given in Table 5.14 and 5.15.

Table 5.14: Proposed CAD system - Results

TP	TN	FP	FN	Accuracy%	Specificity%	Sensitivity%	PPV%	NPV%
59	20	0	1	98.75	100.00	98.33	100.00	95.24

Table 5.15: Proposed CAD system - Comparison with other methods

Method	Accuracy
ABUS[51]	88.75%
Hybrid Filtering[145]	92.50%
Our approach	98.75%

## 5.8 Performance of our proposed CAD system with different set of features

### 5.8.1 Experiment using manually extracted feature (wall thickness)

We added a new feature to the list of the texture features in our proposed system (wall thickness) and repeated the experiments. We also use k-fold cross-validation technique with 16 partitions. The performance of the system does not change when using k-fold cross-validation. The result is shown in Table 5.16 and 5.17.

Table 5.16: Results

TP	TN	FP	FN	Accuracy%	Specificity%	Sensitivity%	PPV%	NPV%
59	20	0	1	98.75	100.00	98.33	100.00	95.24

Table 5.17: Comparison with other methods

Method	Accuracy
ABUS[51]	88.75%
Hybrid Filtering[145]	92.50%
Our approach	98.75%

Including "wall thickness" in the list of features did not improve the accuracy of the system. Radiologists usually do not consider this feature unless there is a lack of other features. This feature is hard to extract and it is very subjective even among experienced radiologists.

### 5.8.2 Experiment using CNN to extract texture features

In our proposed CAD system, we used CNN and performed experiments to see the effect on the accuracy of our classifier. The result of the experiments is shown in Table 5.18 when using k-fold cross-validation technique with 16 partitions. The result in Table 5.19 does not use k-fold cross-validation.

Table 5.18: Result of comparing our proposed classifiers with state-of-the-art classifiers - using CNN for texture feature extraction and using k-fold cross-validation

TP	TN	FP	FN	Accuracy%	Specificity%	Sensitivity%
55	19	4	2	92.25	82.61	96.49

Table 5.19: Result of comparing our proposed classifiers with state-of-the-art classifiers - Using CNN for texture feature extraction

TP	TN	FP	FN	Accuracy%	Specificity%	Sensitivity%
57	19	2	2	95.00	90.48	96.61

It appears that using CNN for feature extraction does not improve the overall accuracy of the system.

### 5.8.3 Experiment using Hu moments to extract texture features

In our proposed CAD system, we used Hu moments as texture features and performed experiments to see the effect on the accuracy of our classifier. The result of the experiments is shown in Table 5.20 when using k-fold cross-validation technique with 16 partitions. The result in Table 5.21 does not use k-fold cross-validation. The performance is the not better than the experiment using Chen et al. [22] texture features.

Table 5.20: Experiment - Using Hu moments - Results using k-fold cross-validation

TP	TN	FP	FN	Accuracy%	Specificity%	Sensitivity%	PPV%	NPV%
56	19	3	2	93.75	86.36	96.55	94.91	90.48

Table 5.21: Experiment - Using Hu moments - Results

TP	TN	FP	FN	Accuracy%	Specificity%	Sensitivity%	PPV%	NPV%
57	21	2	0	97.50	90.91	100.00	96.67	100.00

#### 5.8.4 Experiment using texture features and only Fuzzy for pre-processing

In order to see the effect of texture features on the performance of our CAD system, we performed experiment using Fuzzy logic for pre-processing (no compounding) and used morphological and texture features. The reason was to see if using texture features can compensate for not using compounding. We also use k-fold cross-validation technique with 16 partitions. The performance of the system does not change when using k-fold cross-validation. The result is shown in Table 5.22.

Table 5.22: Experiment using texture features and Fuzzy logic - Results

TP	TN	FP	FN	Accuracy%	Specificity%	Sensitivity%	PPV%	NPV%
58	19	1	2	96.25	95.00	96.67	98.30	90.48

## 5.9 Using concurrent computing

Some of the stages in our CAD system can benefit from concurrent computing to decrease the time required to process an image. In pre-processing, we used fuzzy logic to de-noise breast ultrasound images. This algorithm uses a membership function to perform the task and we make a pixel darker or lighter depending on the membership function. Because each pixel is processed independently from other pixels, we can get benefit of using multi-thread programming to decrease processing time.

Also our multi-layer classifier is a good candidate for using concurrency. As mentioned in previous sections, in the first layer of our proposed classifier, we use three different classifiers (ANN, AdaBoost and FSVM) and the result of each classifier will be passed to a majority vote classifier to assign the test image into malignant and benign classes. In our first layer, we can use three threads for our three classifiers (ANN, AdaBoost and FSVM). We expect this to reduce the time for classifying a test image.

We use a computer with Intel Core i5-3360M processor (4 cores, 2.80 GHz, 4MB L3, 1333MHz FSB), 32GB DDR3 Memory and Windows 7 Professional 64bit operating system. We use 4 different threads in our program to perform de-noising using fuzzy logic and 3 different threads to perform classification using proposed classifier. For de-noising, each pixel is processed by a separate thread and all other pixels wait for their turn to be processed. As soon as a thread is free, another pixel in the queue is picked up and is processed. For classification, 3 threads are created in the program and each classifier is assigned to a thread (i.e. one thread for ANN, one thread for AdaBoost and one thread for FSVM). Majority base classifier waits until all threads are completed and then makes the final decision.

The computational time of our system (on a database of 80 patients) using one core (one CPU, no concurrent computing) and concurrent version of our system that uses 4 threads for de-noising and 3 threads for classification are shown in Table 5.23. The average computational time for processing one ultrasound image using our proposed system and using one CPU is around 5 seconds. Average processing time for one image using the concurrent version of our system is around 4 seconds.

Table 5.23: Computational time for our proposed system (in seconds)

	Using 1 CPU	Using 4 CPU
Pre-processing	105s	71s
Segmentation	127s	127s
Feature Ext./Sel.	134s	134s
Classification	48s	19s
Total	414s	351s

## 5.10 Complete list of experiments

Please see Appendix C for complete list of experiments with the output results.

## 5.11 Conclusion of our experiments

We showed that our proposed pre-processing method (Fuzzy and Compounding) performs better than other well-known pre-processing methods. It also appears that if we do not apply a pre-processing method and use texture features in combination with

morphological features, it can somehow compensate for the accuracy. We also showed that our proposed classifier (ANN, AdaBoost, FSVM and Majority Vote) performs better than other well-known classification methods.

We also manually extracted one morphological feature to evaluate the effect on classification performance. This feature is called "wall thickness" and it seems that it does not affect classification performance. We also used CNN and Hu moments as texture features and evaluated classification performance. It appears that by using those features we get lower accuracy. In general, the accuracy of our proposed classification method combined with our proposed pre-processing method outperforms other state-of-the-art CAD systems.

In our experiments we used relatively low number of ultrasound images. Due to difficulties obtaining more images, we evaluated the performance of our proposed system using ultrasound images from 80 patients. We also had to extract one of the features manually with the help from a physician. We definitely can do more research on the effect of different texture features and morphological features on the performance of the system. Also our proposed classifier could use weighted majority classifier to possibly improve classification accuracy.

# Chapter 6

## Conclusions

An automatic system for classification of breast cancer lesions in ultrasound images is proposed. We reviewed the background and related work and we proposed a methodology to enhance detection of suspicious lesions in breast ultrasound images.

The main problem with processing ultrasound images is speckle noise and shadowing. These two are big challenge for automating detection of suspicious lesions in ultrasound images. To overcome some of the problems, we proposed a fully automated system for detection of breast ultrasound images. To remove the noise, we proposed a fuzzy logic method and a compounding method for the pre-processing stage of our system. By using this Fuzzy logic method and compounding method, we were able to improve the quality of the image before segmentation, therefore we were able to get a better performance out of the system.

We have also identified a sub-set of features for classification purposes. As experimenting with all combinations of features was practically impossible, we extracted most significant features for the purpose of classification.

We also proposed a new approach of segmentation and classification. In our proposed segmentation method, we used an automatic seed selection technique and then used a region growing method to segment the breast ultrasound images in our database. This segmentation method is more accurate compared to other state-of-the-art segmentation methods. For classification, we used a combination of AdaBoost, ANN, FSVM and majority-based classifier and the result suggests that our proposed method performs better than other state-of-the-art classification methods.

We performed our experiments on the database of 80 patients with 3 pathologically



proven images per patient taken at three different angles: 9 o'clock, 0 o'clock and 3 o'clock.

In our experiments we used relatively low number of ultrasound images. Due to difficulties obtaining more images, we evaluated the performance of our proposed system using ultrasound images from 80 patients. We also had to extract one of the features manually with the help from a physician. Future research will focus on the effect of different texture features and morphological features on the performance of the system. We will also investigate weighted majority classifier to possibly improve classification accuracy.

# Appendix A

## Implementation notes

### A.1 Statistical Analysis

Implementation of the algorithms mentioned in this research was done using Microsoft.Net C#. But C# does not natively provide statistical analysis, machine learning, image processing and computer vision methods.

We have used a rich library called Accord.NET. This library provides different interfaces to do statistical analysis, machine learning and image processing.

### A.2 Accord.NET library

Accord.NET provides statistical analysis, machine learning, image processing and computer vision methods for .NET applications. The Accord.NET Framework extends the popular AForge.NET with new features, adding to a more complete environment for scientific computing in .NET.

The framework is divided in libraries, available through an executable installer, standalone compressed archives and NuGet packages. Those libraries are divided among three main functionalities: Scientific computing, Signal and image processing and Support libraries.

#### A.2.1 Scientific computing

**Accord.Math:** Contains a matrix extension library, along with a suite of numerical matrix decomposition methods, numerical optimization algorithms for constrained

and unconstrained problems, special functions and other tools for scientific applications.

**Accord.Statistics:** Contains probability distributions, hypothesis testing, statistical models and methods such as Linear and Logistic regression, Hidden Markov Models, (Hidden) Conditional Random Fields, Principal Component Analysis, Partial Least Squares, Discriminant Analysis, Kernel methods and many other related techniques.

**Accord.MachineLearning:** Support Vector Machines, Decision Trees, Naive Bayesian models, K-means, Gaussian Mixture models and general algorithms such as Ransac, Cross-validation and Grid-Search for machine-learning applications.

**Accord.Neuro:** Neural learning algorithms such as Levenberg-Marquardt, Parallel Resilient Backpropagation, the Nguyen-Widrow initialization algorithm, Deep Belief Networks and Restrictured Boltzmann Machines, and many other neural network related items.

### Signal and image processing

**Accord.Imaging:** Contains interest point detectors (such as Harris, SURF, FAST and FREAK), image filters, image matching and image stitching methods, as well as feature extractors such as Histograms of Oriented Gradients and Haralick's textural feature descriptors.

**Accord.Vision:** Real-time face detection and tracking, as well as general methods for detecting, tracking and transforming objects in image streams. Contains cascade definitions, Camshift and Dynamic Template Matching trackers.

### Support libraries

**Accord.Controls:** Histograms, scatterplots and tabular data viewers for scientific applications.

**Accord.Controls.Imaging:** Windows Forms controls to show and handle images.

Contains a convenient ImageBox control which mimics the traditional MessageBox for quickly displaying or inspecting images.

**Accord.Controls.Audio:** Windows Forms controls to display waveforms and audio-related information.

**Accord.Controls.Vision:** Windows Forms components and controls to track head, face and hand movements and other computer vision related tasks.

A complete listing of the framework's namespaces is presented below:

Namespace	Description
Accord	Contains common classes, such as exceptions, events and framework infrastructure classes.
Accord.Audio	Process, transforms, filters and handle audio signals for machine learning and statistical applications.
Accord.Audio.ComplexFilters	Contains frequency-domain signal filters.
Accord.Audio.Filters	Contains time-domain signal processing filters.
Accord.Audio.Formats	Classes used to handle different audio file formats.
Accord.Audio.Generators	Contains specialized signal generators. Generate square signals, sinusoids, pulse and other filters for use in signal processing.

Namespace	Description
Accord.Audio.Windows	Contains audio window functions which can be used to split signals in time.
Accord.Audition.Beat	Contains beat detection algorithms and related methods.
Accord.Controls	Contains useful Windows Forms controls to help creating scientific applications. Includes histograms, scatterplots, wavecharts and tabular data viewers for scientific applications.
Accord.Controls.Vision	Windows Forms components and controls to track head, face and hand movements and other computer vision related tasks.
Accord.DirectSound	Contains audio devices to reproduce and capture sounds exposed through DirectSound.
Accord.Imaging	Contains Interest point detectors (i.e. Harris, SURF and FAST), image matching and image stitching methods.

Namespace	Description
Accord.Imaging.Converters	Contains classes and methods to convert between different image representations, such as between common images, numeric matrices and arrays.
Accord.Imaging.Filters	Contains the image processing filters such as the Wavelet transform, stereo rectification, image blending and point markers.
Accord.Imaging.Moments	Contains image moments calculators such as central and raw moments.
Accord.MachineLearning	Support Vector Machines, Decision Trees, Naive Bayesian models, K-means, Gaussian Mixture models and general algorithms such as Ransac, Cross-validation and Grid-Search for machine-learning applications.
Accord.MachineLearning.Bayes	Contains discrete and continuous density Naive Bayes models for pattern recognition and concept learning. Supports a wide diversity of probabilistic distributions.

Namespace	Description
Accord.MachineLearning.Boosting	Contains Boosting related techniques for creating classifier ensembles and other composition models.
Accord.MachineLearning.Boosting.Learners	Contains Boosting related learning for training classifier ensembles and other composition models.
Accord.MachineLearning.DecisionTrees	Contains discrete and continuous Decision Trees, with support for automatic code generation.
Accord.MachineLearning.DecisionTrees.Learning	Contains Decision Tree learning algorithms such as the ID3 and C4.5.
Accord.MachineLearning.DecisionTrees.Pruning	
Accord.MachineLearning.Geometry	Contains methods for robust estimation of geometry entities.
Accord.MachineLearning.Structures	Contains specialized search structures, such as K-dimensional Trees.

Namespace	Description
Accord.MachineLearning.VectorMachines	Contains classes related to Support Vector Machines (SVMs). Contains linear machines, kernel machines, multi-class machines, SVM-DAGs (Directed Acyclic Graphs), multi-label classification and also offers support for the probabilistic output calibration of SVM outputs.
Accord.MachineLearning.VectorMachines.Learning	Contains algorithms for training Support Vector Machines (SVMs).
Accord.Math	Mathematics, including matrix algebra and numeric optimization.
Accord.Math.Comparers	
Accord.Math.ComplexExtensions	Contains extension methods to operate over Complex numbers.
Accord.Math.Decompositions	Contains numerical decompositions such as QR, SVD, LU, Cholesky, and NMF with specialized definitions for most .NET data types: float, double, and decimals.
Accord.Math.Differentiation	Contains methods for the automatic differentiation of mathematical formulas, such as the Finite Differences method.



Namespace	Description
Accord.Math.Environments	Contains algorithm environments you can inherit from and let your code be similar to famous environments such as R and Octave.
Accord.Math.Geometry	Contains geometry-related classes. Can identify convex-hulls, detect curvatures and extract convexity defects. When used together with the Imaging and Vision namespaces, can create finger detection components.
Accord.Math.Kinematics	Contains classes to model complex kinematic chains, useful for robotic applications.
Accord.Math.Optimization	Contains classes for constrained and unconstrained optimization. Includes Conjugate Gradient (CG), BroydenFletcherGoldfarb-Shanno (BFGS), and the Goldfarb-Idnani solver for Quadratic Programming (QP) problems.
Accord.Math.Wavelets	Contains Wavelet transforms such as the Cohen-Daubechies-Feauveau and the Haar Wavelet transforms.

Namespace	Description
Accord.Neuro	Neural learning algorithms such as Levenberg-Marquardt, Parallel Resilient Backpropagation, initialization procedures such as Nguyen-Widrow and Deep Learning models, such as Restricted Boltzmann Machines and Deep Belief Networks.
Accord.Neuro.ActivationFunctions	Contains different activation functions for artificial neurons.
Accord.Neuro.Layers	Contains different layer architectures for artificial neural networks.
Accord.Neuro.Learning	Contains neural network learning algorithms such as the Levenberg-Marquardt (LM) with Bayesian Regularization and the Resilient Backpropagation (RProp) for multi-layer networks. This namespace extends the AForge.Neuro namespace of the AForge.NET project.
Accord.Neuro.Networks	Contains different neural network architectures, such as specialized architectures for deep learning and Boltzmann machines.

Namespace	Description
Accord.Neuro.Neurons	Contains different kinds of artificial neurons.
Accord.Neuro.Visualization	Contains methods to visualize information drawn from neural networks.
Accord.Statistics	Statistics, including probability distributions, regression models and hypothesis testing.
Accord.Statistics.Analysis	Contains many statistical analysis, such as PCA, LDA, KPCA, KDA, PLS, IDA, Logistic Regression and Stepwise Logistic Regression Analyses. Also contains performance assessment analysis such as contingency tables and ROC curves.
Accord.Statistics.Analysis.ContrastFunctions	Contains contrast functions to be used with Independent Component Analysis (ICA).
Accord.Statistics.Distributions	Contains more than 30+ statistical distributions, with support for most probability distribution measures and fitting (estimation) methods.
Accord.Statistics.Distributions.DensityKernels	

Namespace	Description
Accord.Statistics.Distributions.Fitting	Contains special options which can be used in distribution fitting (estimation) methods.
Accord.Statistics.Distributions.Multivariate	Contains a multivariate distributions such as the multivariate Normal, Multinomial, Independent, Joint and Mixture distributions.
Accord.Statistics.Distributions.Univariate	Contains univariate distributions such as Normal, Cauchy, Hypergeometric, Poisson, Bernoulli, and specialized distributions such as the Kolmogorov-Smirnov, Nakagami, Weibull, and Von-Mises distributions.
Accord.Statistics.Filters	Contains data processing filters, such as data normalization, discretization, equalization, selection and projection filters.
Accord.Statistics.Formats	Contains readers for specialized formats, such as LibSVM's sparse format and Microsoft (c) Excel formats.

Namespace	Description
Accord.Statistics.Kernels	Contains more than 30+ kernel functions for machine learning and statistical applications. Kernel functions are used in kernel methods such as the Support Vector Machine (SVM).
Accord.Statistics.Kernels.Sparse	Contains kernel function able to deal with sparse data in LibSVM's format.
Accord.Statistics.Links	Contains link functions for generalized linear models, such as the Logit, the Probit and Cauchit link functions.
Accord.Statistics.Models	Contains link functions for generalized linear models, such as the Logit, the Probit and Cauchit link functions.
Accord.Statistics.Links	Contains statistical models with direct applications in machine learning, such as Hidden Markov Models, Conditional Random Fields, Hidden Conditional Random Fields and linear and logistic regressors.
Accord.Statistics.Models.Fields	Contains classes related to Conditional Random Fields, Hidden Conditional Random Fields and their learning algorithms.

Namespace	Description
Accord.Statistics.Models.Fields.Features	Contains CRF feature functions such as Emission, Transition, First and Second Moments features.
Accord.Statistics.Models.Fields.Functions	Contains potential functions for CRFs and HCRFs.
Accord.Statistics.Models.Fields.Functions.Specialized	
Accord.Statistics.Models.Fields.Learning	Contains learning algorithms for CRFs and HCRFs, such as Conjugate Gradient, L-BFGS and RProp-based learning.
Accord.Statistics.Models.Markov	Contains classes related to Hidden Markov Models and their learning algorithms. Offers support for both discrete and continuous-density models, as well as Markov classifiers and threshold models for sequence rejection.
Accord.Statistics.Models.Markov.Hybrid	
Accord.Statistics.Models.Markov.Learning	Contains learning algorithms such as Baum-Welch.
Accord.Statistics.Models.Markov.Topology	Contains topologies for HMMs, such as Forward-only and Ergodic topologies.
Accord.Statistics.Models.Regression	Contains statistical regression models such as logistic and linear regressions.

Namespace	Description
Accord.Statistics.Models.Regression.Fitting	Fitting (learning) algorithms for regression models, such as the Iterative Reweighted Least Squares for standard logistic regressors and the Lower-Bound approximator for multinomial logistic regression.
Accord.Statistics.Models.Regression.Linear	Linear statistical regression models such as simple, polynomial, multiple and multivariate linear regressions.
Accord.Statistics.Moving	Contains classes to estimate moving statistics, i.e. statistics computed within a time frame window.
Accord.Statistics.Running	Contains classes to estimate running statistics, i.e. statistics which should be computed and updated as soon as new data becomes available.

Namespace	Description
Accord.Statistics.Testing	Contains 15+ statistical hypothesis tests, including ANOVA tests, non-parametric tests such as the Kolmogorov-Smirnov test, contingency table tests such as the Kappa test, the Bhapkar and Bowker tests and the more common Chi-Square, Z, F, T and Wald tests.
Accord.Statistics.Testing.Power	Contains methods for power analysis of several related hypothesis tests, including support for automatic sample size estimation.
Accord.Statistics.Visualizations	Contains classes for statistical visualization such as Histograms and Scatterplots.
Accord.Vision	Real-time face detection and tracking, as well as general methods for detecting, tracking and transforming objects in image streams. Contains cascade definitions, Camshift and Dynamic Template Matching trackers.



Namespace	Description
Accord.Vision.Detection	Contains object detectors such as the Viola-Jones (Haar feature) method. The Haar cascades are completely compatible with OpenCV generated definitions and the assembly comes with direct support for bundled definitions for face and nose templates.
Accord.Vision.Detection.Cascades	Built-in Haar cascade definitions to use with the Haar feature object detector. Those definitions can be called directly from code without need for loading XML files.
Accord.Vision.Tracking	Contains classes for object tracking. Include the Camshift algorithm, color segmentation-based trackers and dynamic template matching trackers.

### A.3 Basic linear algebra - DotNetMatrix library

Accord.NET lacks in the area of linear algebra. Therefore we used a combination of Accord.NET and a linear algebra library called DotNetMatrix.

DotNetMatrix is a Microsoft.NET C# library that is used for basic linear algebra operations. The classes in this library give a basic linear algebra package for .NET. It provides user-level C# classes for constructing and manipulating real, dense matrices.

It is meant to provide sufficient functionality for routine problems, packaged in a way that is natural and understandable to non-experts. That said, it is a port of a public domain Java matrix library, called JAMA.

### A.3.1 Background

Currently, the developer of this library (Paul Selormey) works for a small GIS company in Japan developing GIS components for application developers. Coordinate Transformation and therefore Affine Transformation is a very basic part of the development efforts. Recently, he was assigned a task of designing and implementing a new GIS system for the .NET framework with the ability to easily port to Java and other frameworks. He decided to make maximum use of matrix-based affine transformation, which is also a requirement for the OpenGIS Coordinate Transformation Specifications.

Then, he discovered that the Matrix class provided as part of the GDI+ is the .NET implements the affine transformations in a manner different from standard specifications. In short, while the standard 2D Coordinate System Affine Transformation Matrix is define as:

$$\begin{pmatrix} a_{11} & a_{12} & a_{1,3} \\ a_{21} & a_{22} & a_{2,3} \\ 0 & 0 & 1 \end{pmatrix}$$

The matrix defined by GDI+ is:

$$\begin{pmatrix} a_{11} & a_{12} & 0 \\ a_{21} & a_{22} & 0 \\ a_{31} & a_{32} & 1 \end{pmatrix}$$

The effect is that most affine transformations with GDI+ Matrix class will not conform to standard or specifications. For instance, by standard (and mathematically) anti-clockwise (or counter-clockwise) rotations are considered positive but must be negative when using the GDI+ classes. To solve this problem, he decided to implement a standard affine transformation matrix and found this small Java general matrix library JAMA. The presented classes are ported from the JAMA with .NET specific improvements like operator overloading etc. The library is referred to as DotNetMatrix, which provides linear algebra operations.

### A.3.2 Using the library

DotNetMatrix is comprised of the following six C# classes:

- GeneralMatrix
- CholeskyDecomposition
- LUDecomposition
- QRDecomposition
- SingularValueDecomposition
- EigenvalueDecomposition

The GeneralMatrix class provides the fundamental operations of numerical linear algebra. Various constructors create matrices from two dimensional arrays of double precision floating point numbers. Various gets and sets (properties) provide access to submatrices and matrix elements. The basic arithmetic operations include matrix addition and multiplication, matrix norms and selected element-by-element array operations. A convenient matrix print method is also included.

Five fundamental matrix decompositions, which consist of pairs or triples of matrices, permutation vectors, and the like, produce results in five decomposition classes. These decompositions are accessed by the GeneralMatrix class to compute solutions of simultaneous linear equations, determinants, inverses and other matrix functions. The five decompositions are:

- Cholesky Decomposition of symmetric, positive definite matrices
- LU Decomposition (Gaussian elimination) of rectangular matrices
- QR Decomposition of rectangular matrices
- Eigenvalue Decomposition of both symmetric and non-symmetric square matrices
- Singular Value Decomposition of rectangular matrices

The DotNetMatrix deals only with real matrices, there is not support for complex matrices. The design of DotNetMatrix represents a compromise between the need for pure and delegant object-oriented design and the need to enable high performance implementations. The following table illustrates a summary of DotNetMatrix library capabilities as shown in Table A.2:

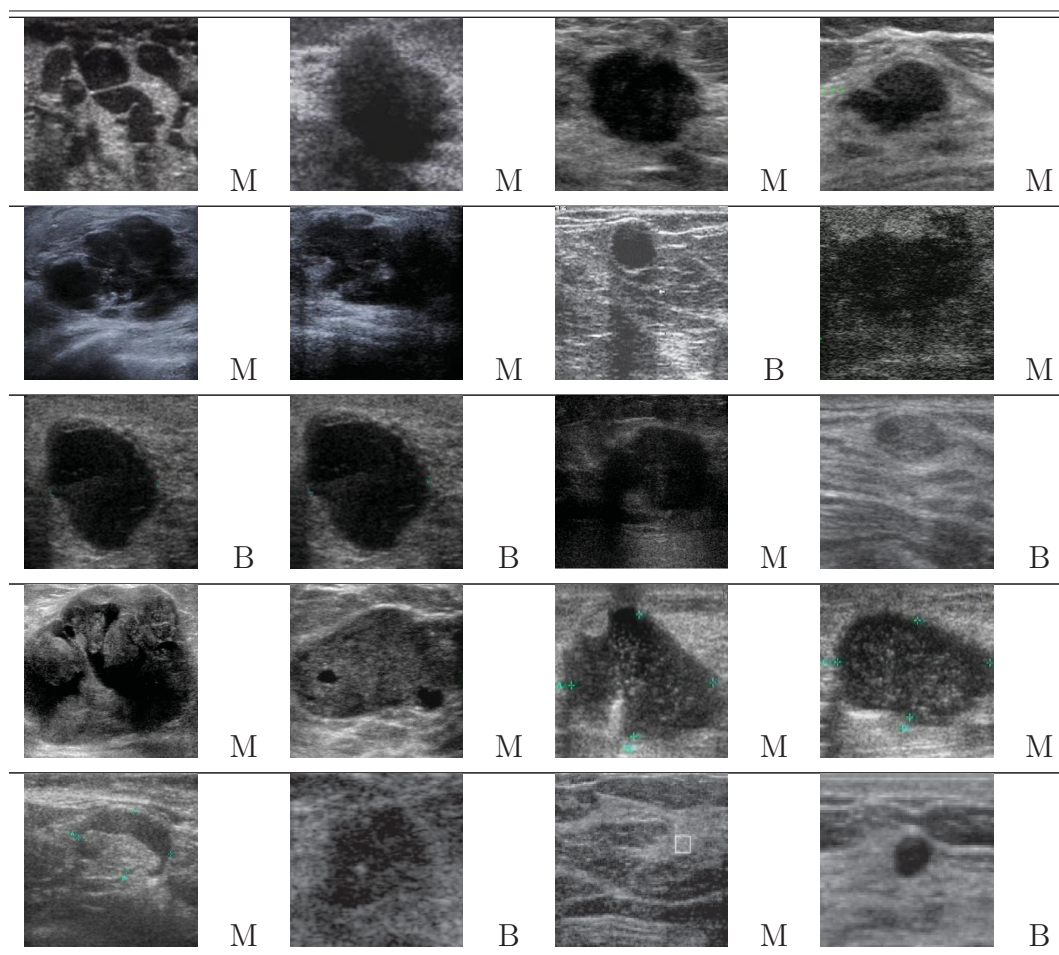
Library	Capabilities
Object Manipulation	
	<ul style="list-style-type: none"> <li>• constructors</li> <li>• set elements</li> <li>• get elements</li> <li>• copy</li> <li>• clone</li> </ul>
Elementary Operations	
	<ul style="list-style-type: none"> <li>• addition</li> <li>• subtraction</li> <li>• multiplications</li> <li>• scalar multiplication</li> <li>• element-wise multiplication</li> <li>• element-wise division</li> <li>• unary minus</li> <li>• transpose</li> <li>• norm</li> </ul>

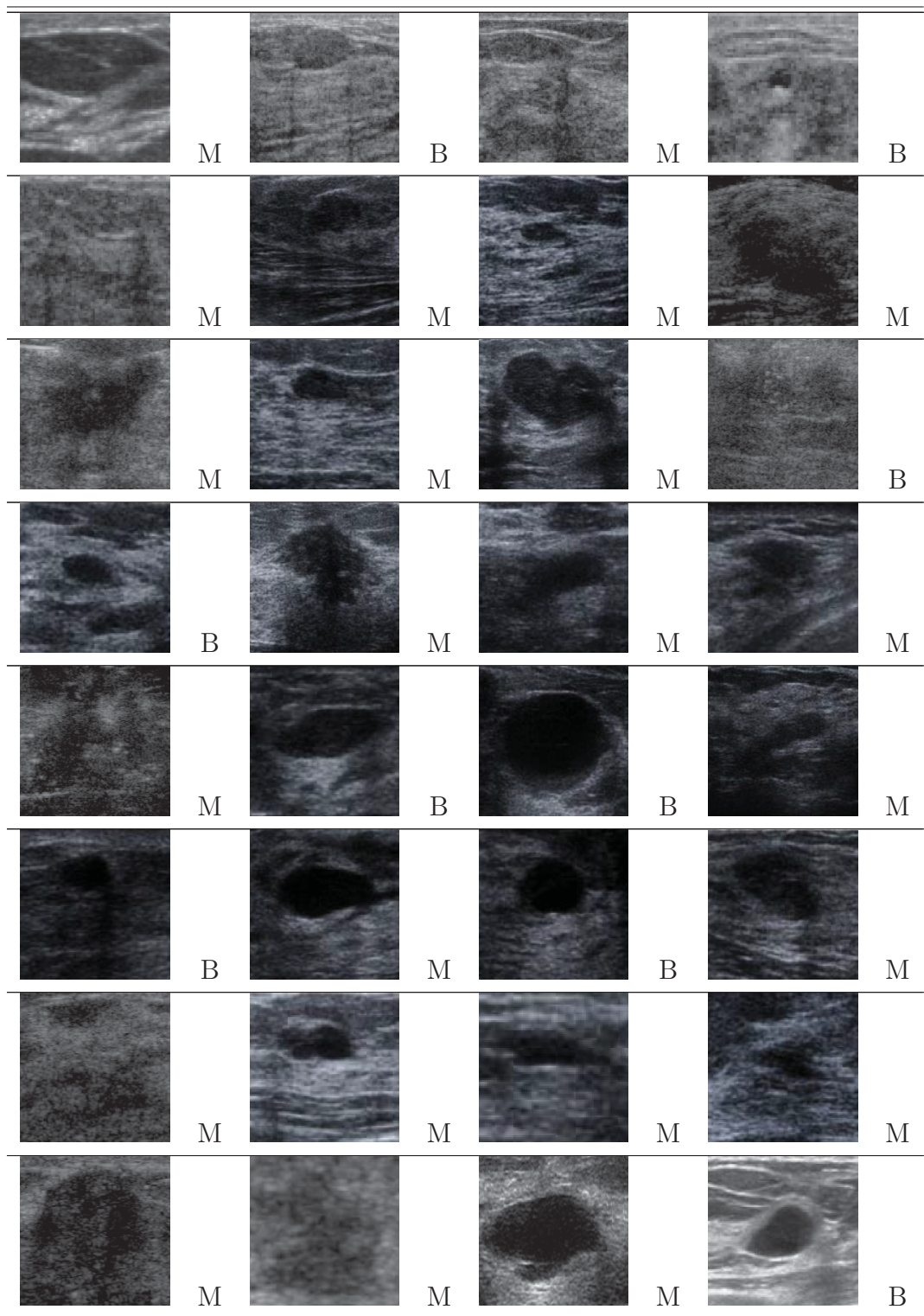
Library	Capabilities
Decompositions	<ul style="list-style-type: none"> <li>• Cholesky</li> <li>• LU</li> <li>• QR</li> <li>• SVD</li> <li>• symmetric eigenvalue</li> <li>• non-symmetric eigenvalue</li> </ul>
Equation Solution	<ul style="list-style-type: none"> <li>• non-singular</li> <li>• least squares</li> </ul>
Derived Quantities	<ul style="list-style-type: none"> <li>• condition</li> <li>• determinant</li> <li>• rank</li> <li>• inverse</li> <li>• pseudoinverse</li> </ul>

Table A.2: DotNetMatrix library capabilities

# Appendix B

## Ultrasound database





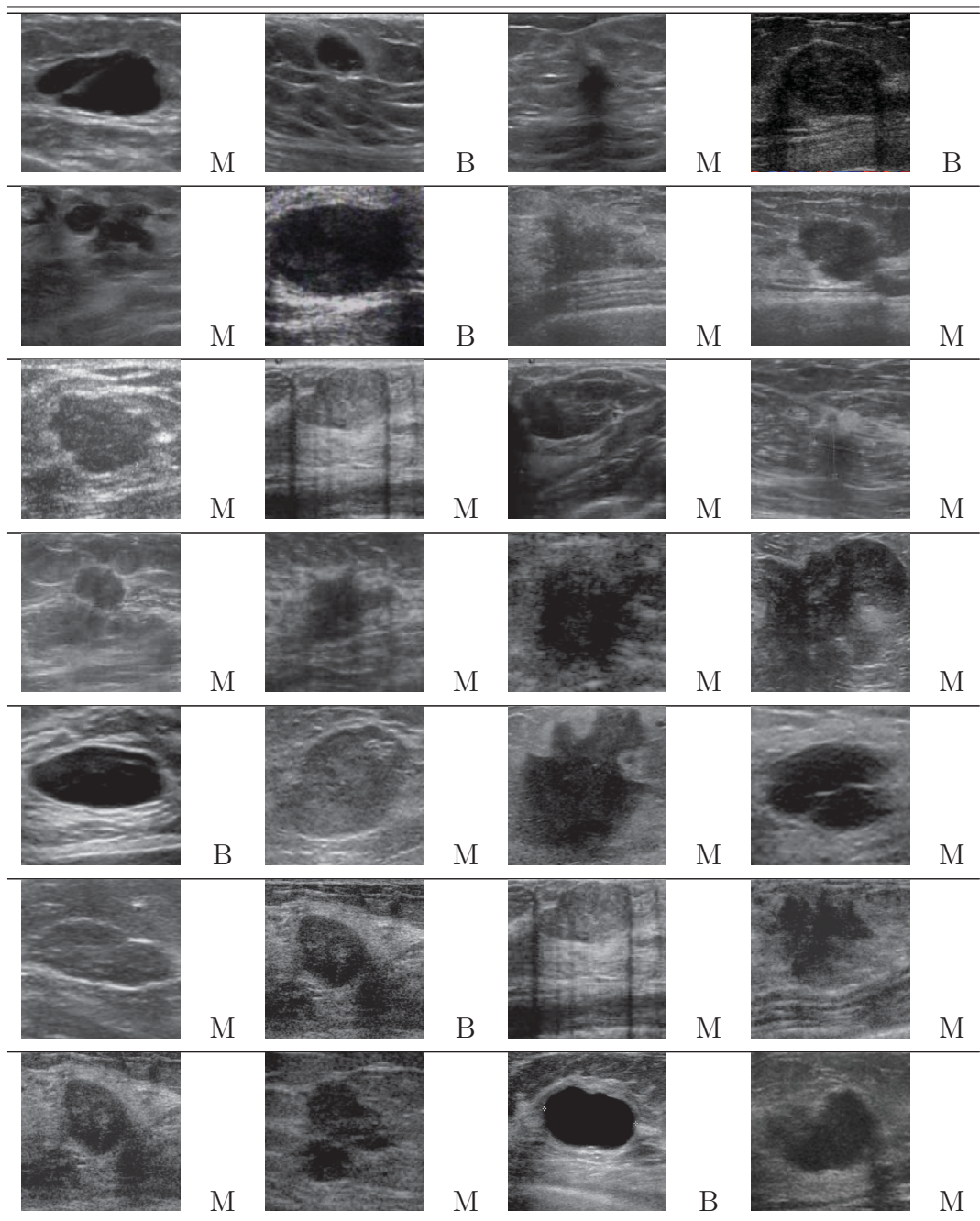


Table B.1: Breast ultrasound database - B: Benign, M: Malignant



# Appendix C

## All Experiments

### C.1 Experiment #1 - Experiment using no pre-processing and using morphological features only

In this experiment, we do not do any pre-processing for ultrasound images. Proposed region growing method is used for segmentation. We used the morphological features that we extracted using MI (mutual information), Sequential Forward Search and Sequential Backward Search methods. For classification, we used our proposed classification method, which uses a combination of FSVM, AdaBoost, ANN and Majority based methods. The selected morphological features are showing in Table C.1. Methods used in each stage of our system are shown in Table C.2.

Table C.1: Experiment #1 - Selected morphological features

#	Morphological Feature
1	Roundness
2	Solidity
3	Convexity
4	TCA Ratio
5	Perimeter
6	Area
7	NSPD
8	Aspect Ratio

Table C.2: Experiment #1 - Methods used in each stage

Stage	Method
Pre-processing	None
Segmentation	Proposed region growing method
Feature Extraction	Morphological features
Feature Selection	MI (mutual information), Sequential Forward Search and Sequential Backward Search
Classification	Our proposed classification method (combination of ANN, AdaBoost, FSVM and Majority base classifier)

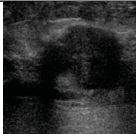
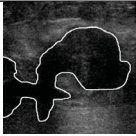
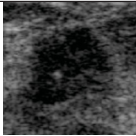
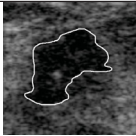
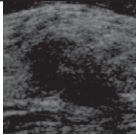
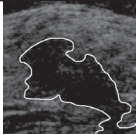
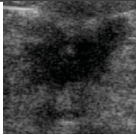
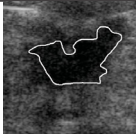
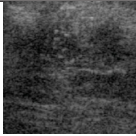
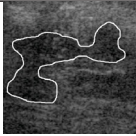
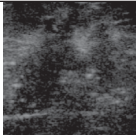
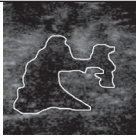
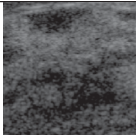
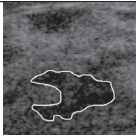
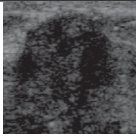
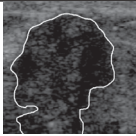
We have performed experiments on our database of 80 patients. For the purpose of this experiment, we only used the 0 o'clock ultrasound images. The results are shown in Table C.3, C.4 and C.5.


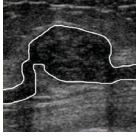
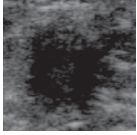
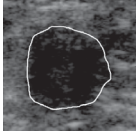
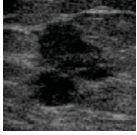
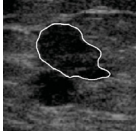
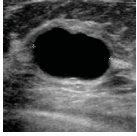

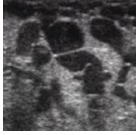

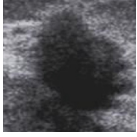

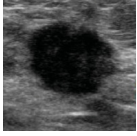
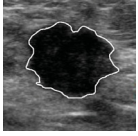
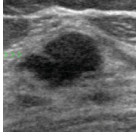
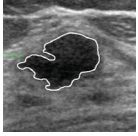
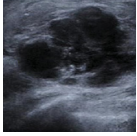



Table C.3: Experiment #1 - Results



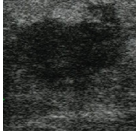

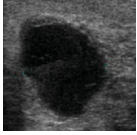

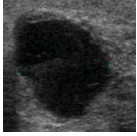

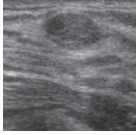



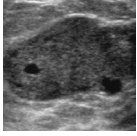
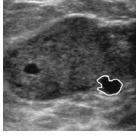
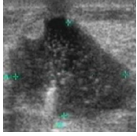
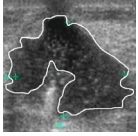
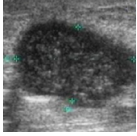
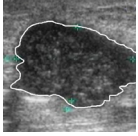
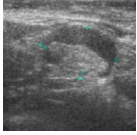
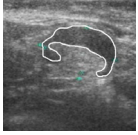
TP	TN	FP	FN	Accuracy%	Specificity%	Sensitivity%	PPV%	NPV%
57	18	2	3	93.75	90.00	95.00	96.61	85.71

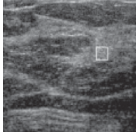

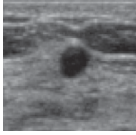

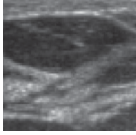
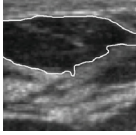
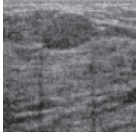
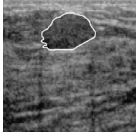
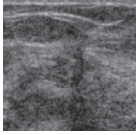
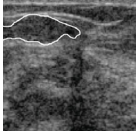
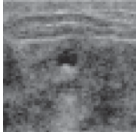
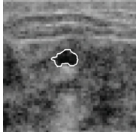
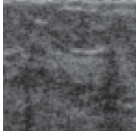

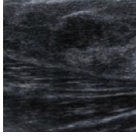
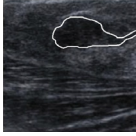
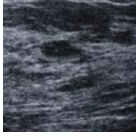

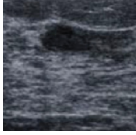

Table C.4: Experiment #1 - Comparison with other methods



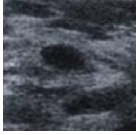



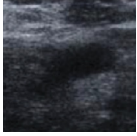

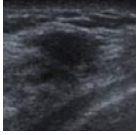

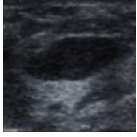

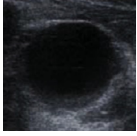

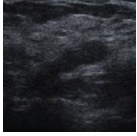

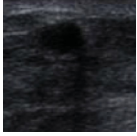



Method	Accuracy
ABUS[51]	88.75%
Hybrid Filtering[145]	92.50%
Our approach	93.75%

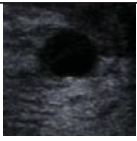

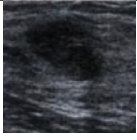

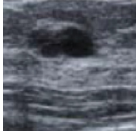
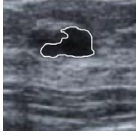
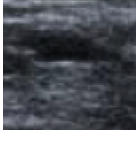

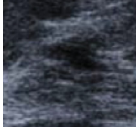

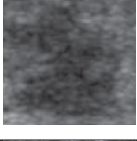
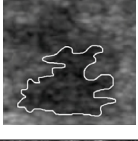
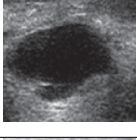
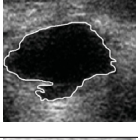
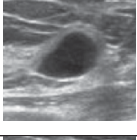





Ultrasound image	Segmented	Classifier output	Gold standard
		Malignant	Malignant
		Malignant	Benign
		Malignant	Malignant
		Malignant	Malignant
		Malignant	Benign
		Malignant	Malignant
		Benign	Malignant
		Malignant	Malignant

Ultrasound image	Segmented	Classifier output	Gold standard
		Malignant	Benign
		Benign	Malignant
		Malignant	Malignant
		Benign	Benign
		Malignant	Malignant
		Malignant	Malignant
		Malignant	Malignant
		Malignant	Malignant
		Malignant	Malignant
		Malignant	Malignant

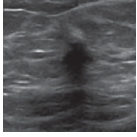

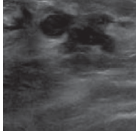

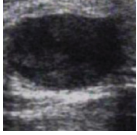
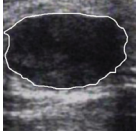
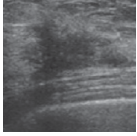
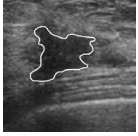
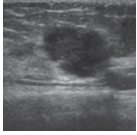
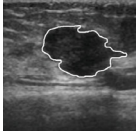
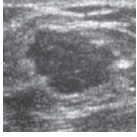
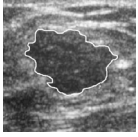
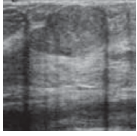
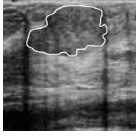
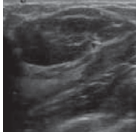

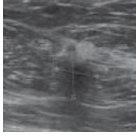

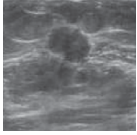
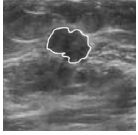
Ultrasound image	Segmented	Classifier output	Gold standard
		Benign	Benign
		Malignant	Malignant
		Benign	Benign
		Benign	Benign
		Benign	Benign
		Malignant	Malignant
		Malignant	Malignant
		Malignant	Malignant
		Malignant	Malignant
		Malignant	Malignant

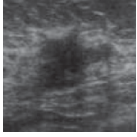
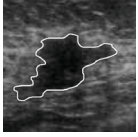


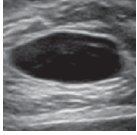

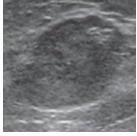

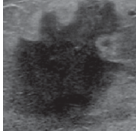

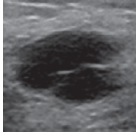
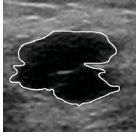
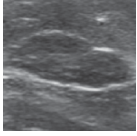

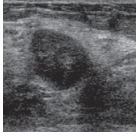

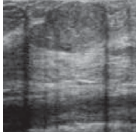
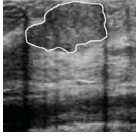
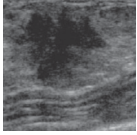

Ultrasound image	Segmented	Classifier output	Gold standard
		Malignant	Malignant
		Benign	Benign
		Malignant	Malignant
		Benign	Benign
		Malignant	Malignant
		Benign	Benign
		Malignant	Malignant
		Malignant	Malignant
		Malignant	Malignant
		Malignant	Malignant

Ultrasound image	Segmented	Classifier output	Gold standard
		Malignant	Malignant
		Benign	Benign
		Malignant	Malignant
		Malignant	Malignant
		Malignant	Malignant
		Benign	Benign
		Benign	Benign
		Malignant	Malignant
		Benign	Benign
		Malignant	Malignant

Ultrasound image	Segmented	Classifier output	Gold standard
		Benign	Benign
		Malignant	Malignant
		Malignant	Malignant
		Malignant	Malignant
		Malignant	Malignant
		Malignant	Malignant
		Malignant	Malignant
		Benign	Benign
		Malignant	Malignant
		Benign	Benign



Ultrasound image	Segmented	Classifier output	Gold standard
		Malignant	Malignant
		Malignant	Malignant
		Benign	Benign
		Malignant	Malignant
		Malignant	Malignant
		Malignant	Malignant
		Malignant	Malignant
		Malignant	Malignant
		Malignant	Malignant
		Malignant	Malignant

Ultrasound image	Segmented	Classifier output	Gold standard
		Malignant	Malignant
		Malignant	Malignant
		Benign	Benign
		Malignant	Malignant
		Malignant	Malignant
		Malignant	Malignant
		Malignant	Malignant
		Benign	Benign
		Malignant	Malignant
		Malignant	Malignant

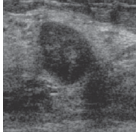
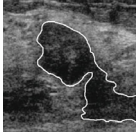
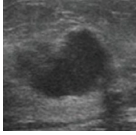

Ultrasound image	Segmented	Classifier output	Gold standard
		Malignant	Malignant
		Malignant	Malignant

Table C.5: Experiment #1 - Output

## C.2 Experiment #2 - Experiment using fuzzy logic for de-noising and using morphological features only

In this experiment, we used Fuzzy logic for pre-processing of ultrasound images. Proposed region growing method is used for Segmentation. We used the morphological features that we extracted using MI (mutual information), Sequential Forward Search and Sequential Backward Search methods. For classification, we used our proposed classification method, which uses a combination of FSVM, AdaBoost, ANN and Majority based methods. The selected morphological features are showing in Table C.6. Methods used in each stage of our system are shown in Table C.7.

Table C.6: Experiment #2 - Selected morphological features

#	Morphological Feature
1	Roundness
2	Solidity
3	Convexity
4	TCA Ratio
5	Perimeter
6	Area
7	NSPD
8	Aspect Ratio

Table C.7: Experiment #2 - Methods used in each stage

Stage	Method
Pre-processing	Fuzzy method
Segmentation	Proposed region growing method
Feature Extraction	Morphological features
Feature Selection	MI (mutual information), Sequential Forward Search and Sequential Backward Search
Classification	Our proposed classification method (combination of ANN, AdaBoost, FSVM and Majority base classifier)


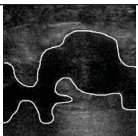
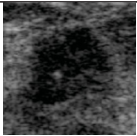
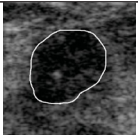
We have performed experiments on the database of 80 patients. For the purpose of this experiment, we only used the 0'clock ultrasound images. The results are given in Table C.8, C.9 and C.10.

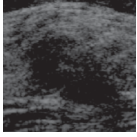
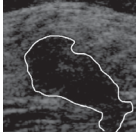
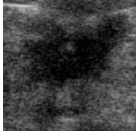
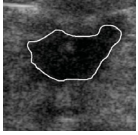
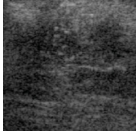
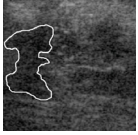
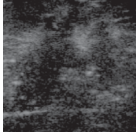
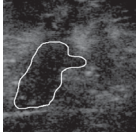
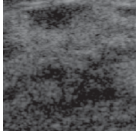
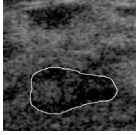
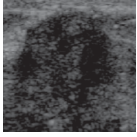
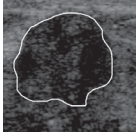


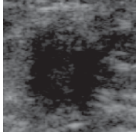
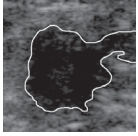
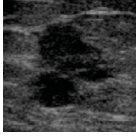

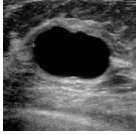

Table C.8: Experiment #2 - Results

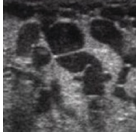

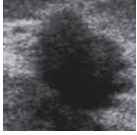
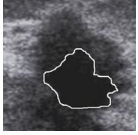
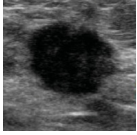

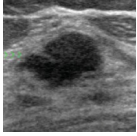
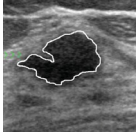
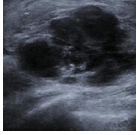



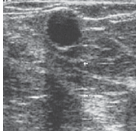

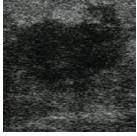

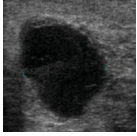

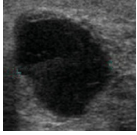

TP	TN	FP	FN	Accuracy%	Specificity%	Sensitivity%	PPV%	NPV%
58	18	1	3	95.00	94.74	95.08	98.30	85.71

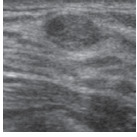



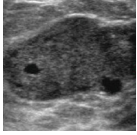
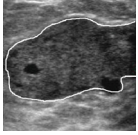
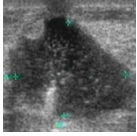
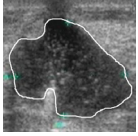
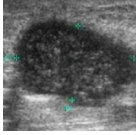
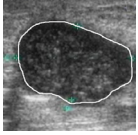
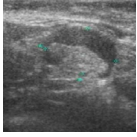
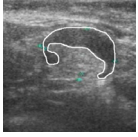
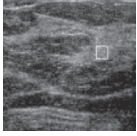

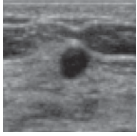

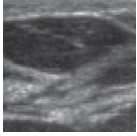
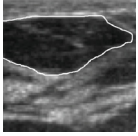
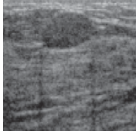

Table C.9: Experiment #2 - Comparison with other methods

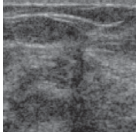
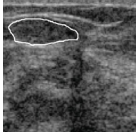
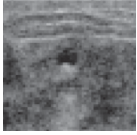
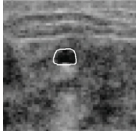
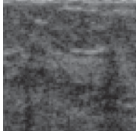

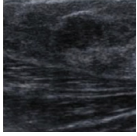
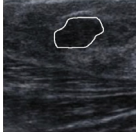
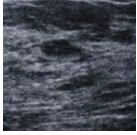

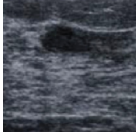
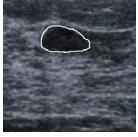


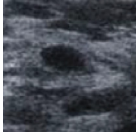



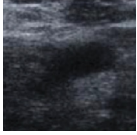

Method	Accuracy
ABUS[51]	88.75%
Hybrid Filtering[145]	92.50%
Our approach	95.00%

Ultrasound image	Segmented	Classifier output	Gold standard
		Malignant	Malignant
		Malignant	Benign

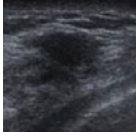



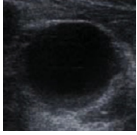
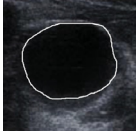
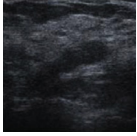

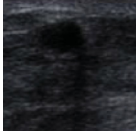

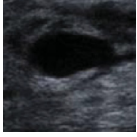


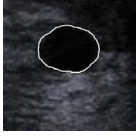
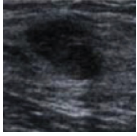

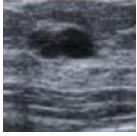
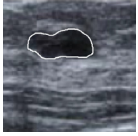


Ultrasound image	Segmented	Classifier output	Gold standard
		Malignant	Malignant
		Malignant	Malignant
		Malignant	Benign
		Malignant	Malignant
		Benign	Malignant
		Malignant	Malignant
		Malignant	Benign
		Malignant	Malignant
		Malignant	Malignant
		Benign	Benign

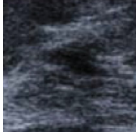

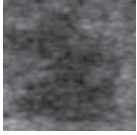
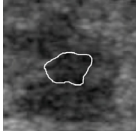
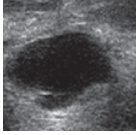
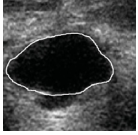
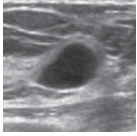

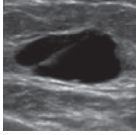

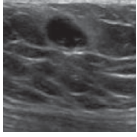

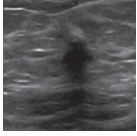
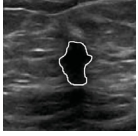
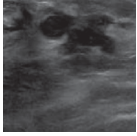

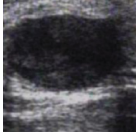
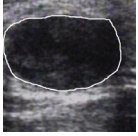
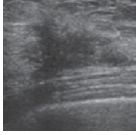

Ultrasound image	Segmented	Classifier output	Gold standard
		Malignant	Malignant
		Malignant	Malignant
		Malignant	Malignant
		Malignant	Malignant
		Malignant	Malignant
		Malignant	Malignant
		Benign	Benign
		Malignant	Malignant
		Benign	Benign
		Benign	Benign

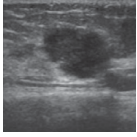
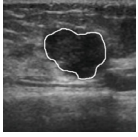
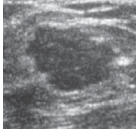
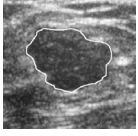
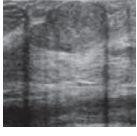
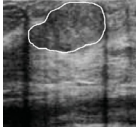




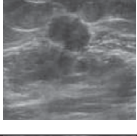
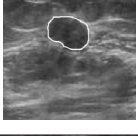
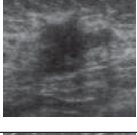

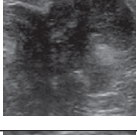

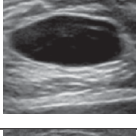

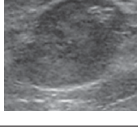

Ultrasound image	Segmented	Classifier output	Gold standard
		Benign	Benign
		Malignant	Malignant
		Malignant	Malignant
		Malignant	Malignant
		Malignant	Malignant
		Malignant	Malignant
		Malignant	Malignant
		Benign	Benign
		Malignant	Malignant
		Benign	Benign

Ultrasound image	Segmented	Classifier output	Gold standard
		Malignant	Malignant
		Benign	Benign
		Malignant	Malignant
		Malignant	Malignant
		Malignant	Malignant
		Malignant	Malignant
		Malignant	Malignant
		Benign	Benign
		Malignant	Malignant
		Malignant	Malignant



Ultrasound image	Segmented	Classifier output	Gold standard
		Malignant	Malignant
		Benign	Benign
		Benign	Benign
		Malignant	Malignant
		Benign	Benign
		Malignant	Malignant
		Benign	Benign
		Malignant	Malignant
		Malignant	Malignant
		Malignant	Malignant

Ultrasound image	Segmented	Classifier output	Gold standard
		Malignant	Malignant
		Malignant	Malignant
		Malignant	Malignant
		Benign	Benign
		Malignant	Malignant
		Benign	Benign
		Malignant	Malignant
		Malignant	Malignant
		Benign	Benign
		Malignant	Malignant

Ultrasound image	Segmented	Classifier output	Gold standard
		Malignant	Malignant
		Malignant	Malignant
		Malignant	Malignant
		Malignant	Malignant
		Malignant	Malignant
		Malignant	Malignant
		Malignant	Malignant
		Malignant	Malignant
		Benign	Benign
		Malignant	Malignant

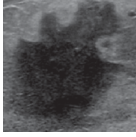

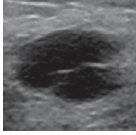

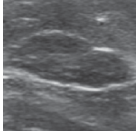
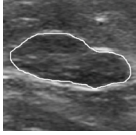
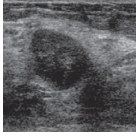

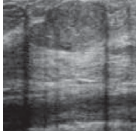

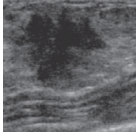

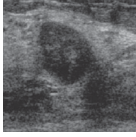

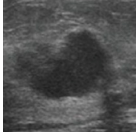

Ultrasound image	Segmented	Classifier output	Gold standard
		Malignant	Malignant
		Malignant	Malignant
		Malignant	Malignant
		Benign	Benign
		Malignant	Malignant
		Malignant	Malignant
		Malignant	Malignant
		Malignant	Malignant

Table C.10: Experiment #2 - Output

### C.3 Experiment #3 - Experiment using fuzzy logic for pre-processing and using morphological and texture features

In this experiment, we used fuzzy logic for pre-processing of ultrasound images. Segmentation is carried out by proposed region growing approach. We used the morphological features that we extracted using MI (mutual information), Sequential Forward Search and Sequential Backward Search. We also included texture features by Chen et al. [22]. For classification, we used our proposed classification method, which uses a combination of FSVM, AdaBoost, ANN and Majority based methods. The selected morphological features and texture features are showing in Table C.11. Methods used in each stage of our system are shown in Table C.12.

Table C.11: Experiment #3 - Selected features (A: 77 auto-covariance matrix; B: SGLDM; C: GLDM; D: BDIP; E: BVLC; F: NGTDM)

#	Morphological Feature	#	Texture Features
1	Roundness	1	AD
2	Solidity	2	ADE
3	Convexity	3	AEF
4	TCA Ratio	4	ABCF
5	Perimeter	5	A
6	Area	6	ADF
7	NSPD	7	ACDE
8	Aspect Ratio		

Table C.12: Experiment #3 - Methods used in each stage

Stage	Method
Pre-processing	Fuzzy method
Segmentation	Proposed region growing method
Feature Extraction	Morphological and texture features
Feature Selection	MI (mutual information), Sequential Forward Search and Sequential Backward Search
Classification	Our proposed classification method (combination of ANN, AdaBoost, FSVM and Majority base classifier)


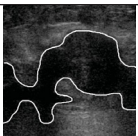
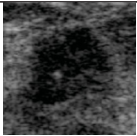
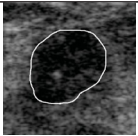
We have performed experiments on the database of 80 patients. For the purpose of this experiment, we only used the 0 o'clock ultrasound images. The results are given in Table C.13, C.14 and C.15.

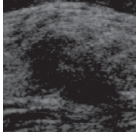
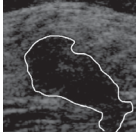
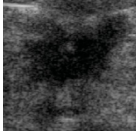
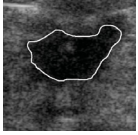
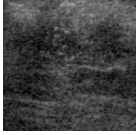
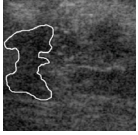
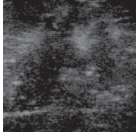
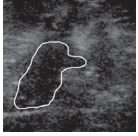
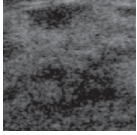
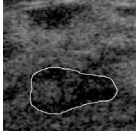
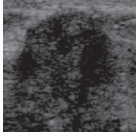
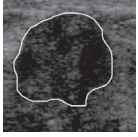


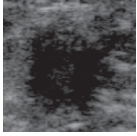
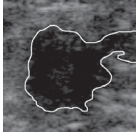
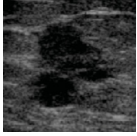

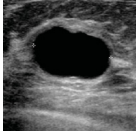

Table C.13: Experiment #3 - Results

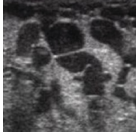
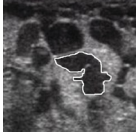
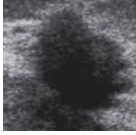
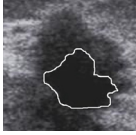
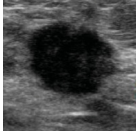
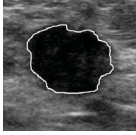
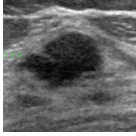
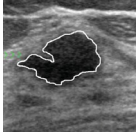
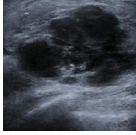



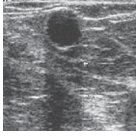

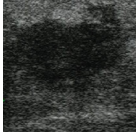

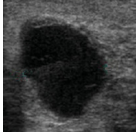
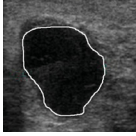
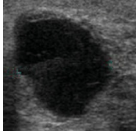

TP	TN	FP	FN	Accuracy%	Specificity%	Sensitivity%	PPV%	NPV%
58	19	1	2	96.25	95.00	96.67	98.30	90.48

Table C.14: Experiment #3 - Comparison with other methods

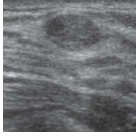



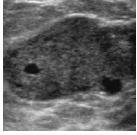
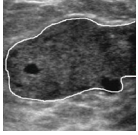
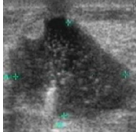
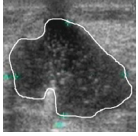
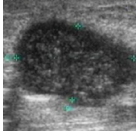
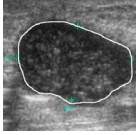
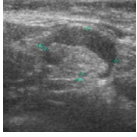
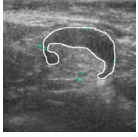
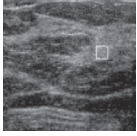

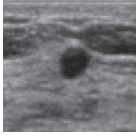

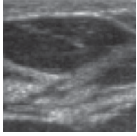
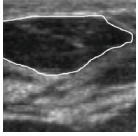
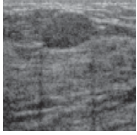

Method	Accuracy
ABUS[51]	88.75%
Hybrid Filtering[145]	92.50%
Our approach	96.25%

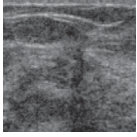
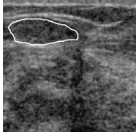
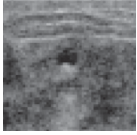
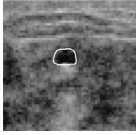
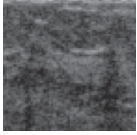

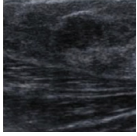
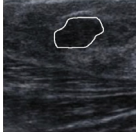
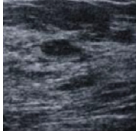

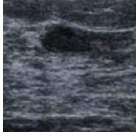
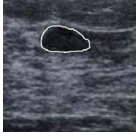


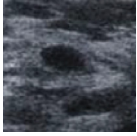



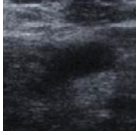

Ultrasound image	Segmented	Classifier output	Gold standard
		Malignant	Malignant
		Malignant	Benign

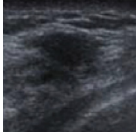



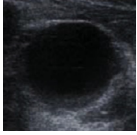
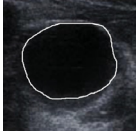
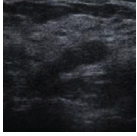

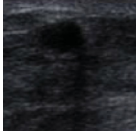

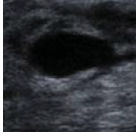


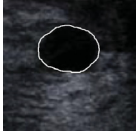
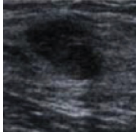

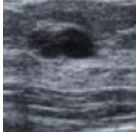
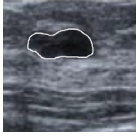


Ultrasound image	Segmented	Classifier output	Gold standard
		Malignant	Malignant
		Malignant	Malignant
		Malignant	Benign
		Malignant	Malignant
		Benign	Malignant
		Malignant	Malignant
		Malignant	Benign
		Malignant	Malignant
		Malignant	Malignant
		Benign	Benign

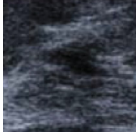

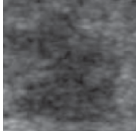
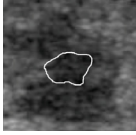
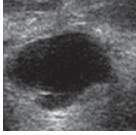
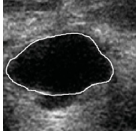
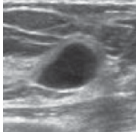
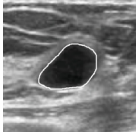
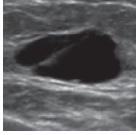

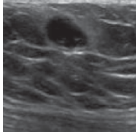
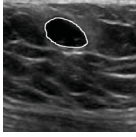
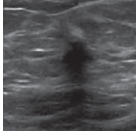
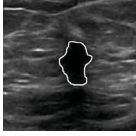
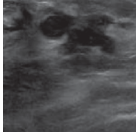

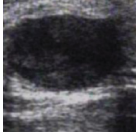
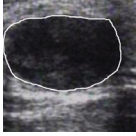
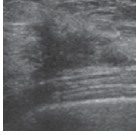

Ultrasound image	Segmented	Classifier output	Gold standard
		Malignant	Malignant
		Malignant	Malignant
		Malignant	Malignant
		Malignant	Malignant
		Malignant	Malignant
		Malignant	Malignant
		Benign	Benign
		Malignant	Malignant
		Benign	Benign
		Benign	Benign

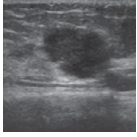
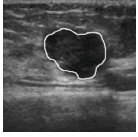
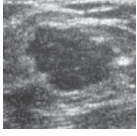
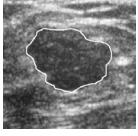
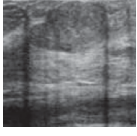
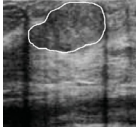




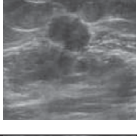
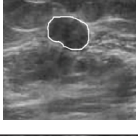
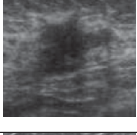

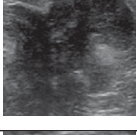

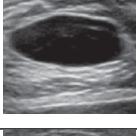

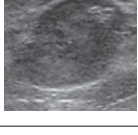



Ultrasound image	Segmented	Classifier output	Gold standard
		Benign	Benign
		Malignant	Malignant
		Malignant	Malignant
		Malignant	Malignant
		Malignant	Malignant
		Malignant	Malignant
		Malignant	Malignant
		Benign	Benign
		Malignant	Malignant
		Benign	Benign

Ultrasound image	Segmented	Classifier output	Gold standard
		Malignant	Malignant
		Benign	Benign
		Malignant	Malignant
		Malignant	Malignant
		Malignant	Malignant
		Malignant	Malignant
		Malignant	Malignant
		Benign	Benign
		Malignant	Malignant
		Malignant	Malignant

Ultrasound image	Segmented	Classifier output	Gold standard
		Malignant	Malignant
		Benign	Benign
		Benign	Benign
		Malignant	Malignant
		Benign	Benign
		Malignant	Malignant
		Benign	Benign
		Malignant	Malignant
		Malignant	Malignant
		Malignant	Malignant

Ultrasound image	Segmented	Classifier output	Gold standard
		Malignant	Malignant
		Malignant	Malignant
		Malignant	Malignant
		Benign	Benign
		Malignant	Malignant
		Benign	Benign
		Malignant	Malignant
		Malignant	Malignant
		Benign	Benign
		Malignant	Malignant

Ultrasound image	Segmented	Classifier output	Gold standard
		Malignant	Malignant
		Malignant	Malignant
		Malignant	Malignant
		Malignant	Malignant
		Malignant	Malignant
		Malignant	Malignant
		Malignant	Malignant
		Malignant	Malignant
		Benign	Benign
		Malignant	Malignant

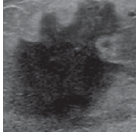
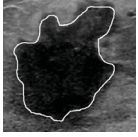
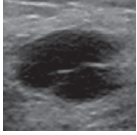

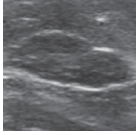
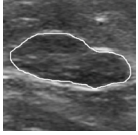
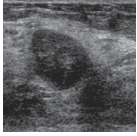

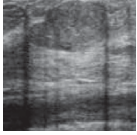

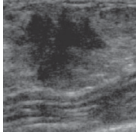





Ultrasound image	Segmented	Classifier output	Gold standard
		Malignant	Malignant
		Malignant	Malignant
		Malignant	Malignant
		Benign	Benign
		Malignant	Malignant
		Malignant	Malignant
		Malignant	Malignant
		Malignant	Malignant

Table C.15: Experiment #3 - Output

## C.4 Experiment #4 - Experiment using fuzzy logic and compounding for de-noising and using morphological and texture features

In this experiment, we used fuzzy logic for pre-processing of ultrasound images. We also used compounding of three images of each patient (9 o'clock, 0 o'clock and 3 o'clock) and performed compounding on the images. Proposed region growing method is used for Segmentation. We used the morphological features that we extracted using MI (mutual information), Sequential Forward Search and Sequential Backward Search methods. We also included texture features by Chen et al. [22]. For classification, we used our proposed classification method, which uses a combination of FSVM, AdaBoost, ANN and Majority based methods. The selected morphological features and texture features are showing in Table C.16. Methods used in each stage of our system are shown in Table C.17.

Table C.16: Experiment #3 - Selected features (A: 77 auto-covariance matrix; B: SGLDM; C: GLDM; D: BDIP; E: BVLC; F: NGTDM)

#	Morphological Feature	#	Texture Features
1	Roundness	1	AD
2	Solidity	2	ADE
3	Convexity	3	AEF
4	TCA Ratio	4	ABCF
5	Perimeter	5	A
6	Area	6	ADF
7	NSPD	7	ACDE
8	Aspect Ratio		

Table C.17: Experiment #4 - Methods used in each stage

Stage	Method
Pre-processing	Fuzzy method + Compounding
Segmentation	Proposed region growing method
Feature Extraction	Morphological and texture features
Feature Selection	MI (mutual information), Sequential Forward Search and Sequential Backward Search
Classification	Our proposed classification method (combination of ANN, AdaBoost, FSVM and Majority base classifier)


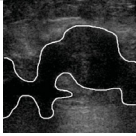
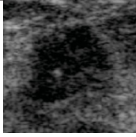
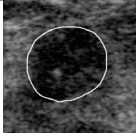
We have performed experiments on the database of 80 patients. The results are given in Table C.18, C.19 and C.20.

Table C.18: Experiment #4 - Results

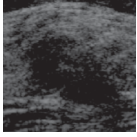
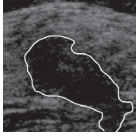
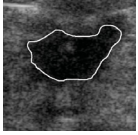
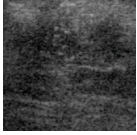
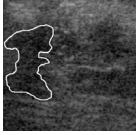
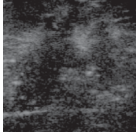
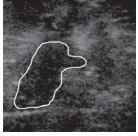
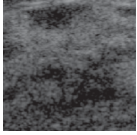
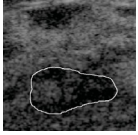
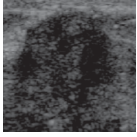
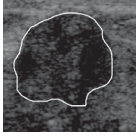


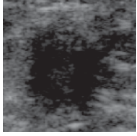
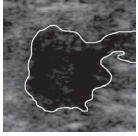
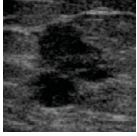

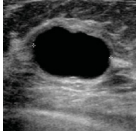

TP	TN	FP	FN	Accuracy%	Specificity%	Sensitivity%	PPV%	NPV%
59	20	0	1	98.75	100.00	98.33	100.00	95.24

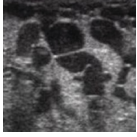

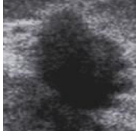
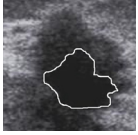
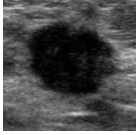

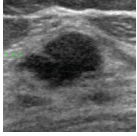
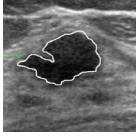
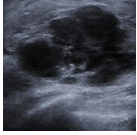



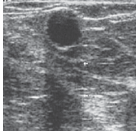

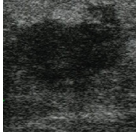

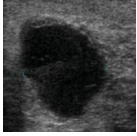

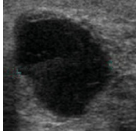

Table C.19: Experiment #4 - Comparison with other methods

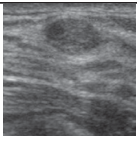
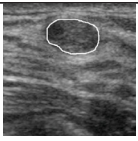


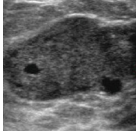
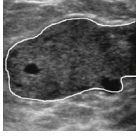
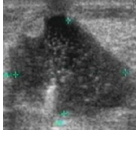
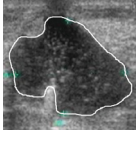
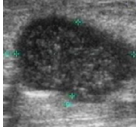
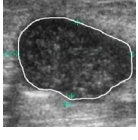
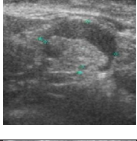

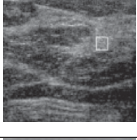
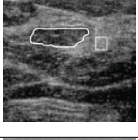
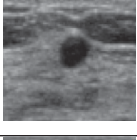

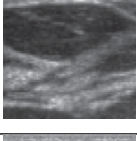
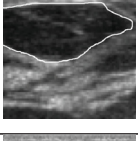
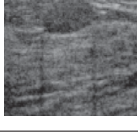

Method	Accuracy
ABUS[51]	88.75%
Hybrid Filtering[145]	92.50%
Our approach	98.75%

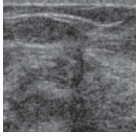
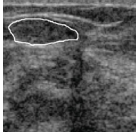
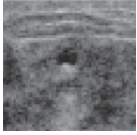
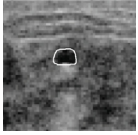
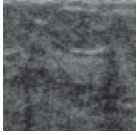

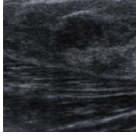
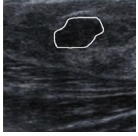
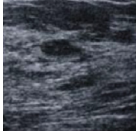

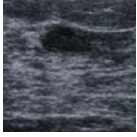
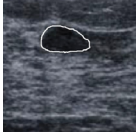


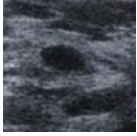



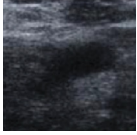

Ultrasound image	Segmented	Classifier output	Gold standard
		Malignant	Malignant
		Benign	Benign

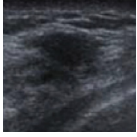



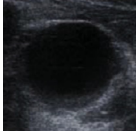
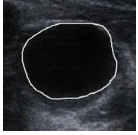
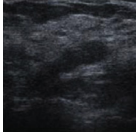

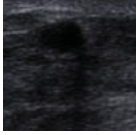

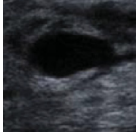


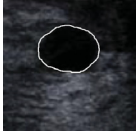
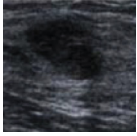

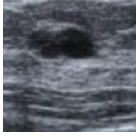
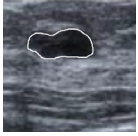




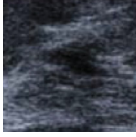

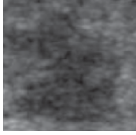
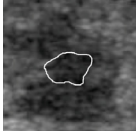
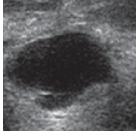
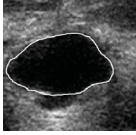
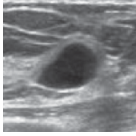
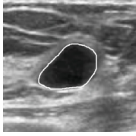
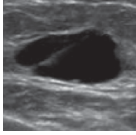

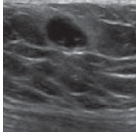
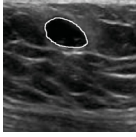
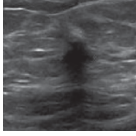
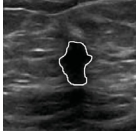
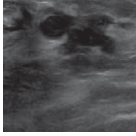

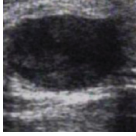
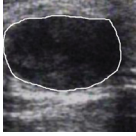
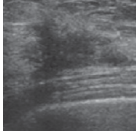

Ultrasound image	Segmented	Classifier output	Gold standard
		Malignant	Malignant
		Malignant	Malignant
		Malignant	Benign
		Malignant	Malignant
		Malignant	Malignant
		Malignant	Malignant
		Benign	Benign
		Malignant	Malignant
		Malignant	Malignant
		Benign	Benign

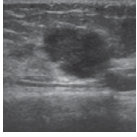
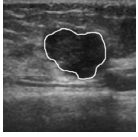
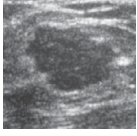
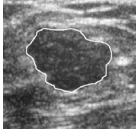
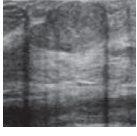
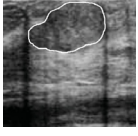




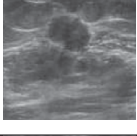
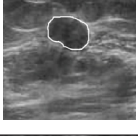
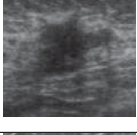

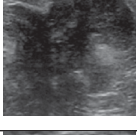

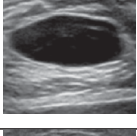

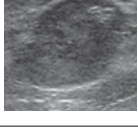

Ultrasound image	Segmented	Classifier output	Gold standard
		Malignant	Malignant
		Malignant	Malignant
		Malignant	Malignant
		Malignant	Malignant
		Malignant	Malignant
		Malignant	Malignant
		Benign	Benign
		Malignant	Malignant
		Benign	Benign
		Benign	Benign

Ultrasound image	Segmented	Classifier output	Gold standard
		Benign	Benign
		Malignant	Malignant
		Malignant	Malignant
		Malignant	Malignant
		Malignant	Malignant
		Malignant	Malignant
		Malignant	Malignant
		Benign	Benign
		Malignant	Malignant
		Benign	Benign

Ultrasound image	Segmented	Classifier output	Gold standard
		Malignant	Malignant
		Benign	Benign
		Malignant	Malignant
		Malignant	Malignant
		Malignant	Malignant
		Malignant	Malignant
		Malignant	Malignant
		Benign	Benign
		Malignant	Malignant
		Malignant	Malignant

Ultrasound image	Segmented	Classifier output	Gold standard
		Malignant	Malignant
		Benign	Benign
		Benign	Benign
		Malignant	Malignant
		Benign	Benign
		Malignant	Malignant
		Benign	Benign
		Malignant	Malignant
		Malignant	Malignant
		Malignant	Malignant

Ultrasound image	Segmented	Classifier output	Gold standard
		Malignant	Malignant
		Malignant	Malignant
		Malignant	Malignant
		Benign	Benign
		Malignant	Malignant
		Benign	Benign
		Malignant	Malignant
		Malignant	Malignant
		Benign	Benign
		Malignant	Malignant

Ultrasound image	Segmented	Classifier output	Gold standard
		Malignant	Malignant
		Malignant	Malignant
		Malignant	Malignant
		Malignant	Malignant
		Malignant	Malignant
		Malignant	Malignant
		Malignant	Malignant
		Malignant	Malignant
		Benign	Benign
		Malignant	Malignant

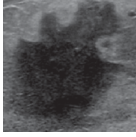

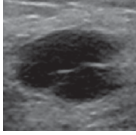

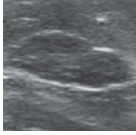
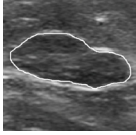
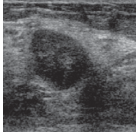

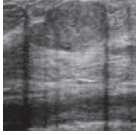

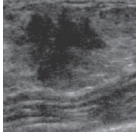

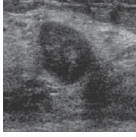

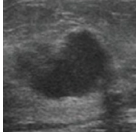

Ultrasound image	Segmented	Classifier output	Gold standard
		Malignant	Malignant
		Malignant	Malignant
		Malignant	Malignant
		Benign	Benign
		Malignant	Malignant
		Malignant	Malignant
		Malignant	Malignant
		Malignant	Malignant

Table C.20: Experiment #4 - Output

## C.5 Experiment #5 - Experiment using an extra feature (wall thickness)

In this experiment, we used fuzzy logic for pre-processing of ultrasound images. We also used correlation of three images for each patient (9 o'clock, 0 o'clock and 3



o'clock) and performed compounding on the images. Proposed region growing method is used for Segmentation. We used the features that we extracted using MI (mutual information), Sequential Forward Search and Sequential Backward Search methods. We also included texture features by Chen et al. [22]. A new feature (wall thickness) is added to the set of features. The outer boundary of the mass was drawn manually by a physician. Feature is defined by the subtracting areas of two regions (Area of outer region - Area of inner region). For classification, we used our proposed classification method, which uses a combination of FSVM, AdaBoost, ANN and Majority based methods. The selected morphological features and texture features are showing in Table C.21. Methods used in each stage of our system are shown in Table C.22.

Table C.21: Experiment #5 - Selected features (A: 77 auto-covariance matrix; B: SGLDM; C: GLDM; D: BDIP; E: BVLC; F: NGTDM)

#	Morphological Feature	#	Texture Features
1	Roundness	1	AD
2	Solidity	2	ADE
3	Convexity	3	AEF
4	TCA Ratio	4	ABCF
5	Perimeter	5	A
6	Area	6	ADF
7	NSPD	7	ACDE
8	Aspect Ratio		
9	Wall Thickness		

Table C.22: Experiment #5 - Methods used in each stage

Stage	Method
Pre-processing	Fuzzy method + Compounding
Segmentation	Proposed region growing method
Feature Extraction	Morphological and texture features + additional morphological feature (Wall Thickness)
Feature Selection	MI (mutual information), Sequential Forward Search and Sequential Backward Search
Classification	Our proposed classification method (combination of ANN, AdaBoost, FSVM and Majority base classifier)

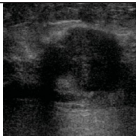
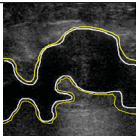
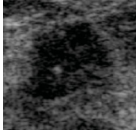
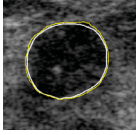
We have performed experiments on the database of 80 patients. The results are given in Table C.23, C.24 and C.25.

Table C.23: Experiment #5 - Results

TP	TN	FP	FN	Accuracy%	Specificity%	Sensitivity%	PPV%	NPV%
59	20	0	1	98.75	100.00	98.33	100.00	95.24

Table C.24: Experiment #5 - Comparison with other methods

Method	Accuracy
ABUS[51]	88.75%
Hybrid Filtering[145]	92.50%
Our approach	98.75%

Ultrasound image	Segmented	Classifier output	Gold standard
		Malignant	Malignant
		Benign	Benign

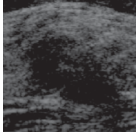
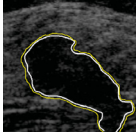
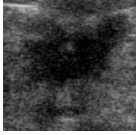
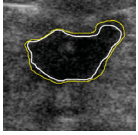
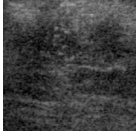
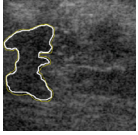
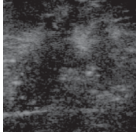
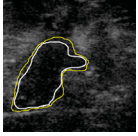
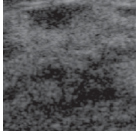
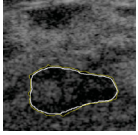
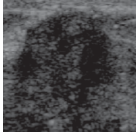
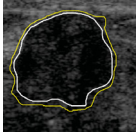


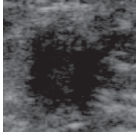
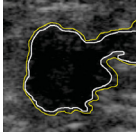
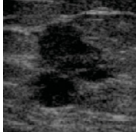
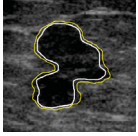
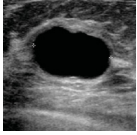

Ultrasound image	Segmented	Classifier output	Gold standard
		Malignant	Malignant
		Malignant	Malignant
		Malignant	Benign
		Malignant	Malignant
		Malignant	Malignant
		Malignant	Malignant
		Benign	Benign
		Malignant	Malignant
		Malignant	Malignant
		Benign	Benign

Table C.25: Experiment #5 - Sample output

Considering "wall thickness" did not make any difference in our results. Radiologists usually do not consider this feature unless there is a lack of other features. This feature is hard to extract and it is very subjective even among experienced radiologists.

Summary of the above experiments are summarized in Table C.26. The summary shows how the system performance improved.

Table C.26: Summary of experiments (Spec.: Specificity, Sen.: Sensitivity)

#	TP	TN	FP	FN	Accuracy%	Spec.%	Sen.%	PPV%	NPV%
1	57	18	2	3	93.75	90.00	95.00	96.61	85.71
2	58	18	1	3	95.00	94.74	95.08	98.30	85.71
3	58	19	1	2	96.25	95.00	96.67	98.30	90.48
4	59	20	0	1	98.75	100.00	98.33	100.00	95.24
5	59	20	0	1	98.75	100.00	98.33	100.00	95.24

## C.6 Experimental results using combination of different methods

In order to know what exactly causes the performance of our system to improve compare to other state-of-the-art CAD systems, we performed the experiments in Table C.27. Please note that for segmentation, we use proposed region growing method. We also use 8 morphological features and 7 texture features we used before. For feature extraction, we use a combination of MI (mutual information), Sequential Forward Search and Sequential Backward Search.

Table C.27: Experiments with different combination of methods in each stage of the CAD system

Experiment #	Pre-processing	Classifier
1	None	ANN
2	None	AdaBoost
3	None	FSVM
4	None	Proposed classifier
5	Fuzzy	ANN
6	Fuzzy	AdaBoost
7	Fuzzy	FSVM
8	Fuzzy	Proposed classifier
9	Fuzzy and Compounding	ANN
10	Fuzzy and Compounding	AdaBoost
11	Fuzzy and Compounding	FSVM
12	Fuzzy and Compounding	Proposed classifier

The result of the experiments mentioned is shown in Table C.28.

Table C.28: Result of comparing our proposed classifiers with state-of-the-art classifiers

#	TP	TN	FP	FN	Accuracy%	Specificity%	Sensitivity%
1	54	16	5	5	87.50	76.19	91.52
2	54	15	4	6	87.50	80.00	90.00
3	56	17	3	4	91.25	85.00	93.33
4	57	18	2	3	93.75	90.00	95.33
5	56	16	3	5	90.00	84.21	91.80
6	57	16	2	5	91.25	88.89	91.93
7	57	20	2	1	93.75	90.00	98.27
8	58	18	1	3	95.00	94.74	95.08
9	57	16	2	5	91.25	88.89	91.93
10	56	20	3	1	95.00	86.96	98.24
11	57	20	2	1	96.25	90.91	98.27
12	59	20	0	1	98.75	100.00	98.33

# Bibliography

- [1] Ge healthcare. <http://www3.gehealthcare.com>. Accessed: 2013-12-30.
- [2] Improved gabor filter for extracting texture edge features in ultrasound kidney images. [www.ccsenet.org/mas](http://www.ccsenet.org/mas). Accessed: 2012-10-14.
- [3] Ultrasound can detect cancers missed by mammography: Why research at center of national debate. [http://medicine.yale.edu/whr/news/232\\_165550\\_Hooley%20Article%20-%20Summer%202013.pdf](http://medicine.yale.edu/whr/news/232_165550_Hooley%20Article%20-%20Summer%202013.pdf). Accessed: 2012-12-30.
- [4] <http://www.breastcancer.org.uk/forum/i/oncotype-dx-test-p387321.html>. Accessed: 2013-10-14.
- [5] [http://en.wikipedia.org/wiki/Medical\\_ultrasonography](http://en.wikipedia.org/wiki/Medical_ultrasonography). Accessed: 2013-10-01.
- [6] C. Ahn, Y. Song, and D. Park. Adaptive template filtering for signal-to-noise ratio enhancement in magnetic resonance imaging. *IEEE Transactions on Medical Imaging*, 18(6):549–556, 1999.
- [7] J. Amores, N. Sebe, and P. Radeva. Boosting the distance estimation; application to the k-nearest neighbor classifier. *Pattern Recognition Letters*, 27: 3307–3318, 2006.
- [8] J. Baker, M. Soo, and E. Rosen. Artifacts and pitfalls in sonographic imaging of the breast. *American Journal of Roentgenology*, 176(5):1261–1266, 2001.
- [9] P. Belhumeur, J. Hespanha, and D. Kriegman. Eigenfaces vs. fisherfaces: Recognition using class specific linear. *IEEE Transactions on Pattern Analysis and Machine Intelligence*, 19(7):711–720, 1997.

- [10] S. Belongie, C. Carson, H. Greenspan, and J. Malik. Color- and texture-based image segmentation using em and its application to content-based image retrieval. In *Proceedings of the International Conference on Computer Vision (ICCV'98)*, pages 675–682, Bombay, India, 1998.
- [11] R. Benes and K. Riha. Noise reduction in medical ultrasound images. *Elektrorevue*, 2(3):1–8, 2011.
- [12] P. Bevan and M. Sherar. B-scan ultrasound imaging of thermal coagulation in bovine liver: log envelope slope attenuation mapping. *Ultrasound Med Biol*, 27:379–387, 2001.
- [13] C. C. Blake, T. L. Elliot, P. J. Downey, and A. Fenster. Variability and accuracy of measurements of prostate brackytherapy seed position *in vitro* using three-dimensional ultrasound: An intra- and inter-observer study. *Medical Physics*, 27(12):2788–2795, 2000.
- [14] L. Bocchi and F. Rogai. Segmentation of ultrasound breast images: Optimization of algorithm parameters. *Applications of Evolutionary Computation. Springer Lecture Notes in Computer Science, LNCS*, 6624:163–172, 2011.
- [15] H. Boveiri. Persian printed numerals classification using extended moment invariants. In *WASET Int. Conf. on Image and Vision Computing*, pages 167–174, Rio de Janeiro, 2010.
- [16] E. Burnside, D. Rubin, R. Sohlich, and E. Sickles. A probabilistic expert system that provides automated mammographic-histologic correlation: Initial experience. *American Journal of Roentgenology*, 182(2):481–488, 2004.
- [17] S. Cang and D. Partridge. Feature ranking and best feature subset using mutual information. *Neural Computing and Applications*, 13:175–184, 2004.
- [18] J. Canny. A computational approach to edge detection. *IEEE Transactions on Pattern Analysis and Machine Intelligence*, 8(6):679–698, 1986.
- [19] R. Chang, W. Wu, W. Moon, and D. Chen. Automatic ultrasound segmentation and morphology based diagnosis of solid breast tumors. *Breast Cancer Research and Treatment*, 89(2):179–185, 2005.



- [20] C. Chen, Y. Chou, K. Han, G. Hung, C. Tiu, H. Chiou, and S. Chiou. Breast lesions on sonograms: computer-aided diagnosis with nearly setting-independent features and artificial neural networks. *Radiology*, 226(2):504–514, 2003.
- [21] D. Chen, R. Chang, and Y. Huang. Computer-aided diagnosis applied to us of solid breast nodules by using neural networks. *Radiology*, 213(2):407–412, 1999.
- [22] D. Chen, Y. Huang, and S. Lin. Computer-aided diagnosis with textural features for breast lesions in sonograms. *Computerized Medical Imaging and Graphics*, 35:220–226, 2011.
- [23] H. Cheng and Y. Guo. A new neutrosophic approach to image thresholding. *New Mathematics and Natural Computation*, 4:291–308, 2008.
- [24] H. Cheng, X. Shi, R. Min, X. Cai, and H. Du. Approaches for automated detection and classification of masses in mammograms. *Pattern Recognition*, 39(4):646–668, 2006.
- [25] H. Cheng, J. Shan, W. Ju, Y. Guo, and L. Zhang. Automated breast cancer detectoin and classification using ultrasound images: A survey. *Pattern Recognition*, 41(1):299–317, 2010.
- [26] H. Chioua, C. Chenc, T. Liuc, S. Chioua, H. Wanga, Y. Choua, and H. Chiang. Computer-aided diagnosis of peripheral soft tissue masses based on ultrasound imaging. *Computerized Medical Imaging and Graphics*, 33:408–413, 2009.
- [27] K. Cobb. Microarrays: The search for meaning in vast sea of data. *Biomedical Computation Review*, 2(4):1–23, 2006.
- [28] B. Deka and D. Ghosh. Ultrasound image segmentation using watersheds and region merging. *In IET International Conference on Visual Information Engineering*, pages 110–115, 2006.
- [29] P. Devijver and J. Kittler. *Pattern Recongnition: A Statistical Approach*. Prentice Hall, 1982.
- [30] Z. Dokur and T. Olmez. Segmentation of ultrasound images by using a hybrid neural network. *Pattern Recognition Letters*, 23(14):1825–1836, 2002.

- [31] Z. Dokur and T. Olmez. Untangling the roots of cancer. *Scientific American*, pages 57–65, 2003.
- [32] K. Drukker, K. Horsch, M. Kupinski, C. Vyborny, and E. Mendelson. Computerized lesion detection on breast ultrasound. *Medical Physics*, 29(7):1438–1446, 2002.
- [33] K. Drukker, C. Sennett, and M. Giger. Automated method for improving system performance of computer-aided diagnosis in breast ultrasound. *IEEE Transactions on Medical Imaging*, 28(1):122–128, 2009.
- [34] R. Duda, P. Hart, and D. Stork. *Pattern Classification*. Wiley, New York, second edition, 2001.
- [35] R. Entekin, P. Jackson, J. Jago, and B. Porter. Real time spatial compound imaging in breast ultrasound: technology and early clinical experience. *Medicamundi*, 43(3), 1990.
- [36] D. Freedman, D. Petiti, and J. Robin. On the efficacy of screening for breast cancer. *International Journal of Epidemiology*, 33(1):43–55, 2004.
- [37] D. Fritsch, S. Pizer, L. Yu, V. Johnson, and E. Chaney. Localisation and segmentation of medical image objects using deformable shape loci. In *Information Processing in Medical Imaging 1997 (IPMI'97)*, Springer Lecture Notes in Computer Science, pages 127–140, 1997.
- [38] I. Gheyas and L. Smith. Feature subset selection in large dimensionality domains. *Pattern Recognition*, 43:5–13, 2010.
- [39] M. Giger. Computerized analysis of images in the detectoin and diagnosis of breast cancer. *Seminars in Ultrasound, CT and MRI*, 25:411–418, 2004.
- [40] W. Gomez, W. Pereira, and A. Infantosi. Analysis of co-occurrence texture statistics as a function of gray-level quantization for classifying breast ultrasound. *IEEE Transactions on Medical Imaging*, 31:1889–1899, 2012.
- [41] Y. Guo, H. Cheng, J. Tian, and Y. Zhang. A novel approach to speckle reduction in ultrasound imaging. *Ultrasound in Medicine and Biology*, 35(4):628–640, 2009.

- [42] S. Gupta, R. Chauhan, and S. Sexena. Robust non-homomorphic approach for speckle reduction in medical ultrasound images. *Medical and Biological Engineering and Computing*, 43:189–195, 2005.
- [43] W. Haihui, W. Yanli, T. Tongzhou, W. Miao, and W. Mingpeng. Images segmentation method on comparison of feature extractoin techniques. *2nd International Workshop on Intelligent Systems and Applications*, pages 1–4, 2010.
- [44] R. Haralick and L. Watson. A facet model for image data. *Computer Vision Graphics Image Process*, 15:113–129, 1981.
- [45] R. Haralick and L. Watson. Evaluation of feature selection techniques for analysis of functional MRI and EEG. In *Proceedings of the 2007 International Conference on Data Mining*, Las Vegas, Nevada, USA, June 25-28 2007.
- [46] T. Hastie, R. Tibshirani, and J. Friedman. *The Elements of Statistical Learning: Data Mining, Inference, and Prediction, Second Edition*. Springer series in statistics. Springer, 2009. ISBN 9780387848587.
- [47] H. Horng, Y. Sun, and X. Lin. Texture feature coding method for classification of liver sonography. *Comput. Med. Imag. Graph*, 6:33–42, 1996.
- [48] M. Hu. Visual pattern recognition by moment invariant. *IRE Trans. Info. Theory*, IT-8:179–187, 1962.
- [49] Y. Huang and D. Chen. Watershed segmentation for breast tumor in 2-d sonography. *Ultrasound Medicin & Biology*, 30(5):625–632, 2004.
- [50] K. Hwang. Computer aided diagnosis (cad) of breast mass on ultrasonography and scintimammography. In *7th International workshop on Enterprise Networking and Computing in Healthcare Industry*, pages 187–189, 2007.
- [51] K. Ikedo, Y., F. D., T. Hara, H. Fujita, E. Takada, T. Endo, and T. Morita. Computerized mass detection in whole breast ultrasound. *Medical Imaging*, 6514:29–36, 2007.
- [52] J. Jackson. *A User's Guide to Principal Components*. Wiley Series in Probability and Statistics, 1991.

- [53] V. Jackson. The role of us in breast imaging. *Radiology*, 177:305–311, 1990.
- [54] A. Jain and F. Farrokhnia. Unsupervised texture segmentation using gabor filters. *Pattern Recognition*, 24(12):1167–1186, 1991.
- [55] A. Jemal, R. Siegel, J. Xu, and E. Ward. Cancer statistics. *CA: A Cancer Journal for Clinicians*, 60:277–300, 2010.
- [56] S. Joo, W. Moon, and H. Kim. Computer-aided diagnosis of solid breast nodules on ultrasound with digital image processing and artificial neural network. *medicine and Biology Society*, 2:1397–1400, 2004.
- [57] A. Jumaat, W. Rahman, A. Ibrahim, and R. Mahmud. Segmentation of masses from breast ultrasound images using parametric active contour algorithm. In *International Conference on Mathematics Education Research*, 8:640–647, 2010.
- [58] T. Kanungo, D. Mount, N. Netanyahu, C. Piatko, R. Silverman, and A. Wu. An efficient k-means clustering algorithm: Analysis and implementation. In *Proc. IEEE Conf. Computer Vision and Pattern Recognition*, pages 881–892, 2007.
- [59] B. Karimi and A. Krzyżak. Computer-aided system for suspicious lesions in breast ultrasound images. In *Proc. 13th International Conference on Artificial Intelligence and Soft Computing, ICAISC 2014*, volume LNAI of *Lecture Notes in Artificial Intelligence*, Zakopane, Poland, June 1-5 2014. Springer.
- [60] B. Karimi and A. Krzyżak. A novel technique for detecting suspicious lesions in breast ultrasound images. *Concurrency and Computation: Practice and Experience*, 2014. After first round of reviews.
- [61] B. Karimi and A. Krzyżak. A novel approach for automatic detection and classification of suspicious lesions in breast ultrasound images. *Journal of Artificial Intelligence and Soft Computing Research*, 2014. Accepted.
- [62] A. Katouzian, E. Angelini, S. Carlier, J. Suri, N. Navab, and A. Laine. A state-of-the-art review on segmentation algorithms in intravascular ultrasound (ivus) images. *IEEE Trans Inf Technol Biomed*, 16(5):823–834, 2012.

- [63] H. Kekre and P. Shrinath. Segmentation of ultrasound breast images using vector neighborhood with vector sequencing on kmcg and augmented kmcg algorithms. *International Journal of Advanced Computer Science and Application (IJACSA)*, 4(2):92–98, 2013.
- [64] H. Kekre, K. Sarode Tanuja, and M. Gharge Saylee. Tumor detection in mammography images using vector quantization technique. *International Journal of Intelligent Information Technology Application*, 2(5):237–242, 2009.
- [65] M. Kenjiro and T. Nishimura. A study for reduction of speckle noise in medical ultrasonic images using neural network. *World Congress on Medical Physics and Biomedical Engineering*, 14(15):2497–2500, 2007.
- [66] B. King. Reforming the theory of invariant moments for pattern recognition. *Pattern Recognition Lett.*, 62:86–101, 1967.
- [67] J. Kling. Put the blame on methylation. *The Scientist*, 16(12):27–41, 2003.
- [68] C. Kotropoulos and I. Pitas. Segmentation of ultrasonic images using support vector machines. pattern recognition letters. *Pattern Recognition Letters*, 24(4):715–725, 2004.
- [69] K. Krishnan and R. Sudhakar. Automatic classification of liver diseases from ultrasound images using glrlm texture features. *Soft Computing Applications*, 195:611–624, 2013.
- [70] L. Kuncheva. *Combining Pattern Classifiers*. Wiley-Interscience, Hoboken, New Jersey, 2004.
- [71] M. Larabi, N. Richard, and C. Fernandez-Maloigne. Using combination of color, texture and shape features for image retrieval in melanomas databases. In *Internet Imaging III, SPIE Photonics West Conference*, San Jose, California, USA, December 2002.
- [72] F. Lauera, C. Suen, and G. Blocha. A trainable feature extractor for handwritten digit recognition. *Pattern Recognition*, 40(6):1816–1824, 2007.
- [73] C. Leondes. *Biomechanical Systems Technology*. World Scientific, 2007.

- [74] Y. Li. Reforming the theory of invariant moments for pattern recognition. *Pattern Recognition Lett.*, 25:723–730, 1992.
- [75] R. Liao, T. Wan, and Z. Qin. Classification of benign and malignant breast tumors in ultrasound images based on multiple sonographic and textural features. *2011 International Conference on Intelligent Human-Machine Systems and Cybernetics(IHMSC)*, 1:71–74, 2011.
- [76] Y. Liao, C. Chang, W. Kuo, K. Chang, and C. Yeh. Classification of benign and malignant breast tumors by 2-d analysis based on contour description and scatterer characterization. *IEEE Transactions on Medical Imaging*, 29(2):513–522, 2010.
- [77] L. Lihua, L. Jiangli, L. Deyu, and W. Tianfu. Segmentation of medical ultrasound image based on markov random field. *Bioinformatics and Biomedical Engineering*, 28(1):968–971, 2007.
- [78] C. Lin and S. Wang. Fuzzy support vector machines: Ieee transactions on neural networks. *IEEE Transactions on Neural Networks*, 13(2):464–471, 2002.
- [79] B. Liu, H. Cheng, J. Huang, J. Tian, J. Liu, and X. Tang. Automated segmentation of ultrasonic breast lesions using statistical texture classification and active contour based on probability distance. *Ultrasound in Medicine & Biology*, 35(8):1309–1324, 2009.
- [80] B. Liu, H. Cheng, J. Huang, J. Tian, X. Tang, and J. Liu. Fully automaticandsegmentation-robustclassificationofbreasttumorsbasedonlocal texture analysisofultrasoundimages. *Pattern Recognition*, 43:280–298, 2010.
- [81] C. Lorenz, I. Carlsen, T. M. Buzug, C. Fassnacht, and J. Weese. Multi-scale line segmentation with automatic estimation of width, contrast, and tangential direction in 2d and 3d medical images. In *Conference on Computer Vision, Virtual Reality and Robotics in Medicine and Medical Robotics and Computer-Assisted Surgery, CVRMed-MRCAS*, Lecture Notes in Computer Science, pages 233–242. Springer, March 1997.

- [82] B. Lui, H. Cheng, J. Huang, J. Tian, X. Tang, and J. Lui. Probability density difference-based active contour for ultrasound image segmentation. journal pattern recognition. *Journal Pattern Recognition*, 43(6):2028–2042, 2010.
- [83] A. Madabhushi and D. Metaxas. Combining low-, high-level and empirical domain knowledge for automated segmentation of ultrasonic breast lesions. *IEEE Transactions on Medical Imaging*, 22(2):155–169, 2003.
- [84] F. Maes, A. Collignon, D. Vandermeulen, G. Marchal, and P. Suetens. Multimodality image registration by maximization of mutual information. *IEEE Transactions on Medical Imaging*, 16(2):187, Apr. 1997.
- [85] S. Mallat and S. Zhong. Characterization of signals from multiscale edges. *IEEE Transactions Pattern Analysis and Machine Intelligence*, 14(7):710–732, 1999.
- [86] M. Mancas, B. Gosselin, and B. Macq. Segmentation using a region growing thresholding. In *Proceedings of 4th Conference on Image Processing (SPIE)*, volume 56, pages 388–398, 2005.
- [87] D. Martin, C. Fowlkes, D. Tal, and J. Malik. A database of human segmented natural images and its application to evaluating segmentation algorithms and measuring ecological statistics. In *Proceedings of the Ninth IEEE International Conference on Computer Vision (ICCV2001)*, pages 416–423, Vancouver, Canada, 2001.
- [88] D. Metaxas. Physics-based techniques for segmentation, modeling and analysis of internal organs. In *Third IEEE-EMBS International Summer School*, pages 326–335, Berder Island, France, June 1998.
- [89] Y. Meyer. *Wavelets and Operators*. Cambridge University Press, Cambridge, 1993.
- [90] O. Michailovich and A. Tannenbaum. Segmentation of medical ultrasound images using active contours. In *International Conference on Image Processing-ICIP*, pages 513–516, 2007.
- [91] W. Moon, C. Lo, J. Chang, C. Huang, J. Chen, and C. R. Computer-aided classification of breast masses using speckle features of automated breast ultrasound images. *Medical Physics*, 39:6465–6473, 2012.

- [92] W. Moon, Y. Shen, M. Bae, C. Huang, and J. Chen. Computer-aided tumor detection based on multi-scale blob detection algorithm in automated breast ultrasound images. *Pattern Recognition*, 32(7):1191–1200, 2013.
- [93] P. Nathangle, W. Chambers, and M. Davidson. *Introduction to Stereomicroscopy*. Nikon, MicroscopyU.
- [94] M. Nicolae, L. Moraru, and A. Gogu. Speckle noise reduction of ultrasound images. *Medical Ultrasonography an International Journal of Clinical Imaging, Supplement*, 11:50–51, 2009.
- [95] M. Nicolae, L. Moraru, and A. Gogu. Speckle noise reduction of ultrasound images. *Medical Ultrasonography an International Journal of Clinical Imaging*, 11:50–51, 2009.
- [96] M. Nicolae, M. Carmen, L. Moraru, and L. Onose. Comparative approach for speckle reduction in medical ultrasound images. *Romanian J. Biophys*, 1:13–21, 2010.
- [97] J. Noble and D. Boukerroui. Ultrasound image segmentation: A survey. *IEEE Transactions on Medical Imaging*, 25(8):987–1010, 2006.
- [98] H. Peng, F. Long, and C. Ding. Feature selection based on mutual information criteria of max-dependency, max-relevance, and minredundancy. *IEEE Transactions on Pattern Analysis and Machine Intelligence*, 27:1226–1238, 2005.
- [99] W. Pereira and A. Infantosi. Analysis of co-occurrence texture statistics as a function of gray-level quantization for classifying breast ultrasound. *IEEE Transactions on Medical Imaging*, 31(10):1889–1899, 2012.
- [100] J. H. Piater and R. A. Grupen. Feature learning for recognition with bayesian networks. In *Proceedings of the 15th International Conference on Pattern Recognition (ICPR 2000)*, pages 17–20, Barcelona, Spain, 2000.
- [101] S. Poonguzhali and G. Ravindran. Automatic classification of focal lesions in ultrasound liver images using combined texture features. *Information Technology Journal*, 7(1):205–209, 2008.



- [102] K. Prasad, B. Zimmermann, G. Prabhui, and M. Pai. Datamining approach for automation of diagnosis of breast cancer in immunohistochemically stained tissue microarray images. *The Open Medical Informatics Journal*, 4:86–93, 2010.
- [103] N. Ragesh, A. Anil, and R. Rajesh. Digital image denoising in medical ultrasound images: A survey. In *ICGST AIML - 11 Conference*, 2011.
- [104] B. Ramana Reddy, A. Suresh, M. Radhika Mani, and V. Vijaya Kumar. Classification of textures based on features extracted from preprocessing images on random windows. *International Journal of Advanced Science and Technology*, 9, 2009.
- [105] N. Rani and T. Thind. Segmentation of ultrasound images using closest neighbour approach. *International Journal of Recent Technology and Engineering (IJRTE)*, 6, 2013.
- [106] A. L. Ratan, O. Maron, W. E. L. Grimson, and T. Lozano-Perez. A framework for learning query concepts in image classification. In *Proceedings of the 1999 IEEE Conference on Computer Vision and Pattern Recognition (CVPR'99)*, Fort Collins, Colorado, USA, 23–25 1999.
- [107] S. Roy, N. Sinha, and A. Sen. A new hybrid image denoising method. *International Journal of Information Technology and Knowledge Management*, 2(2): 491–497, 2010.
- [108] A. Saad. Simultaneous speckle reduction and contrast enhancement for ultrasound images: Wavelet versus laplacian pyramid. *Pattern Recognition and Image Analysis*, 18:63–70, 2008.
- [109] F. Sahba, M. Tizhoosh, and M. Salma. Segmentation of prostate boundaries using regional contrast enhancement. . *The IEEE International Conference on Image Processing (ICIP)*, 2:1266–1269, 2005.
- [110] S. Saini. Ultrasound imaging and image segmentation in the area of ultrasound: a review. *International Journal of Advanced Science and Technology*, 24, 2010.
- [111] A. Sarti, C. Corsi, E. Mazzini, and C. Lamberti. Maximum likelihood segmentation with rayleigh distribution of ultrasound images. *Computers in Cardiology*, 31:329–332, 2004.

- [112] S. Selvan, M. Kavitha, S. Shenbagadevi, and K. Suresh. Feature extraction for characterization of breast lesions in ultrasound elastography and echography. *Journal of Computer Science*, 16:67–74, 2010.
- [113] C. Sennett and M. Giger. Automated method for improving system performance of computer-aided diagnosis in breast ultrasound. *IEEE Trans Med Imaging*, 28(1):122–128, 2009.
- [114] J. Serra. *Image Analysis and Mathematical Morphology. Vol. I*. London Ed. Academic Press, 1982.
- [115] J. Serra and L. Vincent. An overview of morphologic filtering. *Circuits, Systems and Signal Processing*, 11:47–108, 1992.
- [116] J. Shan. Completely automatic segmentation for breast ultrasound using multiple-domain features. In *Image Processing (ICIP2010)*, 2010.
- [117] J. Shan. *A fully automated segmentation method for breast ultrasound images*. PhD thesis, Utah State University, 2011.
- [118] J. Shan, H. Cheng, and Y. Wang. A completely automatic segmentation method for breast ultrasound images using region growing. *11th Joint Conference on Information Science*, 2008.
- [119] J. Shan, H. Cheng, and Y. Wang. A novel segmentation method for breast ultrasound images based on neutrosophic l-means clustering. *Medical Physics*, 39(9):5669–5682, 2012.
- [120] X. Shi, H. Cheng, L. Hu, W. Ju, and J. Tian. Detection and classification of masses in breast ultrasound images. *Digital Signal Processing*, 20(3):824–836, 2010.
- [121] M. Singh, S. Singh, and S. Gupta. An information fusion based method for liver classification using texture analysis of ultrasound images. *Information Fusion*, 2013.
- [122] A. Sohail, P. Bhattacharya, S. Mudur, and S. Krishnamurthy. Classification of ultrasound medical images using distance based feature selection and fuzzy-svm. *Pattern Recognition and Image Analysis*, 6669:176–183, 2011.

- [123] G. Srinivasan and G. Shobha. Statistical texture analysis. *World Academy of Science, Engineering and Technology*, 36, 2008.
- [124] A. Stavros, D. Thickman, C. Rapp, M. Dennis, S. Parker, and G. Sisney. Solid breast nodules: use of sonography to distinguish between benign and malignant lesions. *Radiology*, 196:123–134, 1995.
- [125] S. Sudha, G. Suresh, and R. Sukanesh. Speckle noise reduction in ultrasound images by wavelet thresholding based on weighted variance. *International Journal of Computer Theory and Engineering*, 1(1), 2009.
- [126] M. Talebi, A. Ayatollahi, and A. Kermani. Medical ultrasound image segmentation using genetic active contour. *Biomedical Science and Engineering*, 4: 105–109, 2011.
- [127] P. Tamilselvi and P. Thangaraj. Improved gabor filter for extracting texture edge features in us kidney images. *Modern applied science*, 4, 2010.
- [128] U. Techavipoo, Q. Chen, T. Varghese, A. Zagzebski, and E. Madsen. Noise reduction using spatial-angular compounding for elastography. *IEEE Transactions on Ultrasonics, Ferroelectrics, and Frequency Control*, 51(5), 2004.
- [129] L. Thai, T. Hai, and N. Thuy. Image classification using support vector machine and artificial neural network. *I.J. Information Technology and Computer Science*, 5:32–38, 2012.
- [130] K. Thangavel and M. Karnan. Cad system for preprocessing and enhancement of digital mammograms. *International Journal on Graphics Vision and Image Processing*, 9:69–74, 2005.
- [131] E. Tohno, D. Cosgrove, and J. Sloane. *Ultrasound Diagnosis of Breast Diseases*. Churchill Livingstone, 1994.
- [132] G. Treece, A. Gee, and R. Prager. Ultrasound compounding with automatic attenuation compensation using paired angle scans. *Ultrasound in Medicine and Biology*, 33(4):630–642, 2007.

- [133] H. Tu, J. Zagzebski, A. Gerig, Q. Chen, E. Madsen, and T. Hall. Optimization of angular and frequency compounding in ultrasonic attenuation estimation. *Journal of the Acoustical Society of America*, 117(5):3307–3318, 2005.
- [134] J. Udupa and S. Samarasekera. Fuzzy connectedness and object definition: Theory, algorithms, and applications in image segmentation. *Graphical Models and Image Processing*, 58(3):246–261, 1996.
- [135] V. Ulagamuthalvi and D. Sridharan. Automatic identification of ultrasound liver cancer tumor using support vector machine. *International Conference on Emerging Trends in Computer and Electronics Engineering*, pages 41–43, 2012.
- [136] G. Umamaheswari and R. Vanithamani. Performance analysis of filters for speckle reduction in medical ultrasound images. *International Journal of Computer Applications*, 12(6), 2010.
- [137] H. Vala and A. Baxi. A review on otsu image segmentation algorithm. *International Journal of Advanced Research in Computer Engineering and Technology (IJARCET)*, 2(2), 2013.
- [138] W. Wilhelm, J. Johnson, J. Hatfield, W. Voorhees, and D. Linden. Crop and soil productivity response to corn residue removal: A review of the literature. *Agronomy Journal*, 96:1–17, 2004.
- [139] A. Winder, B. Jadidian, and R. Muratore. Synthetic structural imaging (ssi): A new ultrasound method for tracking breast cancer morphology. *39th Annual Ultrasonic Industry Association Symposium (UIA)*, pages 1–4, 2010.
- [140] H. Wu, H. Tseng, S. Chen, and D. Chen. Speckle reduction imaging of breast ultrasound does not improve the diagnostic performance in morphology-based cad system. *Journal of Clinical Ultrasound*, 40(1):1–6, 2012.
- [141] W. Wu and W. Kyung Moon. Ultrasound breast tumor image computer-aided diagnosis with texture and morphological features. *Academic Radiology*, 15(7): 873–880, 2008.
- [142] Y. Xu and N. T. Segmentation of breast lesions in ultrasound images using spatial fuzzy clustering and structure tensors. *International Journal of Biological and Life Sciences*, 5(3), 2009.

- [143] H. Yang, C. Chang, S. Huang, and P. Li. Correlations among acoustic, texture and morphological features for breast ultrasound cad. *Ultrasound Imaging*, 30(4):228–236, 2008.
- [144] Z. Yang. Breast ultrasound image improvement by pixel compounding of compression sequence. *IEEE Transactions on Ultrasonics, Ferroelectrics, and Frequency Control*, 56(3), 2009.
- [145] M. Yap. A novel algorithm for initial lesion detection in ultrasound breast images. *Journal of Applied Clinical Medical Physics*, 9(4), 2008.
- [146] M. Yap, E. Edirisinghe, A. Gale, and H. Bez. Processed images in human perception: A case study in ultrasound breast imaging. *Eur J Radiol*, 2009.
- [147] C. Yeh, W. Chen, and Y. Liao. A disk expansion segmentation method for ultrasonic breast lesions. *Pattern Recognition*, 42(5):596606, 2008.
- [148] C. Yeh, Y. Chen, W. Fan, and Y. Liao. A disk expansion segmentatoin method for ultrasonic breast lesions. *Pattern Recognition*, 42(5):596–606, 2009.
- [149] A. Yezzi, Jr, S. Kichenassamy, A. Kumar, P. Olver, and A. Tannenbaum. A geometric snake model for segmentation of medical imagery. *IEEE Tr. Med. Im.*, 16(2):199, Apr. 1997.
- [150] T. S. Yoo, M. J. Ackerman, and M. Vannier. Toward a common validation methodology for segmentation and registration algorithms. In *International Conference on Medical Image Computing and Computer-Assisted Intervention MICCAI'2000*, Lecture Notes in Computer Science, pages 422–431, Cambridge, England, 2000. Springer Verlag.
- [151] J. Yu, W. Wang, P. Chen, and H. Xu. Two-dimensional fuzzy clustering for ultrasound image segmentation. *IEEE International Conference on Bioinformatics and Biomedical Engineering*, pages 599–603, 2007.
- [152] Y. Yu and T. Acton. Speckle reduction anisotropic diffusion filter. *IEEE Transaction Image Processing*, 11:1260–1270, 2011.
- [153] L. Zadeh. Fuzzy sets. *Information and Control*, 8(3):338–353, 1965.

- [154] L. Zadeh. The concept of linguistic variable and its application to approximate reasoning - i. *Information Science*, 8:199–249, 1975.
- [155] A. Zaina and A. Asano. Image thresholding by histogram segmentation using discriminant analysis. *Pattern Recognition Letters*, 27(13):1515–1521, 2006.
- [156] H. Zhang, J. Fritts, and S. Goldman. A fast texture feature extraction method for region-based image segmentation. *SPIE*, 5685:957–968, 2005.
- [157] L. Zhang, Y. Ren, C. Huang, and F. Liu. A novel automatic tumor detection for breast cancer ultrasound images. *2011 Eighth International Conference on Fuzzy Systems and Knowledge Discovery (FSKD)*, 1:401–404, 2011.
- [158] M. Zhang. *Novel Approaches to Image Segmentation Based on Neutrosophic Logic*. PhD thesis, Utah State University, 2010.
- [159] Y. Zhu and H. Yan. Computerized tumor boundary detection using a hopfield neural network. *IEEE Tr. Med. Im.*, 16(1):55, Feb. 1997.
- [160] A. Zilkowski, Y. Li, D. Becker, and S. Ishrak. Speckle reduction imaging. *GE Medical Systems Ultrasound*, 2011.